POLITECNICO DI TORINO

Department of Mechanical and Aerospace Engineering

M. Sc. Thesis
in Automotive Engineering

Electrification of an Automatic Nautical Gangway for Boarding Operations

Tutors

Prof. Eng. Mirko Baratta
Prof. Eng. Andrea Cavagnino

Candidate

Alessandro Chiuso

July 2022

Contents

Nomenclature

A	Area
[A]	Ampere
AISI	American Iron and Steel Institute
BLDC	Brushless Direct Current
C	Torque
d	Diameter
DC	Direct Current
E_{abs}	Energy Absorbed
F	Force
f	Friction Coefficient
f_i	Safety coefficient for inertia forces
f_t	Ambient temperature correction factor
f_c	Intermittent utilization correction factor
I	Current
IP	Ingress Protection
[kg]	Kilograms
[kJ]	Kilojoule
[km/h]	Kilometer per Hour
[kN]	Kilonewton
[kV]	Kilovolt
l	Length
l_e	Free Length (buckling)
l_g	Free Length (critic n° of revolution)
[l/min]	Liter per Minute
[m/s]	Meter per Second
[mm]	Millimeter

[mm/s]	Millimeter per Second
N	Normal Force
[N]	Newton
[Nm]	Newton meter
P	Screw Pitch
p	Superficial Contact Pressure
P_{th}	Theoretic Power
P_{abs}	Absorbed Power
Q	Capacity
R	Resultant Force
r_e	External Radius
r_i	Internal Radius
[rad]	Radiant
[rpm]	Revolutions per minute
[s]	Seconds
T	Tangential Force
t	Time
v	Velocity
[V]	Volt
V_{st}	Sliding Velocity
[W]	Watt
%	Percent
α	Thread Angle
γ_a	Angle of Friction
Δp	Change in pressure
Δt	Change in time
η	Efficiency
ω	Angular velocity

Preface

Thesis introduction

A nautical gangway, also called "passerella", is a narrow passage which connects the stern of a boat with the port quay. It is used to allow passengers to get on and off the boat, in particular on yacht and superyacht, where the distance between the end of the boat and the start of the quay is quite large.

This system is usually inserted inside a box, which remains hidden inside the end part of the boat. In this way, when the gangway is not needed, it is practically invisible inside the boat. Instead, when the passengers decide to get on or get off the boat, they just had to push a button, and the passerella will start to exit from its box automatically.

Nowadays, there are different types of gangways, like the foldable one, where the whole passerella fold on itself and then re-enter inside its box, or the telescopic one, where first the second half of the passerella slide underneath the first one, and then both of them re-enter inside the box. Of course, when opening, the gangway does the same movements but in the opposite order. There are also extended versions with more than one telescopic element, which allow to reach greater distances.

Figure 1 Real nautical gangway

In this dissertation, the focus will be on a telescopic gangway, in particular on the model "1041.29" sold by the Opacmare company, which is composed by one telescopic element.

All the movements are performed by hydraulic motors, which take the required energy from the main combustion engine of the boat. Moreover, all the movement are performed with no human body on board, so the passerella have to move just its own weight, while during the static phase it has to sustain also the weight of the passengers that are crossing it.

Movements description

As stated before, the opening of the gangway is divided in three movements, each one independent from the others even if they are subsequent, which means that they cannot be performed simultaneously but they start when the previous one has already finished.

The starting situation is when the whole gangway is packed inside the box, the gate is closed and the system is hidden inside the rear part of the boat.

When the customer decides to open the passerella and press the open button, the first movement takes place: the gate opens, and the gangway starts to exit from the box. This first movement is done by meaning of toothed gear and a belt, with the ladder directly hinged with the movable part of the passerella. When the toothed gear is put in rotation, it moves the belt, which drag the gangway with it. This movement were previously performed using a simple hydraulic motor that is able to actuate the toothed gear, directly placed on top of it.

When the first movement has reached is final position, which means that the passerella is exited completely from the box, the second movement, the so called “telescopic movement”, can start. During the first movement, the gangway exits from the box as a double layer component. During this second movement, the inferior part of the gangway will slowly slide forward, increasing the length of the passerella up to double, while decreasing its thickness. This second movement ends when all the inferior part of the gangway has slid underneath the superior one, creating in this way a unique straight element. At this point, the passerella can be considered fully opened: however, there is

still the last movement, which allows the gangway, and consequently the passenger, to be as close as possible to the quay.

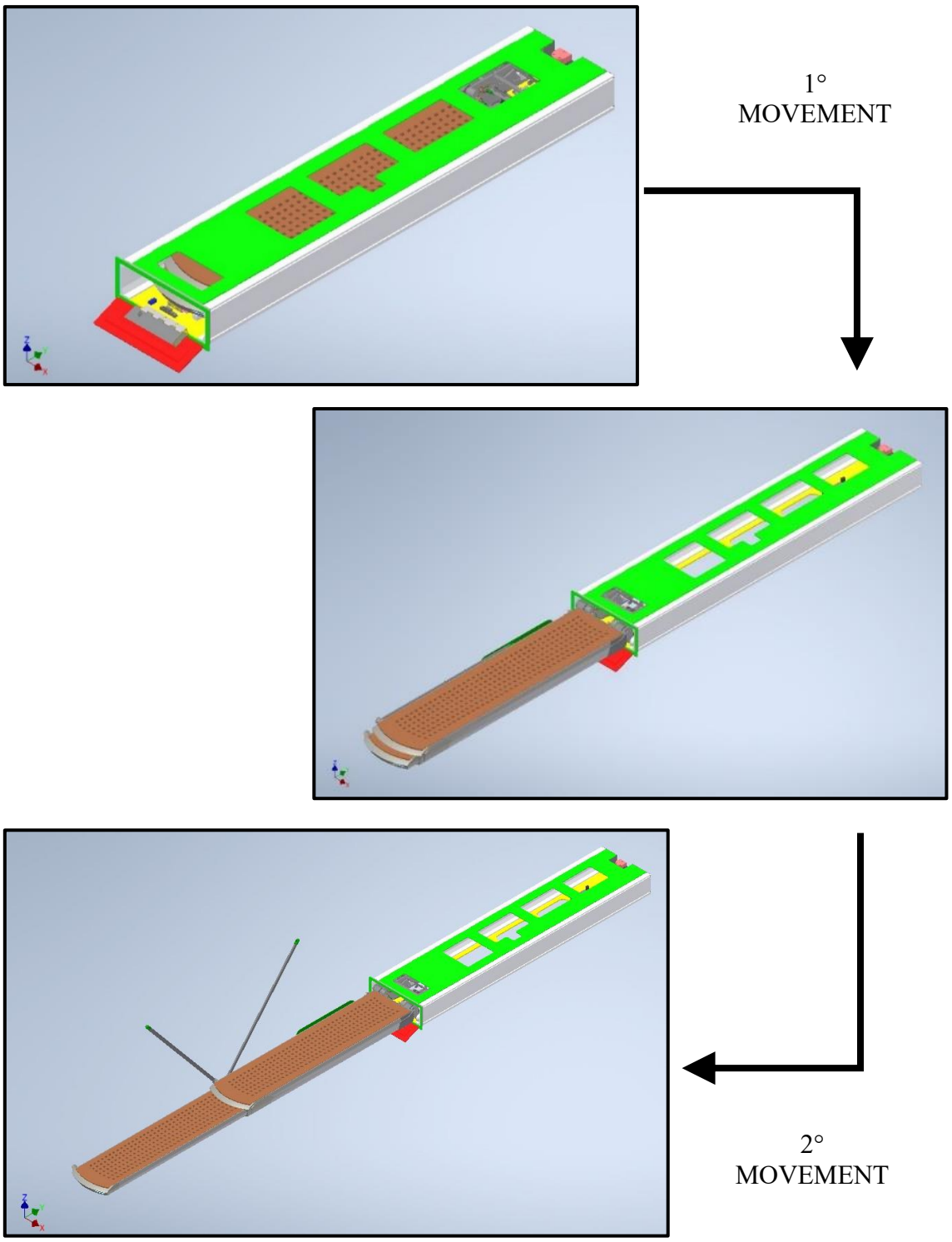

Figure 2 Inventor visualization of the first two analyzed movements

The third and last movement is the so called “tilt” movement: when the gangway is fully extended, it can move its further point towards the sky or towards the sea, creating an angle with the horizontal line. The common adopted angles are between ± 20°, but an acceptable solution can be also between ± 15°. In this way, passengers can accede both an high or low quay without any problem. It is clear that in this situation, the gangway can never be in contact with the quay, but it is always suspended above of it.

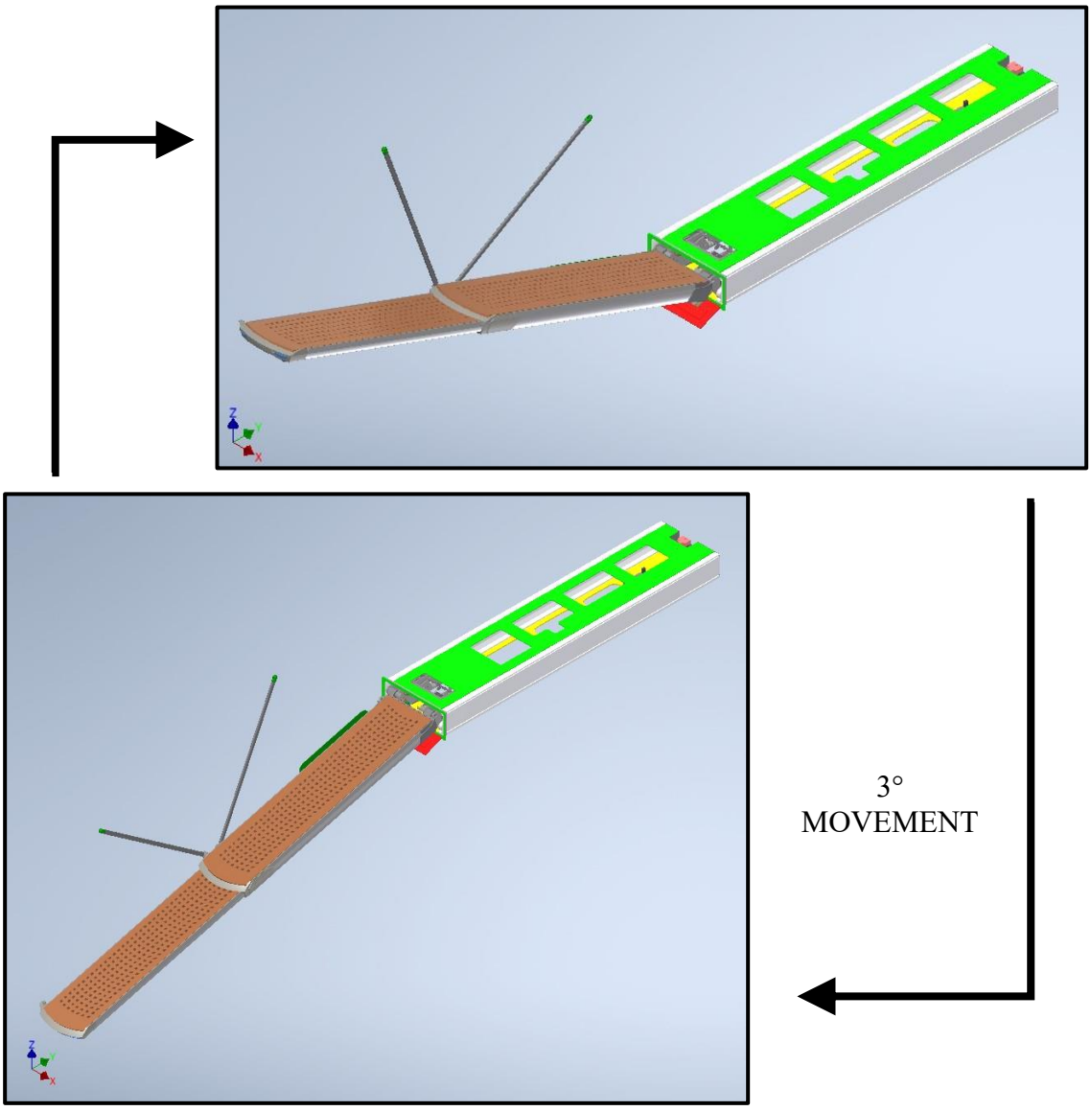

Figure 3 Inventor visualization of the third movement

Objectives

The goal of this dissertation is to analyze, compare and finally create an innovative solution for the predefined movements, with the utilization of electric motors instead of the hydraulic ones. The times and the markets are ready for a further step towards the "green" life, slowly leaving behind the polluting hydraulic motor for the more ecologic electric one.

As it is clear, hydraulics has a lot of advantages, like the very compact and personalized design, the possibility of creating an high torque, the capacity to sustain heavy axial load and so on. However, it has also a lot of drawbacks, first of all the presence of the oil itself, which is the most polluting element inside this motor. Hydraulic fluids can enter the environment through spills and leakages along the wires which connects the motor to the fluids tank, but also from failure inside the motor itself. If spilled on soil, some of the ingredients may rest on the top the surface, while others may sink into the groundwater. The sinking velocity depends on many factors, like the amount of spillage, the amount of rain falls and the type of soil. In water, some ingredients will sink to the bottom of the sea, and fish may contain some of them. Eventually, the ingredients of hydraulic fluids can degrade in the environment, but complete degradation may take more than a year [1].

On the other hand, electric motors present a more complex design, the need of a very well-designed control system, the necessity of a larger space. However, the advantages are countless: first of all, as already stated, they are more ecological, at least for what concern the functioning, they are lighter and usually also less noisy. By eliminating the need of the hydraulic oil, the polluting problem is almost vanished, even if the amount of wiring needed increases. Moreover, the electric solution is usually lighter and less noisy, leading to an higher products rank.

1. First movement analysis

In this first part, the focus will be on the selection of a suitable mechanism for completing the three proposed movements and consequently on the selection of possible gear motors to actuate the mechanisms. The selection is mainly based on power, split between torque and angular speed, overall dimensions, nominal input voltage and Ingress Protection.

The **Ingress Protection IP** classifies the degree of protection provided by an enclosure, for electrical equipment with a rated voltage not exceeding 72.5 kV. It is defined by the international standard EN 60529, which specifies the levels of sealing effectiveness against "ingress" i.e. intrusion from foreign bodies such as tools, dirt and liquid water. The rating consists of the letters IP followed by two digits, the higher the number the better the protection. Sometimes a number is replaced by X, which indicates that the enclosure is not rated for that specification. The first digit stands for the level of protection that the enclosure provides against the ingress of solid foreign objects, from tools or fingers that could be hazardous if they came into contact with electrical conductors or moving parts, to airborne dirt and dust that could damage circuitry. The second digit defines the protection of the equipment inside the enclosure against various forms of moisture (drips, sprays, submersion etc) [2].

First Digit	Intrusion Protection
0	No protection.
1	Protected against solid objects over 50mm, e.g. accidental touch by hands.
2	Protected against solid objects over 12mm, e.g. fingers.
3	Protected against solid objects over 2.5mm, e.g. tools & wires.
4	Protected against solid objects over 1mm, e.g. wires & nails.
5	Protected against dust limited ingress, no harmful deposits.
6	Totally protected against dust.

Second Digit	Moisture Protection
0	No protection.
1	Protected against vertically falling drops of water, e.g. condensation.
2	Protected against direct sprays of water up to 15 degrees from the vertical.
3	Protected against direct sprays of water up to 60 degrees from the vertical.
4	Protected against water splashed from all directions, limited ingress permitted.
5	Protected against low pressure jets of water from all directions, limited ingress permitted.
6	Protected against strong jets of water, e.g. on ships deck, limited ingress permitted.

Table 1.1 Description of the Ingress Protection nomenclature

As already stated, the first movement is done by meaning of toothed gear and a belt, with the ladder directly hinged with the movable part of the passerella. When the toothed gear is put in rotation, the belt is moved and the passerella can slide forward or backward, depending on the sense of rotation of the gear. The solution proposed in this dissertation is to substitute the current hydraulic motor with an electric motor coupled with an orthogonal gear train for space optimization. Moreover, a solution with a coaxial gear train will be proposed in order to demonstrate the effectiveness of the orthogonal solution.

1.1 Requirements

The starting data are directly taken from sensors connected to the hydraulic motor, so they can be considered as real values. The following is the table which summarize them:

TORQUE [Nm]	ω [rpm]	TIME IN/OUT [s]	POWER [W]	VOLTAGE [V]	INGRESS PROTECTION
13	50 - 100	7 - 15	68 - 136	12 - 24	> IP 54

Table 1.2 First movement requirements

The first requirement is about the **torque** that is needed to put in rotation the toothed gear, which depends not only on the weight of the exiting gangway, but also on the friction between the passerella itself and the box outside of it.

The second requirement is about the **angular velocity of the toothed gear**, or better on the **time needed to complete the movement**. The hydraulic solution shows an exit time of about 7 seconds, with an angular velocity of the gear of 100 rpm. However, an acceptable range is between 7 and 15 seconds for the exiting time, leading to a range from 50 to 100 rpm for the toothed gear angular velocity.

In this way, it is possible to compute the **required power** of the motor just by multiplying the torque with the angular velocity. It is clear that also in this case we will have a range of acceptable values since the angular velocity has a range a of values to. We have to take

into account also the efficiency of the gear train, which lead to an increase in the required power. However, a more detailed analysis about this efficiency will be made later in the specific part about the selection of the gear train. As a first approximation, it is possible to state that the required torque is in a range between 68 and 136 W.

Another requirement is set by the **type of current** which feed the electric motor and the **nominal voltage** which is applied. Since this application is studied for yacht and superyacht, usually they can directly provide a direct current exiting from the batteries which are mounted on the boat. Moreover, the state of charge of the batteries is not always the same, so we also have to consider the possibility of a lower voltage as input to the motor, leading to a reduction in the output power of course. This could be avoided by selecting a suitable motor and a suitable driver, creating in this way a mechanism almost independent from the input voltage. The nominal voltage of the batteries usually mounted on boats are 12 V and 24 V. Considering the second one, the possible range of values are between 8 V, which means that the batteries is almost fully discharged, and 32 V, which means that the battery is over charged for some reasons.

Finally, last requirement is about the **class protection** of both the motor and the gear train: its position requires a level of protection greater than IP 54, which means "protected against dust limited ingress, no harmful deposits" and "protected against water splashed from all directions, limited ingress permitted" [2].

1.2 Motor selection

In this paragraph, this preliminary analysis has the goal to select one or more suitable motor solutions, in order to understand the feasibility of the movement with the adoption of one or another type of motor and, moreover, the market availability of the solutions. Obviously, this could not result as the final selection, since during the evolution of the project some other issues could came out and they could be solved by changing even the type of motor; that is why it is better to propose different solutions during this phase.

1.2.1 Motor Architecture

The three most common solution among the DC motor are the **Brushed Direct Current motor**, the **Brushless DC Motor** and the **Stepper motor**. The first solution is the simplest one: the electrical current passes through coils (**rotor**) that are arranged within a fixed magnetic field (**stator**), generating in turn magnetic fields on the coils. In this way, each coil is pushed away from the like pole and pulled toward the unlike pole of the fixed magnetic field. In order to maintain the rotation, it is necessary to reverse continuously the current, so that the coils will continuously chase the unlike fixed pole. The reversal of the current is done using a **rotating commutator**, in contact with fixed conductive brushes that supply the current to the coils [3].

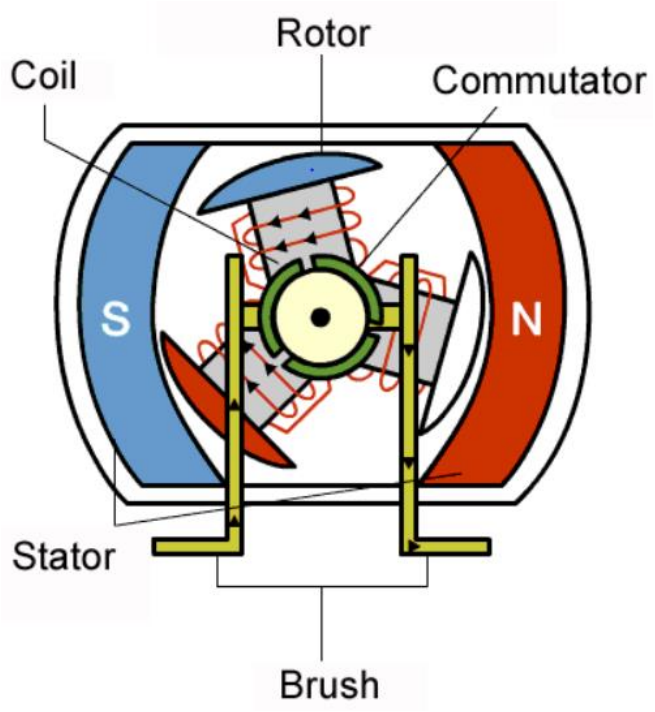

Figure 1.1 Schematic functioning of a Brushed DC motor

The second solution could be seen as evolution of the first one: as the name suggests, the basic difference is the **absence of the brushes**, since the coils are now fixed in place on the stator, while the rotor is a permanent magnet. The rotation of the permanent magnet

is achieved by changing the direction of the magnetic fields generated by the coils, without the need of brushes [3].

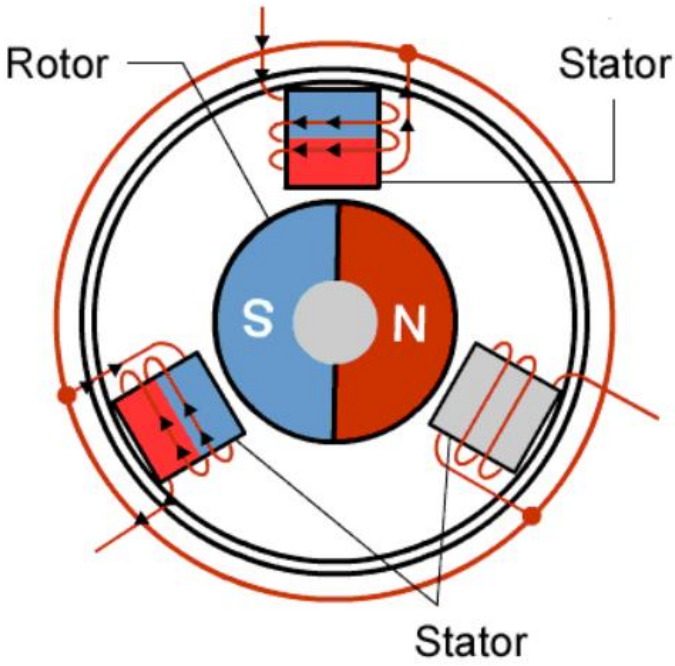

Figure 1.2 Schematic functioning of a Brushless DC motor

The last solution is the Stepper motor, which is a synchronous brushless motor with a **segmented magnetized rotor**. When the coils placed on the stator are energized, they create north and south polls which push or pull the magnetized rotor, putting it in rotation of one step. The fine teeth are evenly spaced around the entire diameter, providing the incremental angular rotation [4].

1.2.2 Input voltage

One important factor that influences the motor selection is the **input voltage**: keeping in mind the previous considerations about the voltage range, it is possible to choose between two situations: the first one is represented by the brushed motor, where the motor is

directly connected with the source without the need of a driver between them; in this way, however, the output torque is strictly dependent on the input voltage, and in the case of a situation in which the batteries can supply a lower voltage, the output torque will be consequently lower than the nominal value and the gangway will struggle to exit. The other situation instead can be found with the brushless and the stepper motor, since they both need a driver placed between the source and them. In this way, the motor will be more independent from the source voltage, since its input voltage will be the one exiting from the driver. Moreover, there is the possibility to increase the operating voltage, using also values well above the 24 V of the batteries.

1.2.3 Others

Other factors that can influence the selection of the motor are the **control strategy** and the possibility to have a **brake on the output shaft of the motor**, which will increase the level of security, since the motor cannot rotate in the opposite direction unless it is operated in that way, preventing the passerella from reentering inside the box when it is not requested. However, there are also other solution that can guarantee the irreversibility of the movement without the need of a brake output. Regarding the **control strategy** instead, there could be some situation in which, depending on the architecture of the motor, the resulting strategy can be very complex, leading to an inconvenient solution. Last, but not least, we always have to keep in mind the required **ingress protection**, typical of every motor: in the case in which the motor does not reach the ingress protection goal, it is possible to encapsulate it in a box, still being careful to other consequences like the resonance effects and so on.

1.3 Gear train selection

The second analysis during this phase is about the gear train that will be coupled with the electric motor: it is a very important analysis, since by introducing this element we

introduce other degrees of freedom in the final solution, with all the subsequent considerations. It is clear that each component that will be added to the final solution presents its own reliability factor, that should be carefully taken into account during the project phase to find all the possible weak points of the assembly. On the other hand, the introduction of a gear train will lead to an increase among the possible motor solutions, just by changing the reduction ratio. Finally, as before, the solutions that will be presented could not be the final solutions, but only an overview of the possible ones.

1.3.1 Gear Train architecture

The currently available gear train architectures are several: the choice is not easy, since different architecture shows different strengths and weaknesses, strongly dependent from the mechanical principle on which they are based. Among the most common solutions there are certainly the **Planetary Gearbox**, the **Bevel Gearbox** and the **Worm Gearbox**; another emerging solution is the **Harmonic Gearbox**, which is an evolution of the Planetary one. In this dissertation the focus will be on the first two gearboxes, since they will be proposed as a solution in our project.

Starting with the **Planetary Gearbox**, it is made of three fundamental components: the central pinion, or "**sun gear**", which is the input gear, three or more "**planet gears**", which rotate outside the central gear, and the fixed outer ring, directly in contact with the outside of all the planet gears. In this way, when the sun gear is put in rotation, also the planet gears start to rotate, but with a slower angular speed, depending on the reduction ratio. The typical configuration is the **coaxial** one, which means that the input and the output shaft are aligned, but there are also configurations where the two shafts are perpendicular to each other, the so-called **orthogonal** configuration, especially used to better occupy the available space; however, the efficiency of this configuration is usually lower with respect to the coaxial one [5].

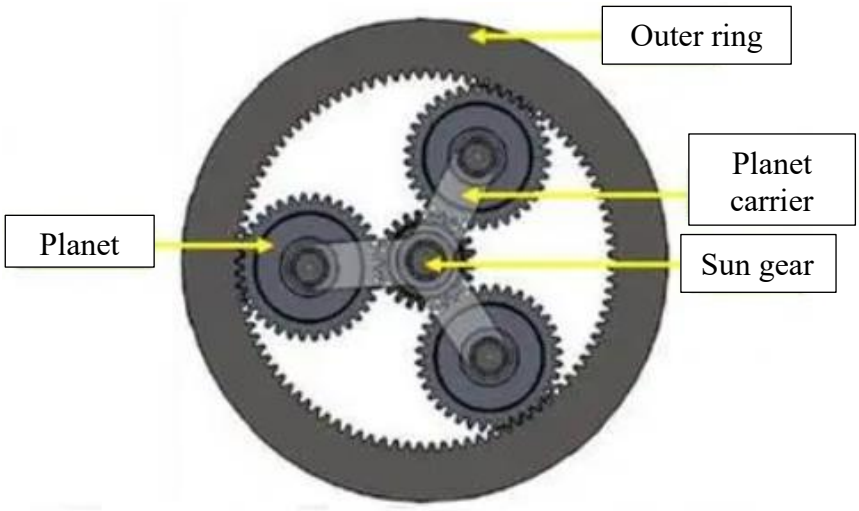

Figure 1.3 Planetary gearbox architecture

The second presented architecture is the **Bevel Gearbox**, where the reduction is done by means of **conic toothed gears**; the angle between the axis of rotation of the two gears is usually 90°, but there is also the possibility of having different angles, while the teeth of the gears can be straight or curved. They are adopted whenever an orthogonal solution is request, since the shows an higher efficiency compared to the Planetary ones in this configuration, while in the coaxial configuration there is the opposite situation. Finally, they can provide reduction ratio lower than Worm Gearbox, and that is why they are often used just to change the direction of the output shaft [6].

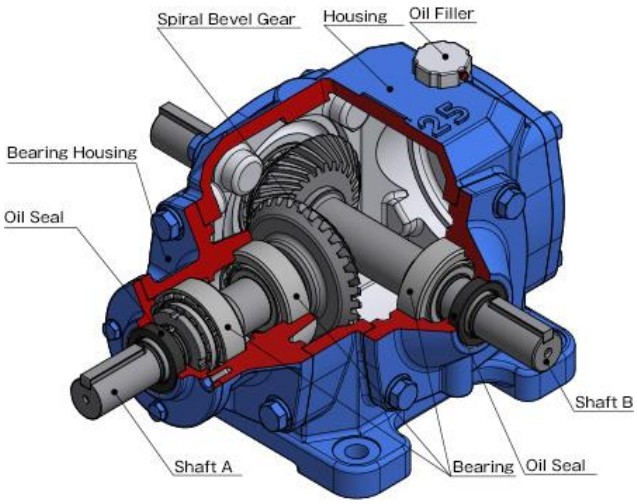

Figure 1.4 Bevel gearbox architecture

1.3.2 Torque and RPM

In this phase, the data about the **torque required** to move the gangway and the **speed of exiting**, directly related to the angular velocity of the output shaft of the gear train are known, so it is possible to start from there. Regarding the required torque, all the gear train show a maximum deliverable output torque, sometimes subdivided in repeatable and momentary. To select the right component, just be sure to remain underneath the repeatable one during standard operation. For what concerns the angular velocity, instead, the limitations are applied on the input shaft, where there is a maximum and an average input shaft velocity. The minimum one is not always specified, but it is better to work always around the average input shaft velocity.

1.3.3 Axial / radial load

Another relevant factor for this analysis is the **axial** and the **radial load** that the gear train can sustain, which is strictly related to the overall dimensions of the component. In this project, the available space is quite limited, which means that each component of the mechanism is designed to occupy the lowest possible space. However, small gear train means low value of both radial and axial sustainable load, but this is not a huge problem: in fact, there are many ways to deal with these kinds of issues, like a washer placed between the output of the gear train and the input of the attached mechanism in order to directly transfer the load on the gear train's case instead of its internal mechanism.

1.3.4 Efficiency

Another important parameter to take into account while choosing the right gear train is its **efficiency**, which means its ability to transfer torque and angular velocity from the input shaft to the output one. Since we are considering gear train's architecture made of toothed gears, the efficiency refers just to the transmittable torque, since a reduction in velocity while passing from a toothed to another placed directly in contact is impossible. For this reason, this specific efficiency has to be considered only while calculating the

output shaft's torque. Moreover, orthogonal gear trains show an efficiency lower the coaxial ones, sometimes with a great difference too.

1.3.5 Ingress protection

Finally, as before, also the gear train has its own **ingress protection**, which should be greater or at least equal to that one of the motor: in the case in which this is not possible, the solutions for this problem are the same presented for the motor, with the subsequent consideration regarding the possible resonance effect or the increasing of the overall dimensions.

1.4 Proposed solutions

Figure 1.5 BG 65x75 Dmove motor

In this section there will be reported a couple of solutions for this first movement; solutions are represented by a coupling of motor with a specific gear train in order to reach the goal in terms of torque and angular velocity. At the end of this section there will be a table which summarizes the presented solutions, very useful to compare them. The first solution is represented by the **BG 65x75 Dmove motor**, sold by the **Dunkermotoren** company, coupled with the **CP 005 MF** gear train sold by the **Wittestein** company. The motor is a Brushless DC, with a nominal output power of 187 W. The nominal output angular velocity is 3650 rpm with a nominal torque of 0,49 Nm. It is clear that since the motor is a brushless DC, by decreasing the angular speed the delivered torque will increase, up to a maximum value of 1,57 Nm. The nominal voltage, instead, is 24 V, but also in this case there is a range of functioning with different combination of torque and angular speed. However, with the introduction of an input driver, this problem will be strongly reduced, and the voltage delivered to the motor will be always around the nominal value. The protection class of the motor is IP65, which is

enough considering the location of the motor. The following table and torque/speed plot are taken from the Dunkermotoren catalogue, as well as the CAD drawings [7].

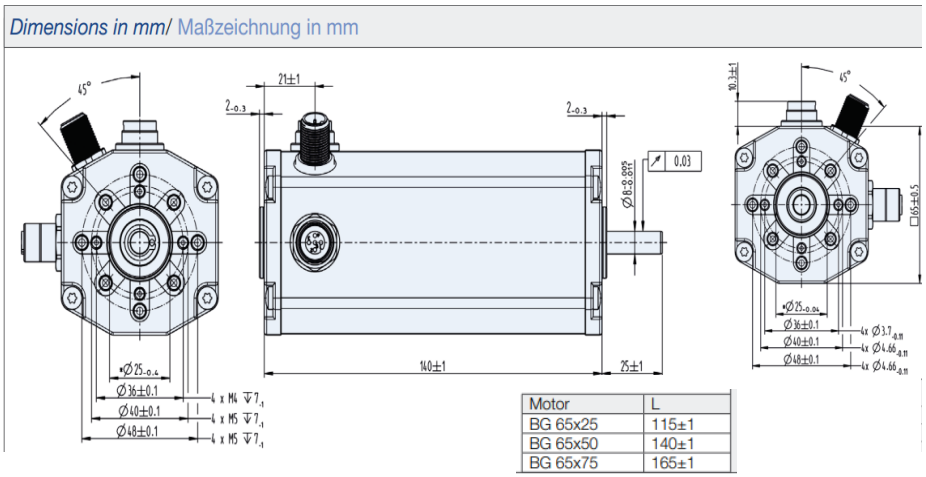

Figure 1.6 CAD drawings of the BG 65x75 motor

Data/ Technische Daten		BG 65x75 dMove	
Nominal voltage/ Nennspannung	VDC	24	48
Nominal current/ Nennstrom	A[1]	10	5
Nominal torque/ Nennmoment	Nm[1]	0.49	0.55
Nominal speed/ Nenndrehzahl	rpm[1]	3650	3390
Maximum torque/ Maximales Moment	Nm[1]	1.57	1.78
No load speed/ Leerlaufdrehzahl	rpm[1]	6250	5870
Nominal output power/ Dauerabgabeleistung	W[1]	187	195
Maximum output power/ Maximale Abgabeleistung	W	367	391
Torque constant/ Drehmomentkonstante	Nm A^{-1}[1]	0.066	0.147
Peak current consumption/ Zulässiger Spitzenstrom Aufnahme	A[1]	23.4	12.1
Peak current phase current/ Zulässiger Spitzenstrom Phasenstrom	mA	40000	21135
Voltage range/ Zulässiger Spannungsbereich	VDC	2...58	2...58
Rotor inertia/ Rotor Trägheitsmoment	gcm²	172	172
Weight of motor/ Motorgewicht	kg	2	2

Table 1.3 Summary of the main motor characteristics

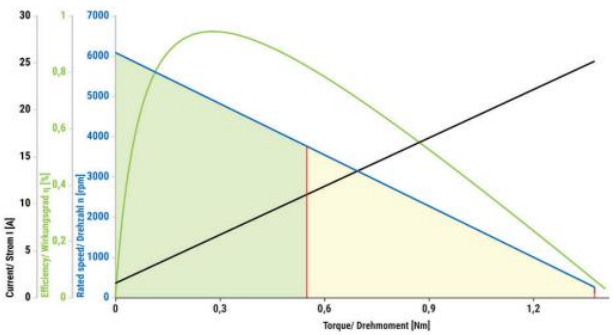

Plot 1.1 Torque Vs Speed plot of the selected motor configuration

For what concerns the selected gear train, it is a planetary gearbox with a reduction ratio of 35: in this way, the output torque will be around 16 Nm while the angular speed will be around 100 rpm. The analyzed configurations are two: the first one with coaxial motor and gear train shafts, the second with orthogonal axis instead. The former shows a greater efficiency with respect to the ladder, but it also has greater overall dimensions since the two components must be aligned; with the orthogonal axis, instead, the available space is better occupied, and the overall dimensions are reduced. The protection class is IP64 for both solutions, which is again enough consideration the location of the component. As before, the following are the table of the characteristics of the two configurations, also with the CAD drawings directly taken form the Wittestein catalogue [8].

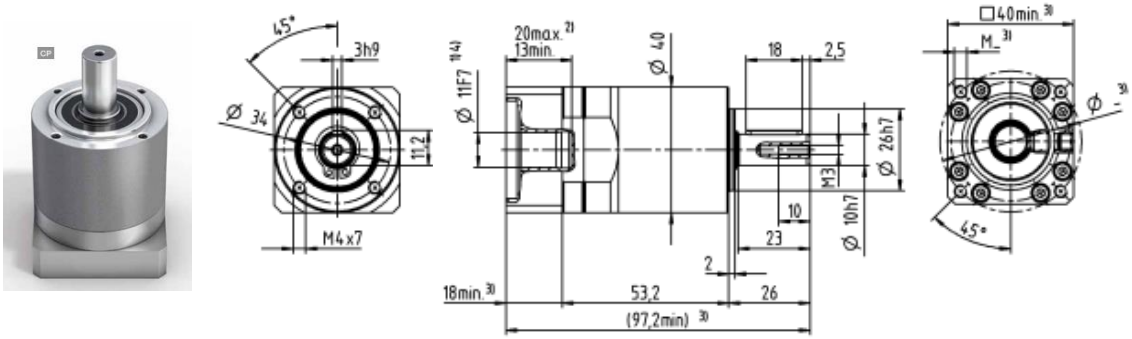

Figure 1.7 CAD drawing of the CP 005 MF gear train

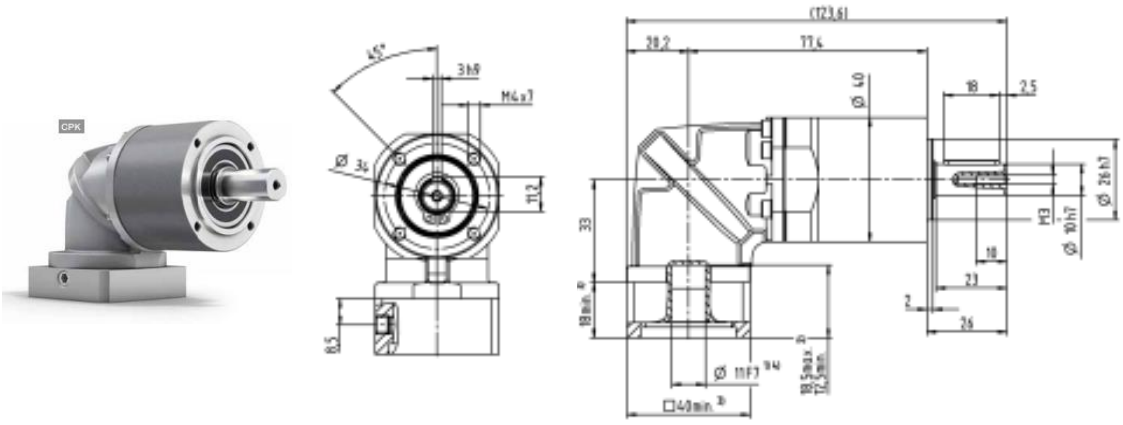

Figure 1.8 CAD drawing of the CPK 005 MF gear train

Rapporto di riduzione	**i**		**35**
Coppia max. [4] [5] [6]	T_{2a}	*Nm*	21
Coppia di accelerazione max. [4] (max. 1000 cicli per ora)	T_{2B}	*Nm*	14
Coppia di emergenza [4] [5] [6] (fino a 1000 volte durante la vita del riduttore)	T_{2Not}	*Nm*	26
Velocità nominale media in ingresso [4] (a T_{2a} e temperatura ambiente di 20°C)	n_{1N}	*rpm*	4300
Velocità max. in ingresso	n_{1Max}	*rpm*	9000
Coppia senza carico media [5] (a n_1 = 3000 rpm e temp. misurata sul riduttore di 20°C)	T_{012}	*Nm*	0,07
Rigidezza torsionale [5]	C_{12}	*Nm/arcmin*	0,58

Forza assiale max. [4]	F_{2AMax}	*N*	240
Forza radiale max. [4] [1]	F_{2CMax}	*N*	170
Coppia di ribaltamento max.	M_{2KMax}	*Nm*	4
Rendimento a pieno carico	η	%	95
Peso (inclusa flangia di adattamento standard)	*m*	*kg*	0,7
Rumorosità (per *i* e n_1 di riferimento consultare cymex®)	L_{PA}	*dB(A)*	≤ 59
Temperatura max. ammissibile sulla carcassa		°C	+90
Temperatura ambiente		°C	da –15 a +40
Lubrificazione			a vita
Senso di rotazione			concorde tra ingresso e uscita
Grado di protezione			IP 64

Table 1.4 General characteristics of the CP 005 MF gear train

Rapporto di riduzione	**i**		**35**
Coppia max. [4] [5] [6]	T_{2a}	*Nm*	21
Coppia di accelerazione max. [4] (max. 1000 cicli per ora)	T_{2B}	*Nm*	14
Coppia di emergenza [4] [5] [6] (fino a 1000 volte durante la vita del riduttore)	T_{2Not}	*Nm*	26
Velocità nominale media in ingresso [4] (a T_{2a} e temperatura ambiente di 20°C)	n_{1N}	*rpm*	3800
Velocità max. in ingresso	n_{1Max}	*rpm*	5000
Coppia senza carico media [5] (a n_1 = 3000 rpm e temp. misurata sul riduttore di 20°C)	T_{012}	*Nm*	0,27
Rigidezza torsionale [5]	C_{12}	*Nm/arcmin*	0,57

Forza assiale max. [4]	F_{2AMax}	*N*	240
Forza radiale max. [4] [1]	F_{2CMax}	*N*	170
Coppia di ribaltamento max.	M_{2KMax}	*Nm*	4
Rendimento a pieno carico	η	%	94
Peso (inclusa flangia di adattamento standard)	*m*	*kg*	0,92
Rumorosità (per *i* e n_1 di riferimento consultare cymex®)	L_{PA}	*dB(A)*	≤ 68
Temperatura max. ammissibile sulla carcassa		°C	+90
Temperatura ambiente		°C	da 0 a +40
Lubrificazione			a vita
Senso di rotazione			concorde tra ingresso e uscita
Grado di protezione			IP 64

Table 1.5 General characteristics of the CPK 005 MF gear train

1.4.1 Components design

This part of the dissertation will be dedicated in showing the preliminary design of the selected components.

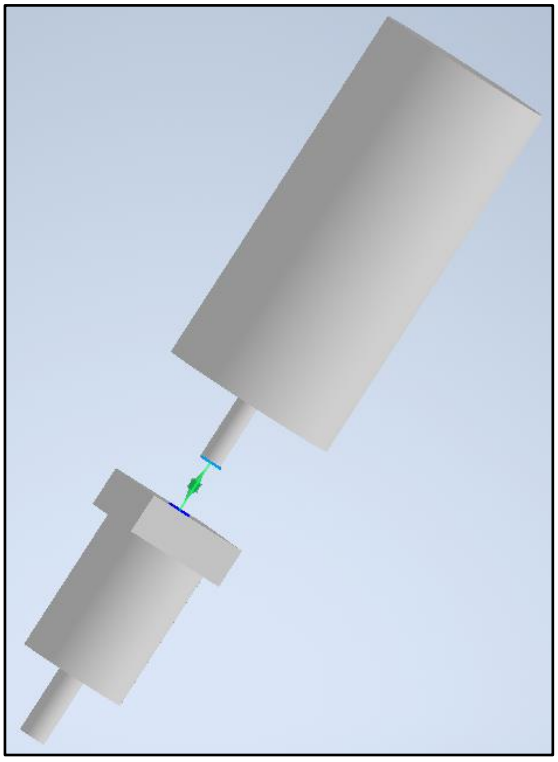

Figure 1.9 Preliminary design of the coupling between the BG 65x75 motor and the CP 005 MF gear train

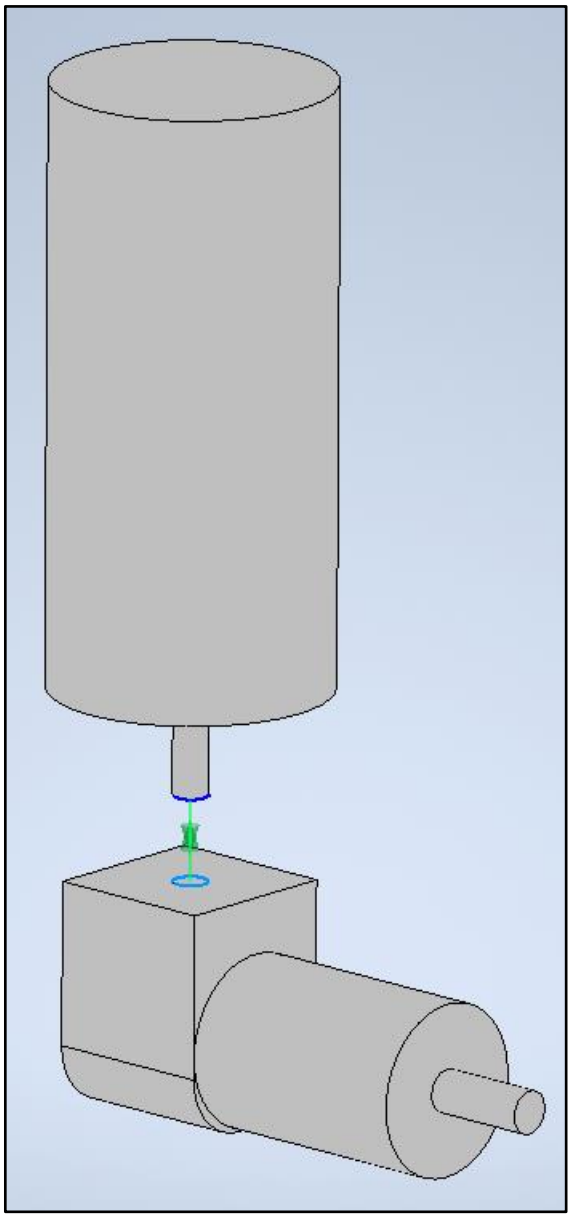

Figure 1.10 Preliminary design of the coupling between the BG 65x75 motor and the CPK 005 MF gear train

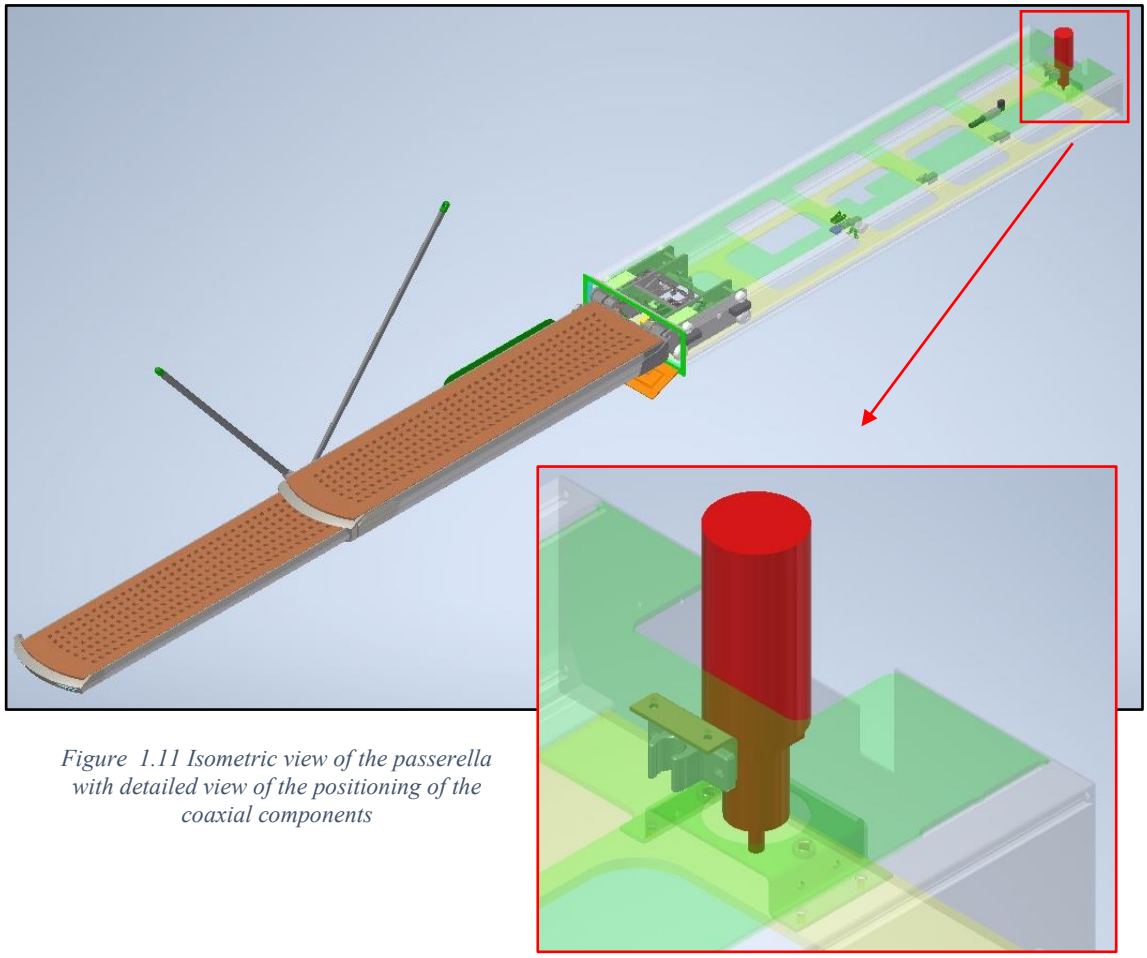

Figure 1.11 Isometric view of the passerella with detailed view of the positioning of the coaxial components

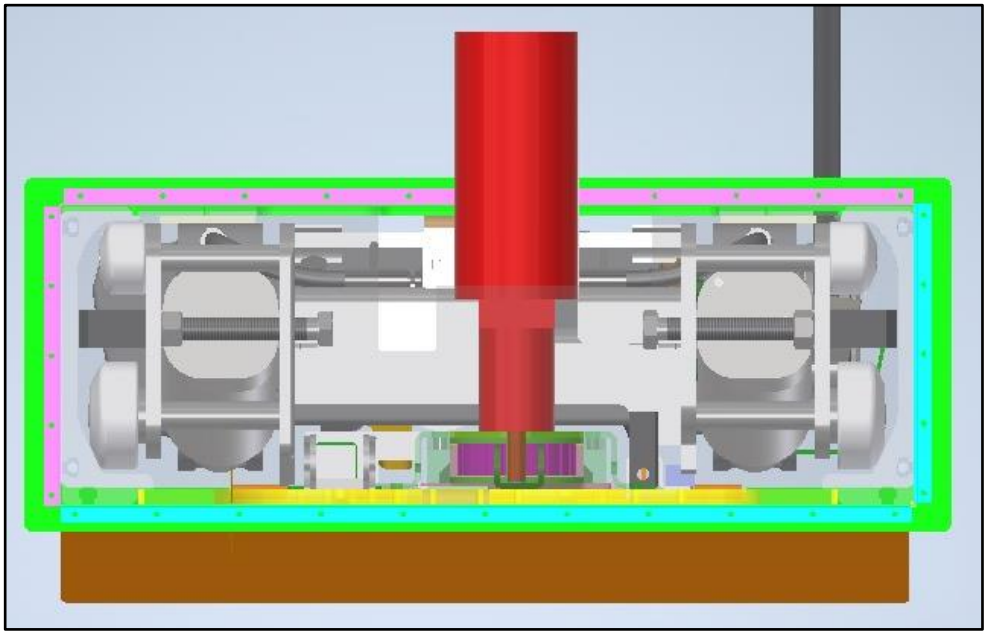

Figure 1.12 Back view of the gangway with highlighted coaxial components

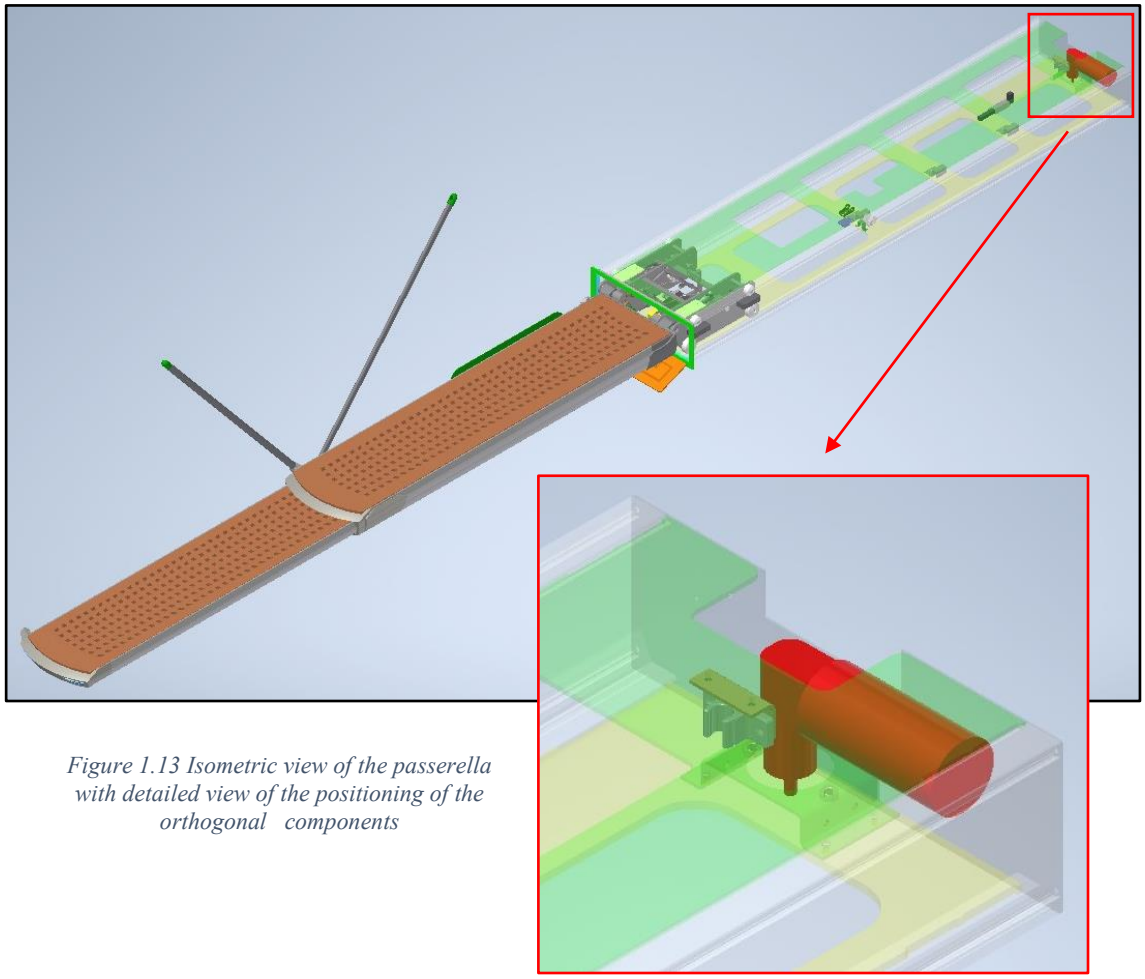

Figure 1.13 Isometric view of the passerella with detailed view of the positioning of the orthogonal components

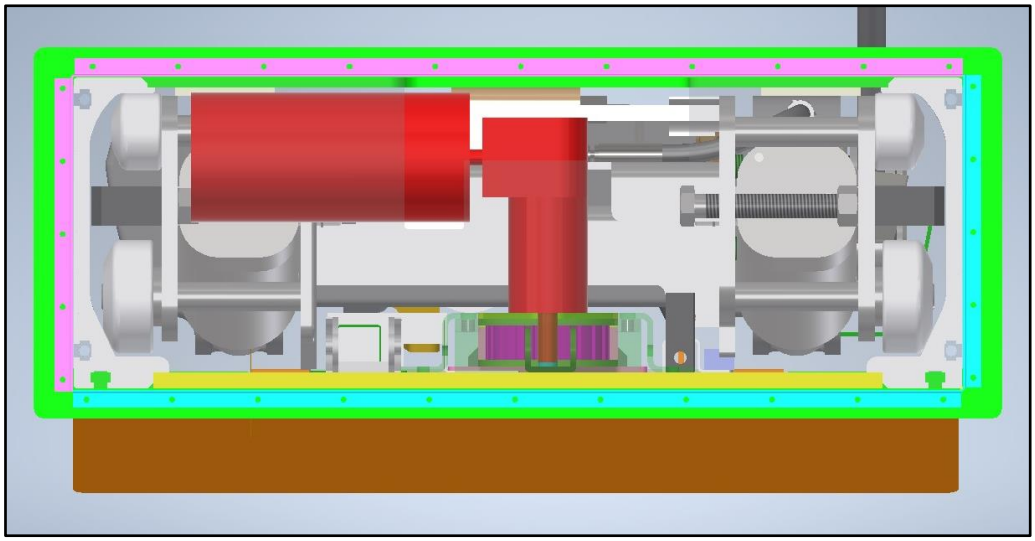

Figure 1.14 Back view of the gangway with highlighted orthogonal components

2. Second movement analysis

The second movement performed by the gangway is the so-called **telescopic movement**, in which the passerella elongates itself to reach furthest distances. In the hydraulic project, this is done by meaning of an hydraulic piston placed under the whole passerella: the pushing rod of the piston pushes the very end of the lower half of the gangway during the opening movement, while during the closing movement, it pull the same end in place, before re-entering inside the box. In this project, the piston is replaced with a **moto-reductor** connected to a **nut and screw**: since the passerella is directly connected with the nut, when the screw is put in rotation by the motor, the nut moves forward or backward along the screw, depending on the direction of rotation of the ladder. The whole mechanism will be placed in the same place of the older hydraulic piston, so the available space is limited both on the direction of the length and of the height.

The following is the table which report the starting data taken directly on the hydraulic piston. In particular, the length of the movement is taken from the CAD of the previous project, the time is taken using a chronometer while the force required to move the part is taken using a manometer directly attached to the input and output of the hydraulic piston.

STROKE [mm]	MOVEMENT TIME [s]	EXIT VELOCITY [mm/s]	FORCE [N]
1200	15	80	3000

Table 2.1 Preliminary requirements for the actuation of the telescopic movement

2.1 Screw dimensioning

Starting from this data, the first aspect that has to be defined is the type of screw which can satisfy the project requirements. The two most common alternatives in this type of situations are the **recirculating ball screw** and the **trapezoidal screw**. Looking at the

requirements, one of them is a sustainable axial force of 3000 N, even if the gangway is inclined towards the sky, and it is a very complex situation to control while using a recirculating ball screw. In fact, using this type of screw, the **irreversibility** of the movement is not always guaranteed, and the nut could come back with load values lower than the calculated ones. Moreover, their **sustainable axial load** is usually lower than the trapezoidal one with equal dimeter, and it's not possible apply neither radial force nor bending moment. Last but not least, they need a constant lubrication to correctly operate, otherwise the efficiency of the mechanism could be reduced by as much as 90%. For these reasons, the selected type for the screw is the trapezoidal one, which can sustain very good axial and radial load, guarantees good irreversibility of the movement, depending on the thread angle of the screw, and does not necessarily need the lubrication, depending on the material of the screw.

2.1.1 Material

Once the type of the screw has been chosen, the second parameter considered is the material: since the ambient of application of the component is very corrosive, the material of the screw has to be carefully selected in order to avoid possible sedimentations coming for the marine water on the thread of the screw, which can cause difficulties in the movement of the nut or even the failure of the nut itself. In general, one of the best materials in terms of structural and corrosive performances is the **AISI 316**, which is an austenitic steel with a typical chemical composition of 0.04 % of Carbon, 17.2 % of Chromium, 10.1 % of Nickel and 2.1 % of Molybdenum, while the maximum values are 0.07 % of Carbon, 2.0 % of Manganese, 1.0 % of Silica, 18.5 % of Chromium, 13 % of Nickel, 0.04 % of Phosphorus, and 2.25 % of Molybdenum. Austenitic, instead, means that the steel must have less than 18 % of Chromium, less than 8-9 % of Nickel and other noble element like Titanium or Molybdenum. There is also another type of steel used in this kind of application, which is a kind of evolution of the 316, the so called **316L**, in which the main difference is the reduction is the acceptable amount of Carbon, which is less than 0.03 % this time. For this calculation, will be adopted the AISI 316 since it has a greater availability on the market and not so strong drawback compared to the 316L [9].

Once the material has been selected, it is possible to start taking the general dimensions of the screw from the catalogue: again, for this calculation, the catalogue of the well-known company "CONTI" will be adopted [10]. The following table summarize these data:

CONTI®

Viti trapezie tipo KAM – materiale INOX A4 - AISI 316

Codice per vite **DESTRA**	Codice per vite **SINISTRA**	**Diametro per passo**	n° principi	Classe di precisione µm/300 mm	Rettilineità mm / mm	Peso kg/mt
□ KAM 10 J R …	□ KAM 10 J L …	**Tr 10x4 (P2)**	2	200	0,7 / 1000	0,48
□ KAM 12 B R …	□ KAM 12 B L …	**Tr 12x6 (P3)**	2	200	0,7 / 1000	0,65
□ KAM 14 B R …	□ KAM 14 B L …	**Tr 14x6 (P3)**	2	200	0,7 / 1000	0,93
□ KAM 16 B R …	□ KAM 16 B L …	**Tr 16x8 (P4)**	2	200	0,7 / 1500	1,17
□ KAM 18 B R …	□ KAM 18 B L …	**Tr 18x8 (P4)**	2	200	0,7 / 1500	1,53
■ KAM 20 B R …	□ KAM 20 B L …	**Tr 20x8 (P4)**	2	200	0,6 / 2000	1,94
□ KAM 20 E R …	□ KAM 20 E L …	**Tr 20x20 (P4)**	5	200	0,6 / 2000	1,94
□ KAM 20 D R …	□ KAM 20 D L …	**Tr 20x20 (P5)**	4	200	0,6 / 2000	1,84
□ KAM 22 B R …	□ KAM 22 B L …	**Tr 22x10 (P5)**	2	200	0,6 / 2000	2,29
□ KAM 24 B R …	□ KAM 24 B L …	**Tr 24x10 (P5)**	2	200	0,4 / 2000	2,78
□ KAM 25 B R …	□ KAM 25 B L …	**Tr 25x10 (P5)**	2	200	0,4 / 2000	3,05
□ KAM 26 B R …	□ KAM 26 B L …	**Tr 26x10 (P5)**	2	200	0,4 / 2000	3,33
□ KAM 28 B R …	□ KAM 28 B L …	**Tr 28x10 (P5)**	2	200	0,4 / 2000	3,92
□ KAM 30 B R …	□ KAM 30 B L …	**Tr 30x12 (P6)**	2	200	0,4 / 3000	4,38
□ KAM 32 B R …	□ KAM 32 B L …	**Tr 32x12 (P6)**	2	200	0,4 / 3000	5,06
□ KAM 36 B R …	□ KAM 36 B L …	**Tr 36x12 (P6)**	2	200	0,3 / 3000	6,56
□ KAM 40 B R …	□ KAM 40 B L …	**Tr 40x14 (P7)**	2	200	0,3 / 3000	8,03

Viti trapezie tipo KAM – materiale INOX A4 - AISI 316

Codice per vite **DESTRA**	Codice per vite **SINISTRA**	**Diametro per passo**	n° principi	Classe di precisione µm/300 mm	Rettilineità mm / mm	Peso kg/mt
□ KAM 08 A R …	□ KAM 08 A L …	**Tr 8x1,5**	1	200	0,9 / 1000	0,30
■ KAM 10 T R …	■ KAM 10 T L …	**Tr 10x2**	1	200	0,7 / 1000	0,48
■ KAM 10 A R …	■ KAM 10 A L …	**Tr 10x3**	1	200	0,7 / 1000	0,42
■ KAM 12 A R …	■ KAM 12 A L …	**Tr 12x3**	1	200	0,7 / 1000	0,65
■ KAM 14 R R …	□ KAM 14 R L …	**Tr 14x3**	1	200	0,7 / 1000	0,93
□ KAM 14 A R …	□ KAM 14 A L …	**Tr 14x4**	1	200	0,7 / 1000	0,86
■ KAM 16 A R …	■ KAM 16 A L …	**Tr 16x4**	1	200	0,7 / 1500	1,17
■ KAM 18 A R …	□ KAM 18 A L …	**Tr 18x4**	1	200	0,7 / 1500	1,53
■ KAM 20 A R …	■ KAM 20 A L …	**Tr 20x4**	1	200	0,6 / 2000	1,94
■ KAM 22 A R …	□ KAM 22 A L …	**Tr 22x5**	1	200	0,6 / 2000	2,29
■ KAM 24 A R …	■ KAM 24 A L …	**Tr 24x5**	1	200	0,4 / 2000	2,78
□ KAM 25 A R …	□ KAM 25 A L …	**Tr 25x5**	1	200	0,4 / 2000	3,05
■ KAM 26 A R …	□ KAM 26 A L …	**Tr 26x5**	1	200	0,4 / 2000	3,33
■ KAM 28 A R …	□ KAM 28 A L …	**Tr 28x5**	1	200	0,4 / 2000	3,92
□ KAM 30 P R …	□ KAM 30 P L …	**Tr 30x5**	1	200	0,4 / 3000	4,57
■ KAM 30 A R …	■ KAM 30 A L …	**Tr 30x6**	1	200	0,4 / 3000	4,38
■ KAM 32 A R …	■ KAM 32 A L …	**Tr 32x6**	1	200	0,4 / 3000	5,06
□ KAM 35 P R …	□ KAM 35 P L …	**Tr 35x5**	1	200	0,3 / 3000	6,40
□ KAM 35 A R …	□ KAM 35 A L …	**Tr 35x6**	1	200	0,3 / 3000	6,16
■ KAM 36 A R …	■ KAM 36 A L …	**Tr 36x6**	1	200	0,3 / 3000	6,56
□ KAM 40 P R …	□ KAM 40 P L …	**Tr 40x5**	1	200	0,3 / 3000	8,51
□ KAM 40 O R …	□ KAM 40 O L …	**Tr 40x6**	1	200	0,3 / 3000	8,26
■ KAM 40 A R …	■ KAM 40 A L …	**Tr 40x7**	1	200	0,3 / 3000	8,03
■ KAM 44 A R …	■ KAM 44 A L …	**Tr 44x7**	1	200	0,3 / 3000	9,90
□ KAM 50 P R …	□ KAM 50 P L …	**Tr 50x5**	1	200	0,3 / 3000	13,70
□ KAM 50 O R …	□ KAM 50 O L …	**Tr 50x6**	1	200	0,3 / 3000	13,35
■ KAM 50 A R …	■ KAM 50 A L …	**Tr 50x8**	1	200	0,3 / 3000	12,90
□ KAM 55 A R …	□ KAM 55 A L …	**Tr 55x9**	1	200	0,3 / 3000	15,51
□ KAM 60 O R …	□ KAM 60 O L …	**Tr 60x6**	1	200	0,3 / 3000	19,67
□ KAM 60 N R …	□ KAM 60 N L …	**Tr 60x7**	1	200	0,3 / 3000	19,36
■ KAM 60 A R …	■ KAM 60 A L …	**Tr 60x9**	1	200	0,3 / 3000	18,74
■ KAM 70 A R …	■ KAM 70 A L …	**Tr 70x10**	1	200	0,3 / 3000	25,80
■ KAM 80 A R …	■ KAM 80 A L …	**Tr 80x10**	1	200	0,3 / 3000	34,39
□ KAM 90 A R …	□ KAM 90 A L …	**Tr 90x12**	1	200	0,5 / 3000	43,07
□ KAM A0 A R …	□ KAM A0 AL …	**Tr 100x12**	1	200	0,5 / 3000	53,99

Figure 2.1 General characteristics of the available screws from the Conti's catalogue

As it is clear from these tables, there are a lot of possible configurations regarding the dimensions of the screw. The following considerations will be done on almost all the configurations, in order to find the smallest possible diameter which satisfies the requirements but also possible improvements like increasing the pitch.

	SCREW	PITCH	MEAN DIAMETER [mm]	THREAD ANGLE [°]	THREAD ANGLE [rad]	ANGLE OF FRICTION [°]	ANGLE OF FRICTION [rad]	RADIAL VELOCITY [mm/s]	ω [rpm]
1 PRINCIPLE	KAM 16 T R	4	13,75	5,12	0,09	11,20	0,20	892,86	1239,77
	KAM 20 T R	4	17,77	4,03	0,07	11,20	0,20	1135,51	1220,23
	KAM 25 T R	5	22,24	4,03	0,07	11,20	0,20	1135,51	974,94
	KAM 28 T R	5	25,24	3,34	0,06	11,20	0,20	1370,80	1037,09
	KAM 30 T R	6	26,71	4,03	0,07	11,20	0,20	1135,51	811,79
	KAM 40 T R	7	36,20	3,30	0,06	11,20	0,20	1387,45	732,05
2 PRINCIPLES	KAM 16 T R	8	13,75	10,19	0,18	11,20	0,20	445,07	617,99
	KAM 20 T R	8	17,77	8,03	0,14	11,20	0,20	567,07	609,39
	KAM 25 T R	10	22,24	8,03	0,14	11,20	0,20	567,07	486,89
	KAM 28 T R	10	25,24	7,07	0,12	11,20	0,20	645,03	488,01

Table 2.2 General data and first calculations on the selected screws

2.1.2 Radial and angular velocity

In order to have an approximate calculation of the **angular velocity of the screw**, it is possible to start calculating the liner velocity of the nut while opening the gangway. Considering that the length of the stroke is $\boldsymbol{l}$**=1200 mm** and the time of exiting is $\boldsymbol{t}$**=15 s**, the linear velocity $\boldsymbol{v}$ of the nut is:

$$v = \frac{l}{t} = \frac{1200}{15} = 80\frac{mm}{s} \tag{2.1}$$

Now, the linear velocity of the screw can be considered equal to the tangential velocity of the screw and, since it is an approximative calculation, it can be used to obtain the radial velocity of the screw $\boldsymbol{v}'$ considering:

$$v = v' \tan\alpha \tag{2.2}$$

which means

$$v' = \frac{v}{\tan\alpha} \tag{2.3}$$

Remembering that

$$\omega' = \frac{v'}{r} \tag{2.4}$$

it is possible to directly convert this velocity from *mm/s* to *rpm* considering:

$$\omega = \omega' \cdot \frac{30}{\pi} \tag{2.5}$$

2.1.3 Efficiency

The term efficiency means the attitude of the screw/nut mechanism to transform the rotational motion into linear one. This parameter allows to understand the amount of rotational energy which is transformed in useful energy for the linear movement, and also the amount of energy dissipated into heat. It is possible to calculate it using the following formula, where alpha is the helix angle and f is the dynamic friction coefficient between the nut and the screw materials, taken as 0,15 for self-lubricating plastic materials:

$$\eta = \frac{1 - f \bullet \mathrm{tg}\alpha}{1 + \frac{f}{\mathrm{tg}\alpha}}$$

η = efficiency
f = dynamic friction coefficient between screw and nut
α = thread angle

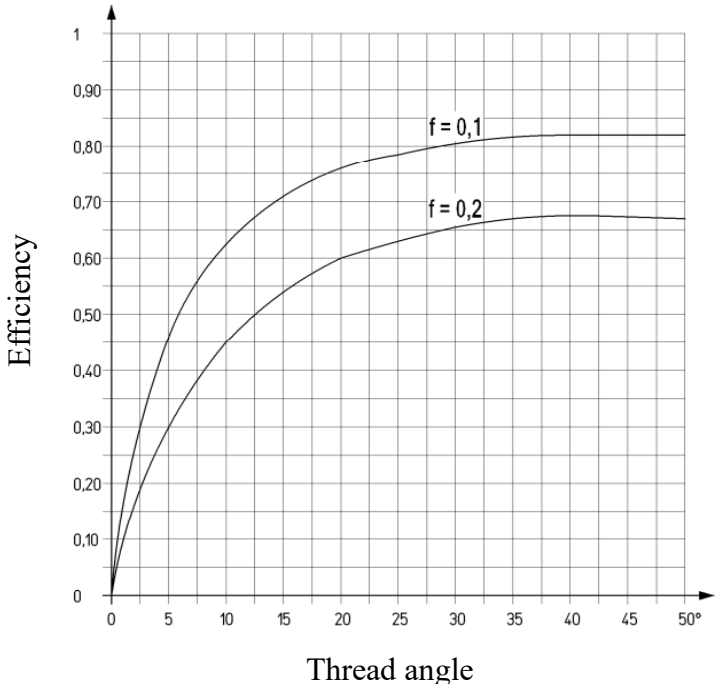

Plot 2.1 Efficiency of the transmission between nut and screw as function of the thread angle [10]

From the graph 2.1, it is clear that increasing the helix angle, also the efficiency of the mechanism will increase, up to a certain value where the efficiency will increase in a less steep way. However, increasing too much the helix angle will have a negative effect on the irreversibility of the movement, as it will be showed in the next paragraph. Moreover, the efficiency is inversely proportional to the dynamic friction coefficient, which means that using materials with dynamic friction coefficient as low as possible will guarantee the lowest waste of energy. This is the reason why self-lubricating plastic materials will be adopted as nut material.

2.1.4 Irreversibility

One of the most important characteristics of the mechanism is the irreversibility of the movement, which is guarantee by an helix angle < 2° 30'. If this angle in greater, some torsion could be applied to the actuator in stationary screw situation, in particular with the presence of vibrations [10].

Moreover, it is possible to demonstrate this statement also from a theoretical point of view. Considering the following system, it can be considered *reversible* if, without the torque C, the weight Q is able to move the nut and consequently to rotate the screw.

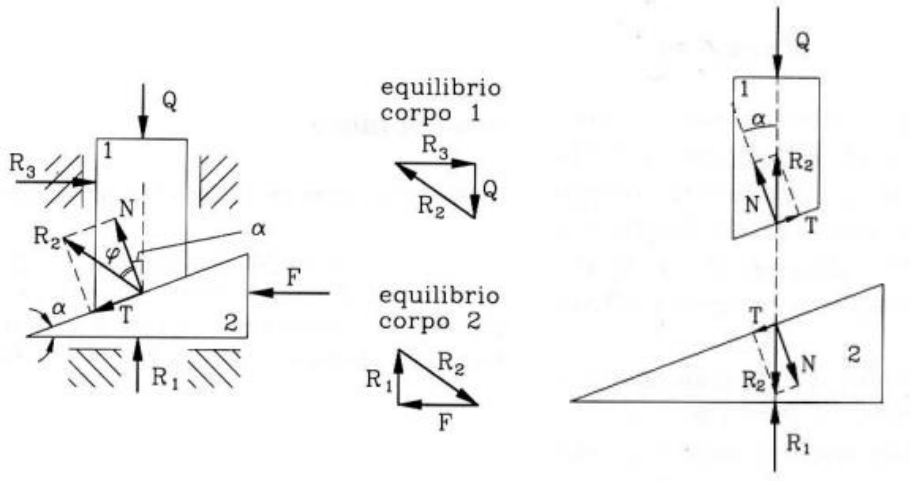

Figure 2.2 Schematic drawing of the forces exchanged between the screw and the nut during their relative movement [11]

Considering moreover the absence of relative movement between the two wedges which means complete adherence between them, the tangential force T and the normal force N exchanged by the two wedges can be written as:

$$T \leq f_a N \tag{2.6}$$

Since there is no friction on the constraints of the elements, forces exchanged on wedge 2, and consequently on wedge 1, cannot have horizontal components, but only vertical. This is equivalent to state that the resultant of the forces R_2 will be sloped of the helix angle α with respect to the normal, which means:

$$T = N \tan \alpha \tag{2.7}$$

Considering the two previous equations, in order to satisfy the first one, it has to be:

$$f_a \geq \tan \alpha \tag{2.8}$$

And consequently:

$$\varphi_a \geq \alpha \tag{2.9}$$

Which means that the angle of friction has to be higher than the helix angle to guarantee the irreversibility of the movement [11].

2.1.5 Buckling

One important factor to keep in mind in this specific application is the so called buckling phenomenon, which means the tendency of the screw to bend itself when loaded in axial compression. The sustainable axial load depends on the core diameter d_2 of the screw, on the constraints placed in the extremities and on the free length "l_e". Additionally, a safety factor of 2, for example, can be added in this calculation to increase the margin of error. The following graph and drawings were used for this purpose [10].

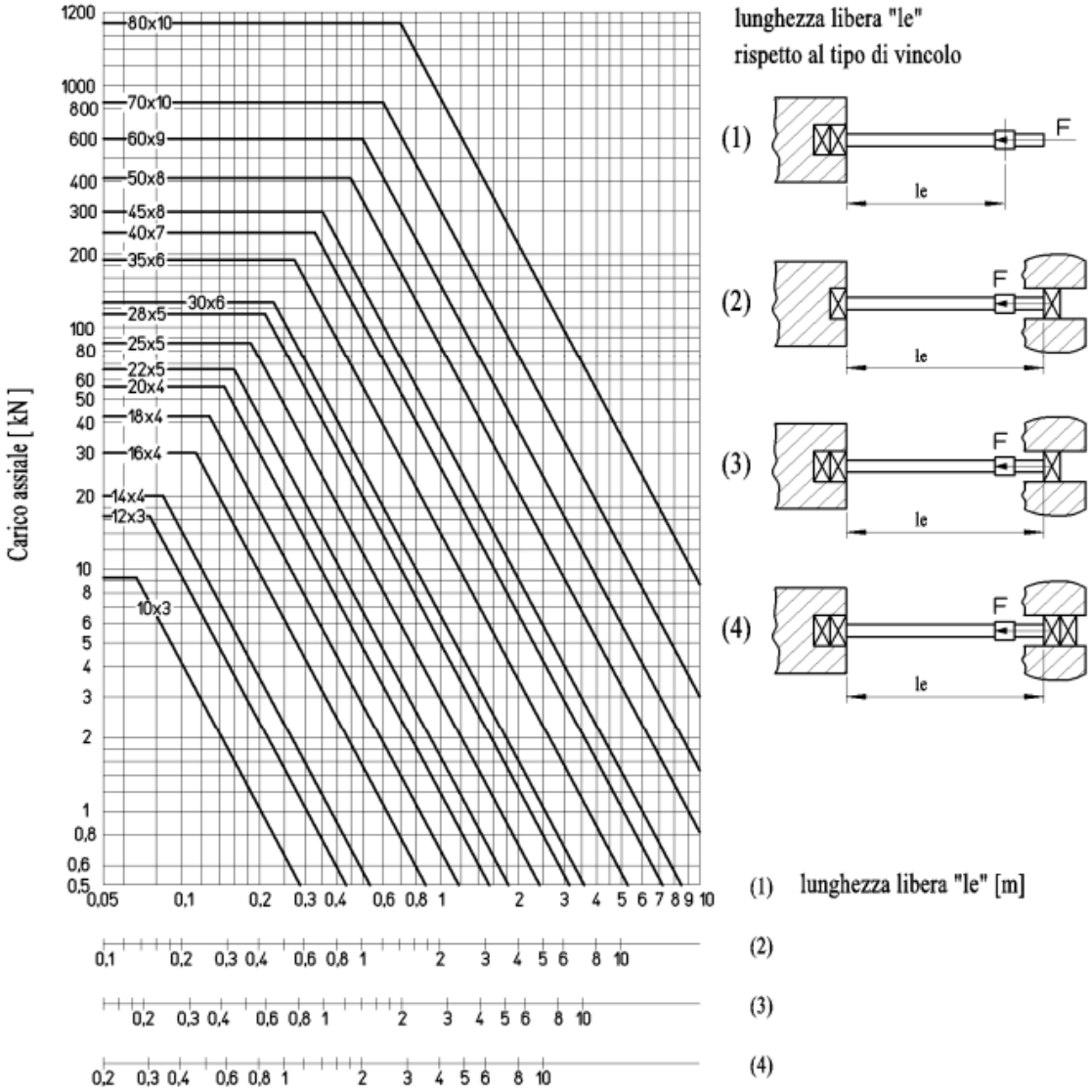

Plot 2.2 Reference plot for the calculation of the sustainable axial load as function of the screw diameter

2.1.6 Critical number of revolutions

The critical number of revolutions for the screw is the frequency of rotation at which the screw starts to vibrate. This revolution velocity should never be reached since these kinds of vibrations will strongly affects the functioning of the mechanism. This critic velocity depends on the diameter of the screw, on the constraints placed at the extremities and on the free length "lg", but also on the mounting precision; however, this last parameter will not be considered in this dissertation. As before, also in this case is possible to add a safety factor, equal to 1,5 in this calculation. The following graph and drawings were used for this purpose [10].

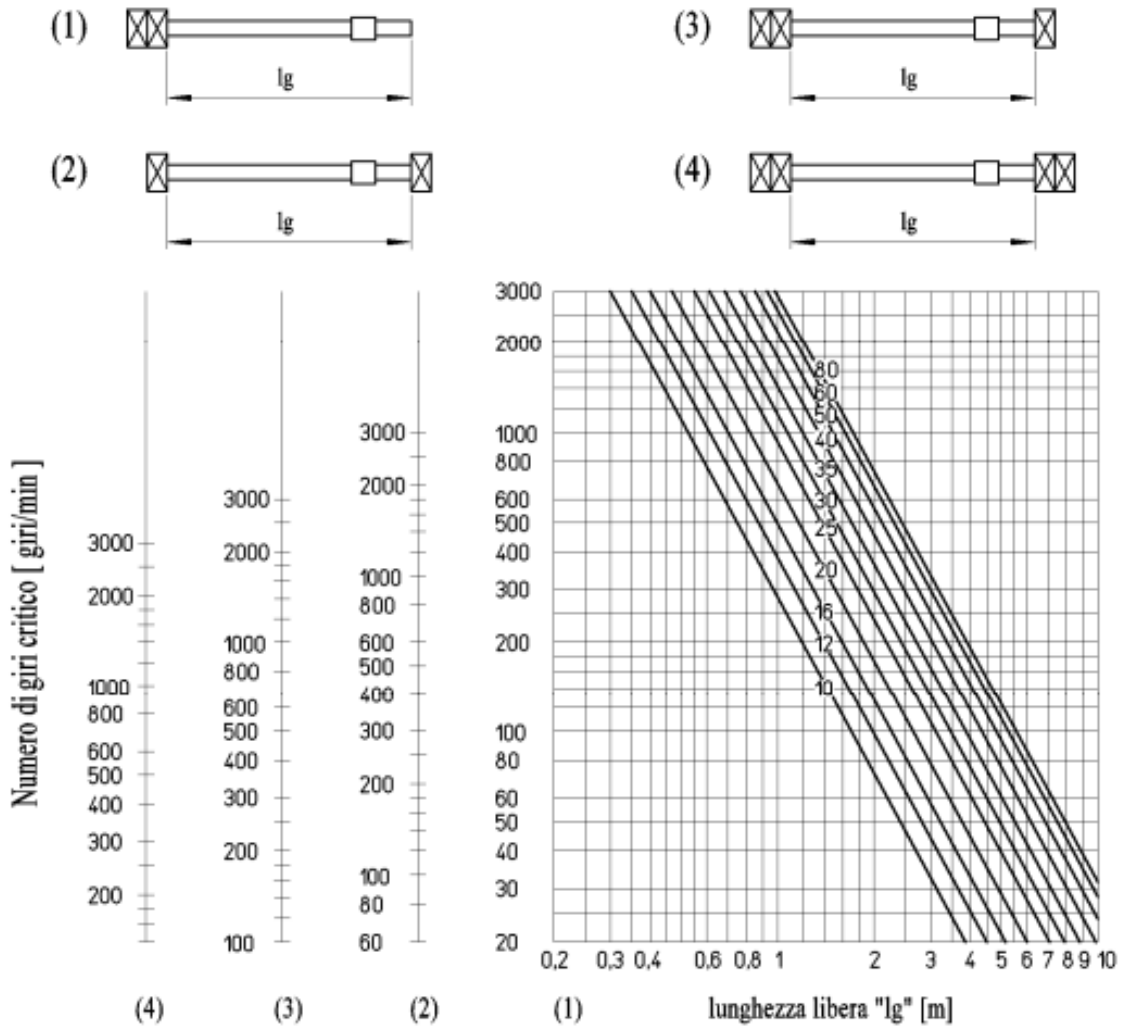

Plot 2.3 Reference plot for the calculation of the critical number of rotations as function of the screw diameter

2.1.7 Motor torque

The torque required by this mechanism is simply calculated as:

$$C = \frac{F \bullet P}{2 \pi \eta 1000}$$

C = torque [Nm]
F = axial force on the nut [N]
P = screw pitch [mm]
η = efficiency

Here is reported the table which summarize the calculations done in this way on the available screw diameter.

	SCREW	BUCKLING [kN]	CRITIC N° OF REVOLUTIONS [rpm]	EFFICIENCY	MOTOR TORQUE [Nm]
1 PRINCIPLE	KAM 16 T R	0,50	666,67	0,304	5,18
	KAM 20 T R	1,75	933,33	0,257	6,04
	KAM 25 T R	4,00	1200,00	0,257	7,55
	KAM 28 T R	7,00	1333,33	0,223	8,59
	KAM 30 T R	9,00	1600,00	0,257	9,07
	KAM 40 T R	35,00	2133,33	0,221	12,15
2 PRINCIPLES	KAM 16 T R	0,50	666,67	0,456	8,37
	KAM 20 T R	1,75	933,33	0,402	9,50
	KAM 25 T R	4,00	1200,00	0,402	11,88
	KAM 28 T R	7,00	1333,33	0,373	12,79

Table 2.3 Calculations on the available screws from the Conti's catalogue

2.2 Nut dimensioning

2.2.1 Material

Once the screw has been selected, the next component which is analyzed is the nut: again, the first parameter to consider is the material, for the same reasons listed above for the screw. This time, the choice is between two very specific materials, the EN 1982 CuAl11Fe6Ni6-C (CC333G) and the PA6 + MoS2 DIN 7728 + additives.

The first one is an alloy of Bronze and Aluminum, in particular with high content of Aluminum between the 8.5 and 12 %, very useful in maritime ambient and in application where the mechanical parts are strongly stressed. The chemical composition which characterizes this specific material is 76 – 83 % of Copper, 0.1 % of Tin, 0.5 % of Zinc, 0.03 % of Lead, 4 – 6 % of Nickel, 4 – 5.5 % of Iron, 0.1 % of Silica, 3.0 % of Manganese and 8.5 – 10.5 % of Aluminum [12].

The second one, instead, is a polymer with optimal mechanical characteristics, very low friction coefficient, good impact resistance, compression and wear resistance, very strong against aging and atmospheric agent. It is obtained by adding molybdenum disulfide to the base polymer PA6-G and its commercial name is Veramyd 6 + MOS_2 [13].

For the current application, they are both very useful, since they both have good resistance to corrosive environments such as the marine water, good mechanical resistance such as impact and compression resistance and good wear resistance, but they also have some differences, of course. The most important one, which will also be the tiebreaker in this situation, is the ability of the Veramyd 6 + MOS_2 to lubricates itself during the movement, guarantying a very low friction coefficient with the screw, while the Bronze-Aluminum alloy requires an external lubricant to reach the same performances; however, considering the location of the mechanism under the passerella, the presence of the external lubricant can cause spill and leakages on the visible part of the boat, and of course this is not acceptable in a yacht and superyacht solution. For these reasons, the choice material for the nut will be the Veramyd 6 + MOS_2 [12] [13].

Once the material has been chosen, it is possible to take the overall dimensions of the nut which couple with the pre-selected screw from the catalogue. As matter of fact, not all the possible screw dimeters have a corresponding plastic nut, which means that the first step is to find the possible coupling between them.

The following are the possible matching between the AISI 316 screw and the polymer nut [10]:

Codice per chiocciola **DESTRA**	Codice per chiocciola **SINISTRA**	**Diametro per passo**	n° principi	**d1** mm	**d2** mm	**d3** mm	**d4** mm	**d5** mm	**p** mm	**L** mm	**s** mm	**n°** fori per viti	Viti di fissaggio (classe 8.8)	Peso kg/cad.	**At** mm^2 (1)
FCS 12 A R	FCS 12 A L	**Tr 12x3**	1	18	26	37	4,5	7,5	4,2	36	12	4	M4	0,016	594
FCS 16 A R	FCS 16 A L	**Tr 16x4**	1	22	32	45	5,5	9,5	5,2	48	16	4	M5	0,030	1056
FCS 20 A R	FCS 20 A L	**Tr 20x4**	1	30	40	52	5,5	9,5	5,2	60	20	4	M5	0,057	1696
FCS 20 B R	--	**Tr 20x8 (P4)**	2	30	40	52	5,5	9,5	5,2	60	20	4	M5	0,057	1696
FCS 25 A R	FCS 25 A L	**Tr 25x5**	1	35	48	62	6,5	11	6,5	75	25	6	M6	0,094	2650
FCS 28 A R	FCS 28 A L	**Tr 28x5**	1	40	53	68	6,5	11	6,5	90	30	6	M6	0,142	3600
FCS 28 B R	--	**Tr 28x10 (P5)**	2	40	53	68	6,5	11	6,5	90	30	6	M6	0,142	3600
FCS 30 A R	FCS 30 A L	**Tr 30x6**	1	40	53	68	6,5	11	6,5	90	30	6	M6	0,135	3816
FCS 35 A R	FCS 35 A L	**Tr 35x6**	1	50	63	78	8,5	14	8,5	105	35	6	M8	0,221	5277
FCS 40 A R	FCS 40 A L	**Tr 40x7**	1	55	68	84	8,5	14	8,5	120	40	6	M8	0,289	6880
FCS 40 I R	--	**Tr 40x10**	1	55	68	84	8,5	14	8,5	120	40	6	M8	0,252	6597
FCS 50 A R	FCS 50 A L	**Tr 50x8**	1	65	80	100	10,5	17	10,5	150	50	6	M10	0,476	10840

Table 2.4 Available polymer nuts from the Conti's catalogue

2.2.2 Contact area & superficial contact pressure

The first parameter is the contact area between the threads of the screw and the nut, which is directly taken from the Conti's catalogue. This data is used to calculate the second presented parameter, which is the superficial contact pressure, obtained by dividing the maximum axial force F_a by the previous contact area.

2.2.3 Sliding velocity

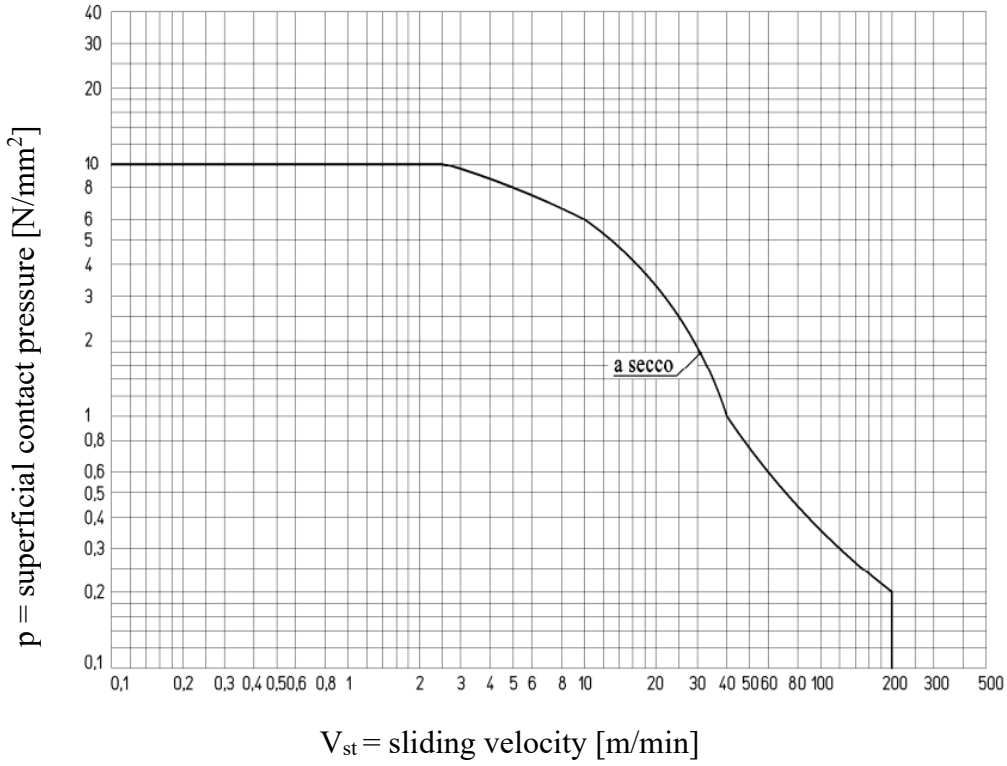

Plot 2.4 Reference plot for the calculations of the sliding velocity of the polymer nut without lubricant [10]

The sliding velocity can be considered as the velocity at which the nut slides against the screw. It is a very important parameter since it plays a fundamental role in the maximum velocity that the nut can reach but also in the heat generation, since too much angular velocity or a continuous use of the mechanism could drastically increase the temperature of the nut, leading to a possible failure of it.

In order to calculate it, it is possible to take the previously obtained translating velocity of the nut and divide it by the sine of the thread angle α. In formula:

$$v_{st} = \frac{v_{tr}}{\sin \alpha} \tag{2.10}$$

Then, it is possible to calculate the maximum sliding velocity of the selected plastic nut as function of the superficial contact pressure typical of the mechanism under studying using the graph 2.4.

$$p \cdot v_{st\,max} = p \cdot v_{st\,graph} \tag{2.11}$$

2.2.4 Various coefficients

In order to calculate the admissible sliding velocity that characterize the mechanism under studying, the next step is the definition of a series of coefficients that define the influence of some parameters to this velocity, like the time of usage time with respect to the stop time.

– **Safety coefficient for the inertia forces (f_i)**

During the dimensioning phase of the project, it is necessary to ensure that the inertia forces created during the acceleration and the deceleration of the mechanism remain under a certain value so that also the product $p \cdot v_{st}$ remains controlled. For this reason, a coefficient called safety coefficient for the inertia forces will be introduced in the calculation of the admissible sliding velocity of the nut against the screw. It is possible to use the following table, taken once again from the Conti's catalogue, which reports typical values for this coefficient depending on the load condition under exam. For this project, a value of f_i = 0,8 can be considered representative of the load conditions.

Type of load	f_i
Constant loads with controlled acc./dec.	from 1 to 0,5
Constant loads with quick start and stop	from 0,5 to 0,33
Very variable loads and speed	from 0,33 to 0,25
Loads with shocks and vibrations	from 0,25 to 0,17

Table 2.5 Reference table for determining the load coefficient [10]

– **Ambient temperature correction factor (f_t)**

While using plastic nuts, the admissible $p \cdot v_{st}$ value should be corrected also as function of the ambient temperature. In fact, the plastic material will soften with an increasing temperature, and consequently will sustain lower loads. On the other hand, with a decreasing temperature, the material will harden and will sustain higher values of load. This correction factor can be obtained from the following graph, taken from the Conti's catalogue. For the mechanism under studying, is obtained a value of f_t = 0,8, considering that ambient temperature can reach values up to 50 °C during the hottest summer days.

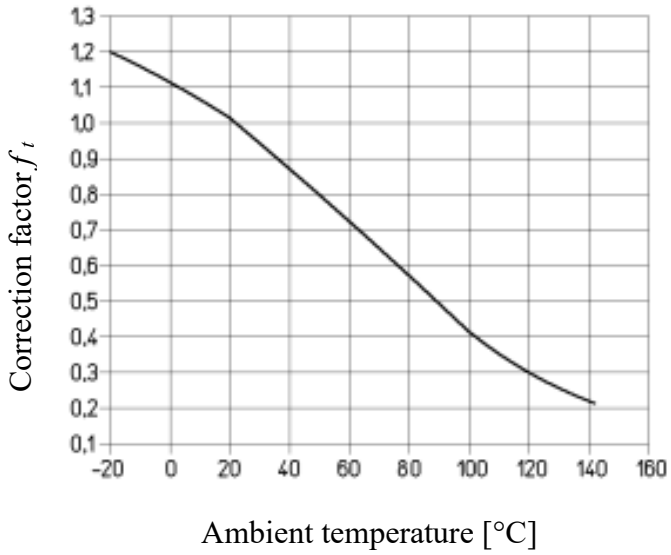

Plot 2.5 Reference plot for the correction factor as function of the ambient temperature for polymer nuts [10]

– **Intermittent utilization correction factor (f_c)**

Nuts which are made with plastic material can reach high temperature if their utilization is quite continuous; on the other hand, when they are utilized in a more intermittent way, with quite long idle time, they usually do not reach dangerous temperature. For these reasons, the last coefficient that will be introduced in this calculation is the so-called intermittent utilization correction factor, which represents the previously described temperature increasing as function of the frequency of utilization of the mechanism. This coefficient is usually an integer number equal or greater than one: if it is equal to one, it means that the stop time is equal to the working time, while if it is two, it means that the stop time is double with respect to the working time and so on. In this specific situation, where the stop time is far greater than the working time, the Intermittent utilization correction factor will be equal to 6, which means that during a whole day, it can be operated for a maximum of 4 hours, which is still far greater than a reasonable working time.

2.2.5 Admissible sliding velocity vs calculated

Once that all the previous coefficients have been defined, it is possible to calculate the admissible sliding velocity, or better the admissible $p \cdot v_{st}$, which is just the superficial contact pressure multiplied by the sliding velocity. As a matter of fact, this product is more representative of the interaction between nut and screw than the sliding velocity alone.

In order to calculate the admissible $p \cdot v_{st}$ it is possible to use this simple formula:

$$p \cdot v_{st\,amm} = p \cdot v_{st} \cdot f_i \cdot f_t \cdot f_c \tag{2.12}$$

Now it is possible to calculate the calculate the specific $p \cdot v_{st}$ of the mechanism under studying by simply multiplying the previously calculated sliding velocity v_{st} with the superficial contact pressure, which means:

$$p \cdot v_{st\,calc} = p \cdot v_{st} \tag{2.13}$$

Finally, to select the possible solution, it is necessary to compare the calculated $p \cdot v_{st}$ with the admissible one: if the former is lower than the ladder, the solution can be considered acceptable.

The following is the table which summarize all the previous calculation with different screw and nut diameters.

NUT	CONTACT AREA At [mm^2]	SUPERFICIAL CONTACT PRESSURE p [N/mm^2]	V_{st} [m/min]	V_{st} [m/min]
FCS 16 A R	1056,00	2,84	55,57	22,00
FCS 20 A R	1696,00	1,77	69,45	30,00
FCS 25 A R	2650,00	1,13	69,36	37,00
FCS 28 A R	3600,00	0,83	89,00	45,00
FCS 30 A R	3816,00	0,79	69,31	47,00
FCS 40 A R	6880,00	0,44	89,02	80,00
FCS 20 B R	1696,00	1,77	34,90	30,00
FCS 28 B R	3600,00	0,83	39,65	45,00

NUT	$P*V_{st\ max}$	INERTIA FORCE FACTOR	TEMPERATURE FACTOR	FREQUENCY OF ACTUATION FACTOR	$P*V_{st\ amm}$	$P*V_{st\ calc}$
FCS 16 A R	62,50	0,80	0,80	6,00	240,00	**157,87**
FCS 20 A R	53,07	0,80	0,80	6,00	203,77	**122,85**
FCS 25 A R	41,89	0,80	0,80	6,00	160,85	**78,52**
FCS 28 A R	37,50	0,80	0,80	6,00	144,00	**74,17**
FCS 30 A R	36,95	0,80	0,80	6,00	141,89	**54,49**
FCS 40 A R	34,88	0,80	0,80	6,00	133,95	**38,82**
FCS 20 B R	53,07	0,80	0,80	6,00	203,77	**61,73**
FCS 28 B R	37,50	0,80	0,80	6,00	144,00	**33,04**

Table 2.6 Summary of the previous calculations performed on the available nuts from the Conti's catalogue

This last section of this chapter will be dedicated to the proposal of a combination of a moto reductor already available on the market, coupled with the nut and screw mechanism previously selected, which can satisfy both the functional but also the general dimensions requirements.

2.3 Screw selection

From the previous calculations, it is possible to see that the smallest screw which can satisfy the project requirements is the KAM 25x5, since it can sustain a buckling load of 4 kN. However, its number of revolutions is quite high, which means that also the power requested to the motor is quite high. To deal with this issue, one possible solution is to increase the principle of the thread of the screw, which means decrease the number of revolutions of the screw while maintaining constant the torque requested to actuate the screw. For example, passing from a screw with 1 principle to a 2 principles screw, halve the number of revolutions while keeping the requested motor torque constant. However, the smallest screw with 2 principles produced by CONTI is the KAM 28x10, which will be adopted screw for this mechanism. As it is clear, this is not the only solution, but the solution that will be adopted and discussed during this dissertation. The following are the characteristics that describe this specific type of screw.

SCREW	PITCH	MEAN DIAMETER [mm]	THREAD ANGLE [°]	ANGLE OF FRICTION [°]	RADIAL VELOCITY [mm/s]	ω [rpm]
KAM 28 T R	10	25,24	7,07	11,20	645,03	488,01

SCREW	BUCKLING [kN]	CRITIC N° OF REVOLUTIONS [rpm]	EFFICIENCY	MOTOR TORQUE [Nm]
KAM 28 T R	7	1333,33	0,373	12,79

Table 2.7 Summary of the calculations performed on the final screw selection

2.4 Nut selection

Regarding the possible selection of the nut, it is clear that almost all the proposed configurations can be considered acceptable from a sliding velocity point of view. However, the nut must be coupled with the correct screw, which means that the limitations applied to the screw are also applied to the nut. For these reasons, the nut final selection is the FCS 28 B R, which is a plastic nut with auto lubricant features and very good wear resistance. As the screw, it presents 2 principles, limited external diameter and a total length of 3xTr, very good in terms of sustainable load [10].

The following is the table which summarize the features of the final nut selection:

NUT	CONTACT AREA At [mm^2]	SUPERFICIAL CONTACT PRESSURE p [N/mm^2]	V_{st} [m/min]	V_{st} [m/min]	P*$V_{st\ max}$
FCS 28 B R	3600,00	39,65	34,90	45,00	37,50

NUT	INERTIA FORCE FACTOR	TEMPERATURE FACTOR	FREQUENCY OF ACTUATION FACTOR	P*$V_{st\ amm}$	P*$V_{st\ calc}$
FCS 28 B R	0,80	0,80	6,00	144,00	**33,04**

Table 2.8 Summary of the calculations performed on the final nut selection

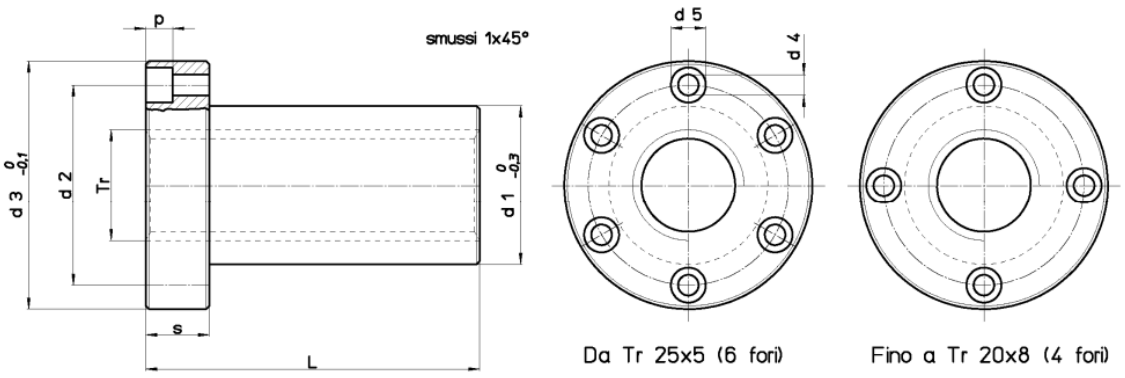

Figure 2.3 CAD drawing of the polymer nut from the Conti's catalogue

2.5 Motor selection

Looking at the market, there are a lot of solutions for what concern the actuation of this movement. For this specific application, the final selection will be represented by the motor "**SERIE E**" of the ElipTagliente srl company, located in Monopoli (Bari), Italy. This motor is a permanent magnet DC motor, which is a DC motor that uses a permanent magnet to create the magnetic field required for its operations. The main characteristics of this motor are summarized in the following table, where it is clear that the possible solutions are the 12V or the 24V.

Volt	12	24	36	48
Watt	800			
Rpm	3300			
Amp	80	40	26,6	20

Table 2.9 Main characteristics of the SERIE E motor

The Ingress Protection of this motor is customizable up to IP68, while its nominal output torque is 2,2 Nm. This motor was selected thanks to its very compact design (the total

DIMENSIONI

FLANGIA B14	*B*	C	D	d1	E	H	M
MEC 63	*114*	60	11	75	2,5	23	M5
MEC 71	*114*	70	14	85	2,5	30	M6

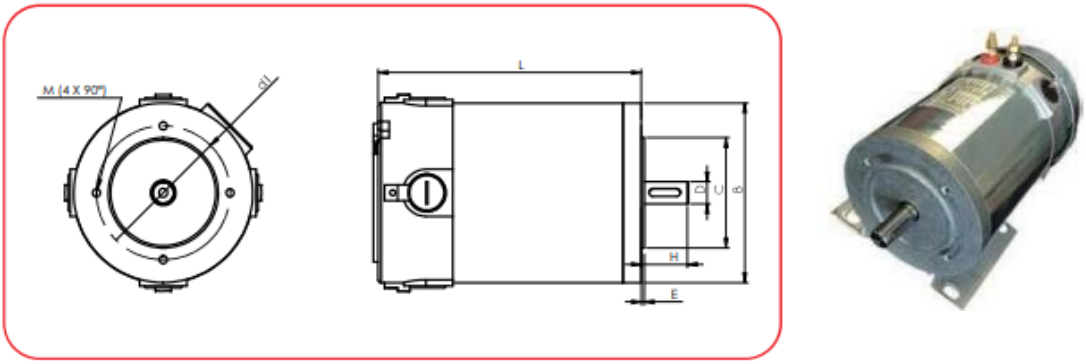

Figure 2.4 CAD drawing and general dimensions of the SERIE E motor

length is only 168 mm), its output torque, the possibility to customize the class protection and, last but not least, the possibility to obtain it in short time, since the facility of this productor is near to the production facility of the gangway. The following are the CAD of the SERIE E motor, directly taken from the ElipTagliente's catalogue [14].

2.6 Gear train solution

Regarding the possible gear train solution, there are a lot of possibilities available on the market. One of the most famous productor of gear train mechanisms is the Wittenstein company, which presents a lot of very useful solutions in all the possible market segments. Looking at their catalogue, it is clear that there are infinite solutions, from the smallest to the most efficient gear train. For this specific application, one of the most important features is the smallest as possible overall dimensions, still maintaining the right reduction ratio and a sustainable axial load. For these reasons, the final gear train selection will be the **CP 005 MF**, with a **reduction ratio** equal to **7**. It is a planetary gearbox, with a class protection equal to IP64. The Ingress protection of this component could be increased up to IP69K, which is the highest as possible, but on the other hand also the length of the component will increase.

The main characteristics which allow this gear train to become the final solution are the very compact design (the total length neglecting the shaft is about 80 mm) and a very high efficiency, equal to 0,97 [8].

Rapporto di riduzione	i		7
Coppia max.	T_{2a}	*Nm*	21
Coppia di accelerazione max. (max. 1000 cicli per ora)	T_{2B}	*Nm*	14
Coppia di emergenza (fino a 1000 volte durante la vita del riduttore)	T_{2Not}	*Nm*	26
Velocità nominale media in ingresso (a T_{2N} e temperatura ambiente di 20°C)	n_{1N}	*rpm*	4300
Velocità max. in ingresso	n_{1Max}	*rpm*	9000
Coppia senza carico media (a n_1 = 3000 rpm e a temp. misurata sul riduttore di 20°C)	T_{012}	*Nm*	0,06
Rigidezza torsionale	C_{12}	*Nm/arcmin*	0,58

Forza assiale max.	F_{2AMax}	*N*	240
Forza radiale max.	F_{2QMax}	*N*	170
Coppia di ribaltamento max.	M_{2KMax}	*Nm*	4
Rendimento a pieno carico	η	%	97
Peso (inclusa flangia di adattamento standard)	*m*	*kg*	0,5
Rumorosità (per *i* e n_1 di riferimento consultare cymex®)	L_{PA}	*dB(A)*	≤ 59
Temperatura max. ammissibile sulla carcassa		°C	+90
Temperatura ambiente		°C	da –15 a +40
Lubrificazione			a vita
Senso di rotazione			concorde tra ingresso e uscita
Grado di protezione			IP 64

Table 2.10 Main characteristics of the selected gear train

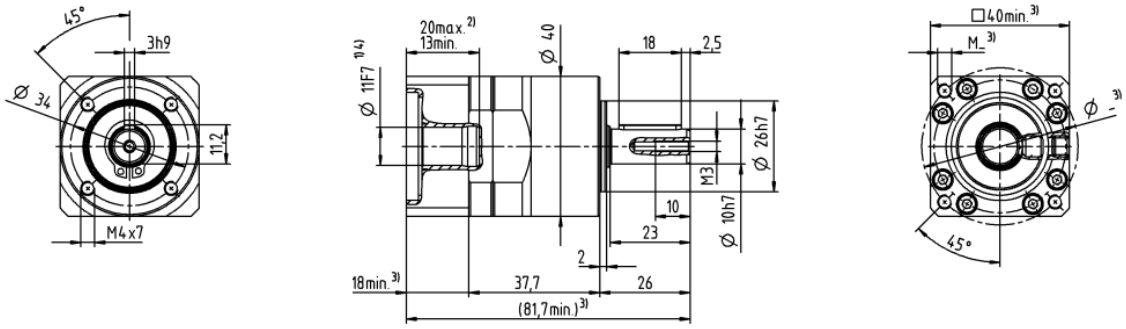

Figure 2.5 CAD drawing of the selected gear train

To conclude, this is the table which shows the features of the coupling between the motor and the gear train, and it is possible to see how they respect both the project requirements and the actuation limitations applied by the nut and screw mechanism.

MOTOR TORQUE [Nm]	MOTOR SPEED [rpm]	REDUCTION RATIO	EFFICIENCY	OUTPUT TORQUE [Nm]	OUTPUT SPEED [rpm]
2,2	3300	7	0,97	14,94	471

Table 2.11 Summary of the final selected mechanism features

2.7 Components design

This section will be dedicated in showing the preliminary design of the selected components.

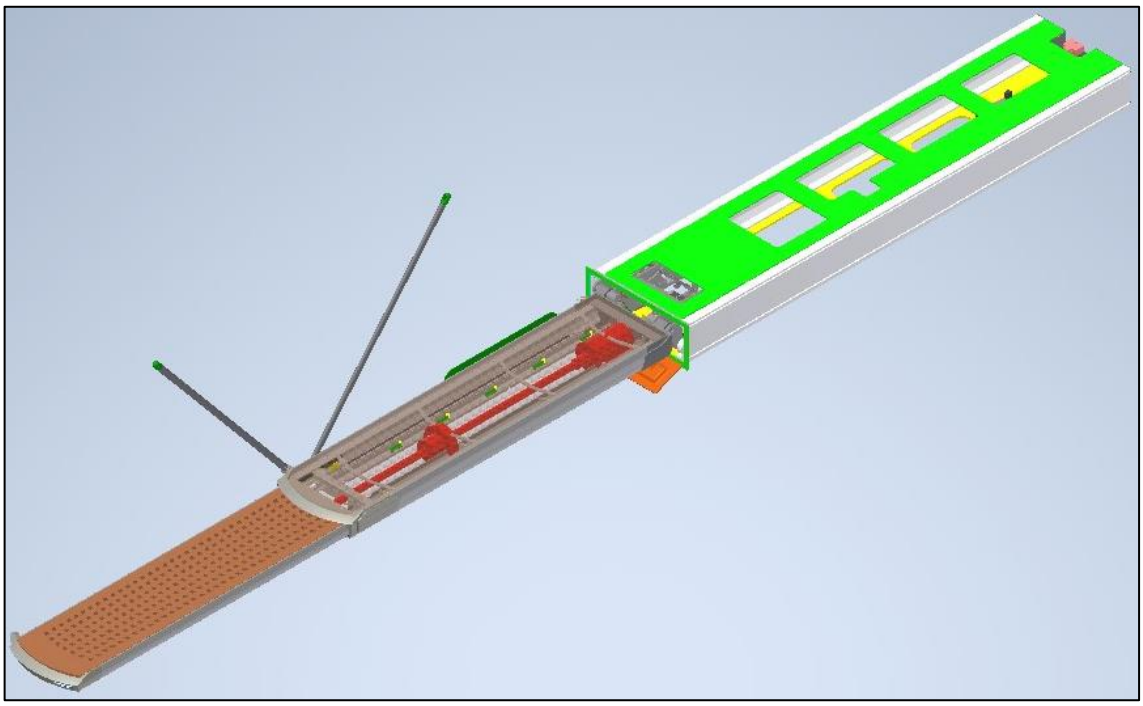

Figure 2.7 Isometric view of the passerella showing the position of the selected component, highlighted in red

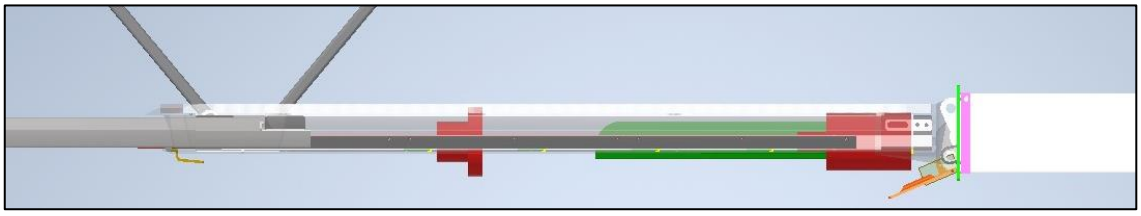

Figure 2.8 Side view of the positioning of the designed component

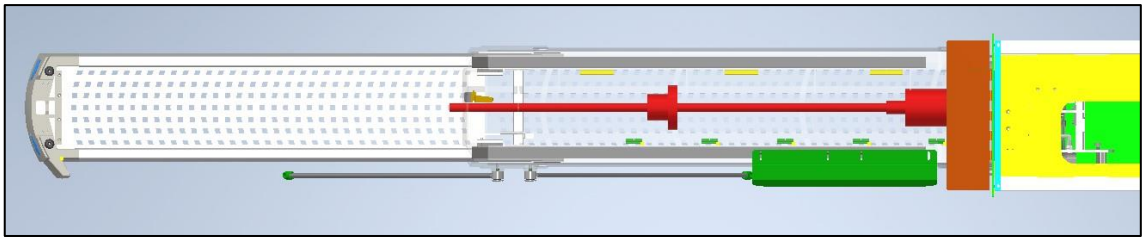

Figure 2.6 Bottom view of the positioning of the selected component

3. Third movement analysis

The third and last movement which is performed by the gangway is the vertical movement, which allows the passerella to place itself as close as possible to the dock. This is movement were performed by an hydraulic piston hinged to the box on one hand and to the passerella on the other end, while the passerella was hinged only in one point to the box. The hydraulic piston was inclined in such a way that when the piston elongates itself, the passerella move its farthest end towards the sky, while when the piston compresses itself, the passerella moves the same end towards the see. The following are some photos which describes this behavior.

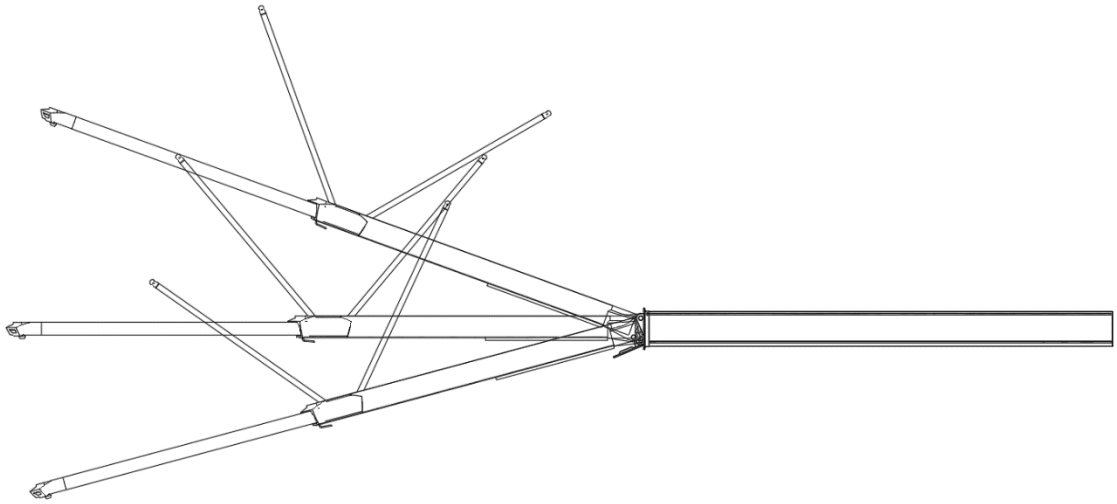

Figure 3.1 Sketch of the performed movements of the passerella

The solutions proposed for this movement are multiple, since the problem is quite complicated both from a structural and a dimensional point of view. In particular, the proposed solutions are a nut and screw mechanism very similar to the previous one and an electric piston that replace the previously present hydraulic piston. These solutions were be analyzed more in detail in the following paragraph.

In order to calculate the force required to the mechanism to move the passerella but also to sustain an heavy load placed on the farthest end of the gangway, some data was taken from the previous hydraulic solution, such as the stroke of the piston or the movement velocity. These are summarized in the following table:

STROKE [mm]	TIME [s]	MOVEMENT VELOCITY [mm/s]
55	30	1,8

Table 3.1 Starting data for the third movements analysis

The first data that can be calculated is the force required to the mechanism both in static and in the dynamic condition. For what concern the static situation, it is possible to consider the equilibrium in the hinge point of the passerella between the momentum created by the load placed in the farthest end of the passerella and the momentum created by the replacement mechanism. The following is the free body diagram and the calculations to obtain the required static force applied by the mechanism.

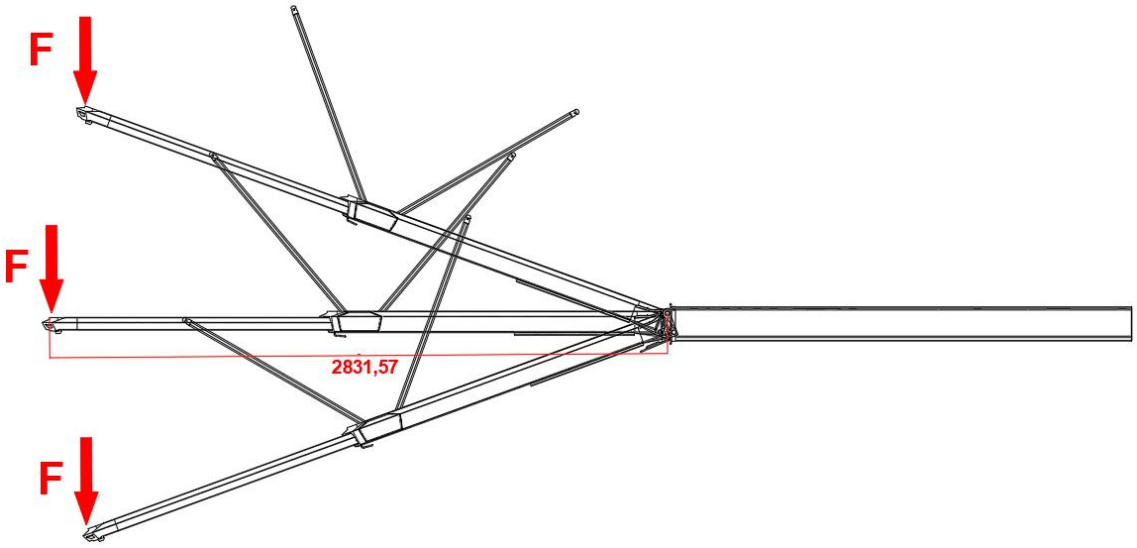

Figure 3.2 Load condition for the static analysis

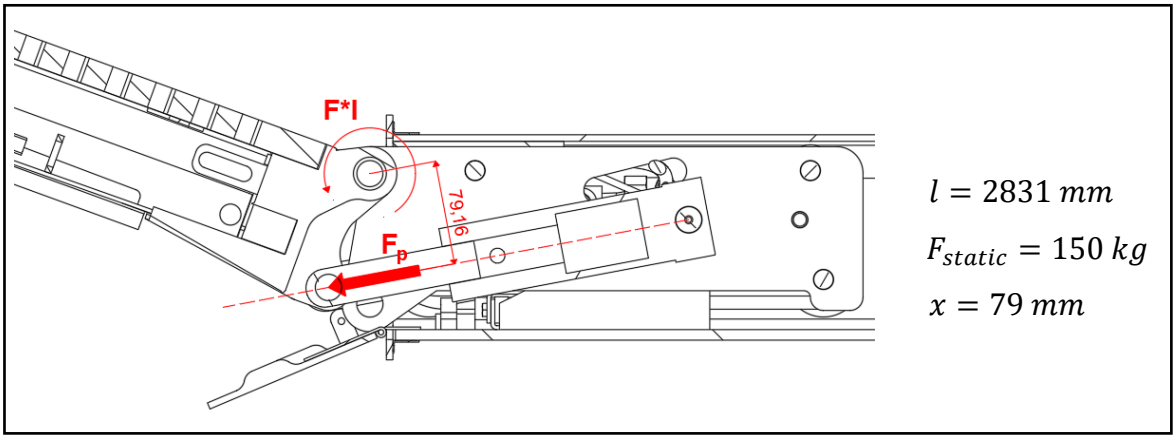

Figure 3.3 Detailed free body diagram for the static situation

EQUILIBRIUM EQUATION

$$F_{static} \cdot l = F_{p\ static} \cdot x \tag{3.1}$$

$$F_{p\ static} = \frac{F_{static} \cdot l}{x} \tag{3.2}$$

$$F_{p\ static} = \frac{150 \cdot 9{,}81 \cdot 2831}{79} = 52731{,}854\ N \tag{3.3}$$

For what concern the dynamic situation, the calculations are almost the same, with the only difference that the dynamic movement is performed without any types of loads on the passerella, which means that the only force to counteract is the weight of the gangway itself. The following are again the free body diagram and the calculations regarding the required dynamic force.

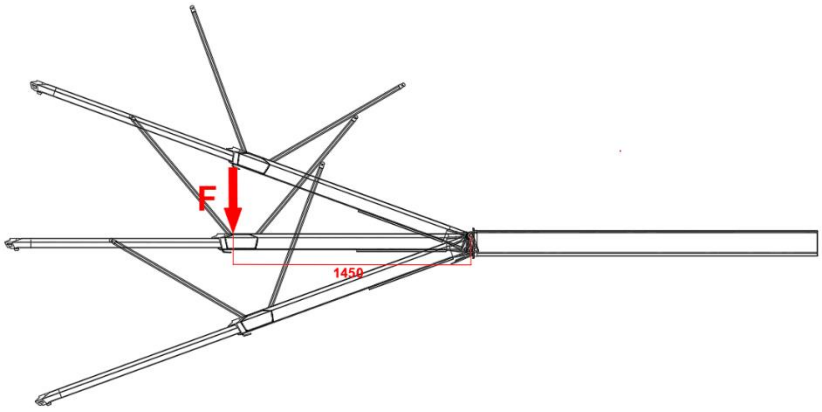

Figure 3.5 Load condition for the dynamic analysis

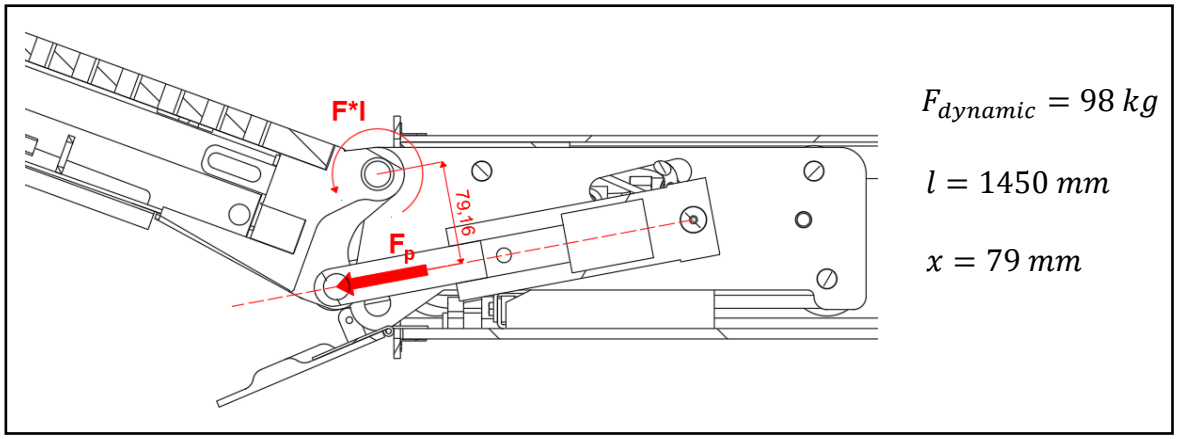

Figure 3.4 Detailed free body diagram for the dynamic situation

$$F_{p\ dynamic} = \frac{F_{dynamic} \cdot l}{x} \tag{3.4}$$

$$F_{p\ dynamic} = \frac{98 \cdot 9{,}81 \cdot 1450}{79} = 17645\ N \tag{3.5}$$

As it is clear from these calculations, the force required in the static situation is way greater than the one required during the dynamic movement: this aspect could be fundamental for the project, since it allows to divide the tasks between static and dynamic: in this way, one mechanism could satisfy the dynamic performance, while another one, also completely independent from the first one, could satisfy the static performance, instead of having one mechanism that has to satisfy both requirements.

3.1 Linear actuator solution

The first proposed solution for this specific application is the placement of two electric linear actuators. This solution could be very useful, since it does not require the presence of a motor coupled with a gear train, since it is all integrated inside the actuator. The selected product is the CON60 actuator sold by the Concerns company. It is the most compact solution available on the market, thanks to "in-line" technology: for example, the gear train is in linear extension with the spindle part itself, meaning all parts placed in line, resulting in a as compact as possible solution. Moreover, this actuator satisfies the IEC standard 60529, 'harsh environment' (HE), tested according to IP68/69 standards, and it is also available in stainless steel (AISI316), which makes them well suited for Maritime operation. Last but not least, there is also the possibility to add Hall sensors, which enables controlling the position of the piston rod very precisely and allows driving of two or more electric in-line actuators synchronously [15]. This last feature, in particular the possibility to drive synchronously tow ore more actuators, is very important since, in order to satisfy the dynamic requirement, there will be the necessity of at least two actuators that work in parallel, and since they are very close between each other, they must move very synchronously, to avoid failure inside the actuator itself due to the little arm distance. The following are the most relevant characteristics of this specific actuator.

Standard Specifications (Specifications for non-standard actuators eg. HE-version, may vary)

Motor/Gear

24 VDC power supply, permanent magnet motor (max. current is 11,5 A, absolute max. voltage is 28 VDC)

Gear ratio		19	43	66	81	100
Maximum load	[N]	1900	4300	6600	8100	10000
Speed at maximum load	[mm/s]	26	12	8	6	5

Max. static load/ Self locking force	Alu/Stainless steel: 18100 N Depending on stroke length for push-applications Max. load limited to 5000 N for stroke length > 400 mm
Temperature	■ Operation: - 20 °C to + 50 °C ■ Storage: - 40 °C to + 70 °C
Protection class	IP66
Cable specification	1 m, 2 x 1.3 mm² (AWG16), Ø = 6.4 mm, black, Molex Mini-Fit Jr. 6 pin
Bending Radius	6 x cable diameter
Materials	Motor and actuator tube are powder coated steel Piston rod is stainless steel Front and rear brackets are aluminium
Duty cycle	Max. 10 % or 2 minutes in use followed by 18 minutes rest
Color	Black (RAL 9005)

Stroke length/weight

Stroke	[mm]	50	100	150	200	250	300	350	400	500	750
Weight	[kg]	4.1	4.4	4.7	5	5.3	5.6	5.9	6.2	6.8	7.6

Figure 3.6 General characteristic of the CON60 linear actuator [15]

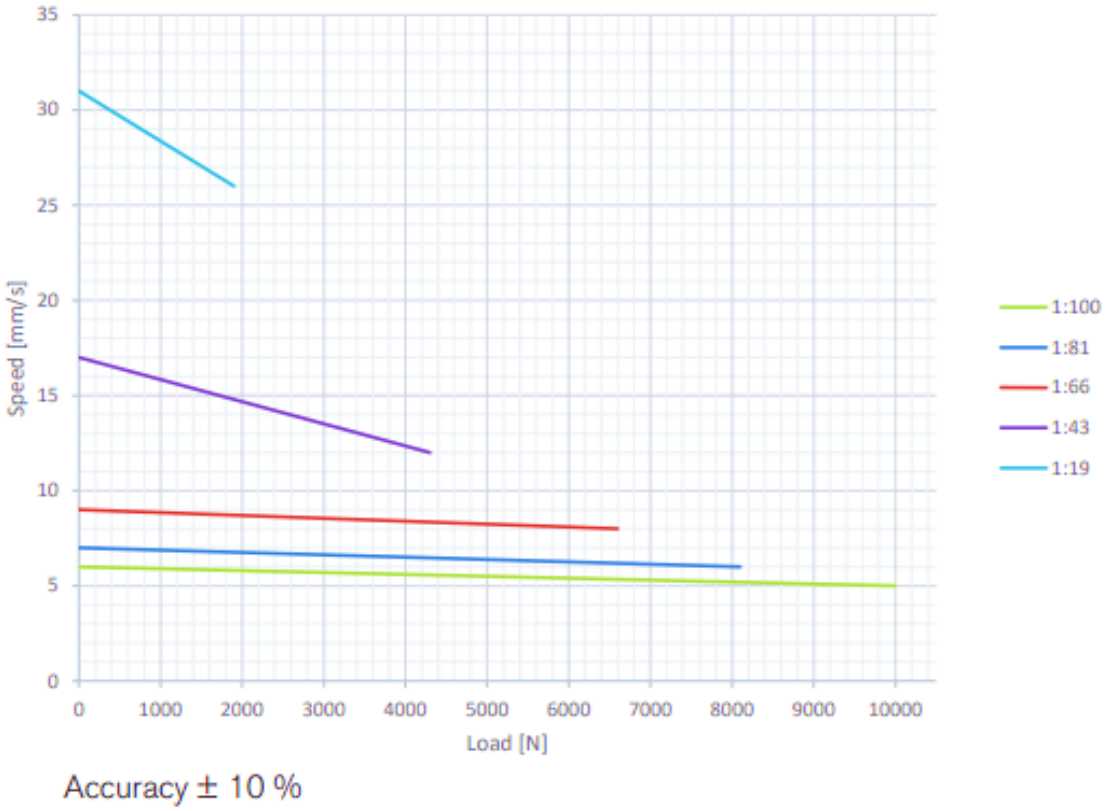

Plot 3.1 Characteristic plot of the speed of movement of the linear actuator as function of the applied force [15]

From the graph 3.1. it is possible to see how the reduction ratio of the linear actuator strongly influences both the sustainable force and the speed of movement. Clearly, decreasing the reduction ratio, the sustainable force increases, while the speed of movement tend to decrease. Moreover, it is also possible to see the difference in range of the movement speed while changing the reduction ratio: with a high reduction ratio (light blue line) the slope of the line is significant, which means that the speed of movement decreases steeply while increasing the applied force, while with a lower reduction ratio (green line), the line is practically horizontal and the speed of movement remains constant.

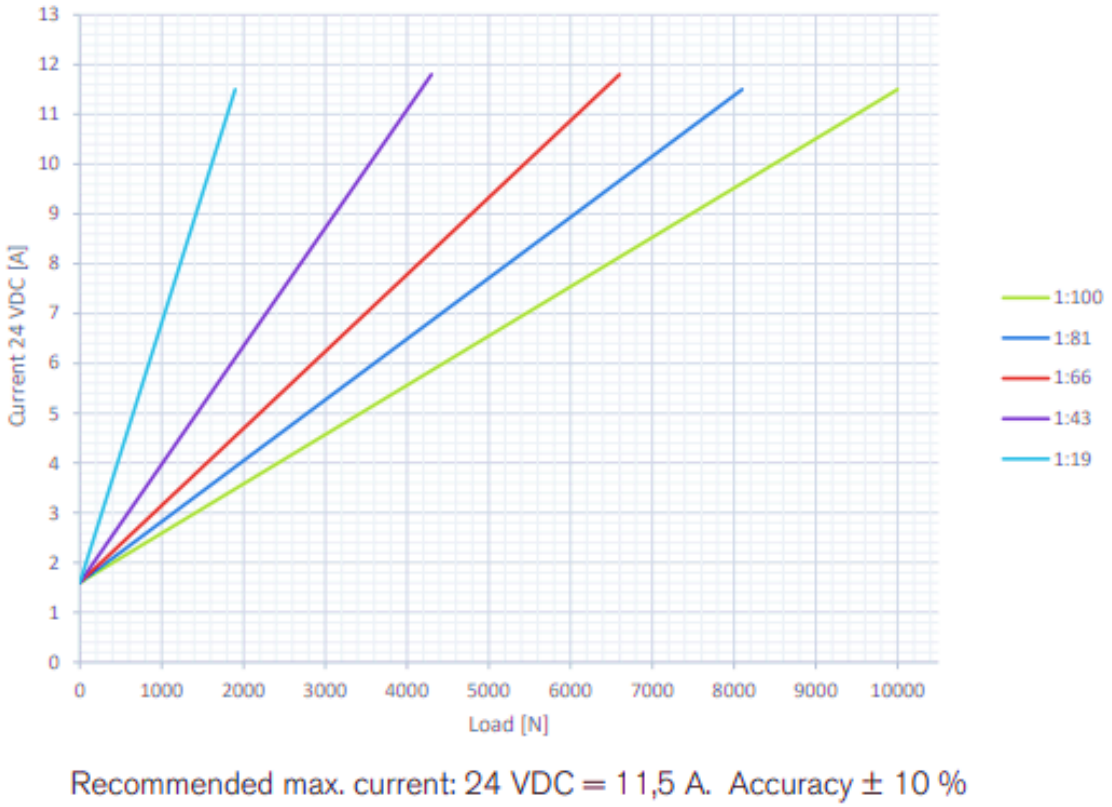

Plot 3.2 Characteristic plot of the drawn current as function of the applied load [15]

In the graph 3.2, instead, is shown the effect of the applied force on the required current, while keeping a constant 24 V voltage in DC. It is possible to see that, clearly, the required current increase with an increasing applied force, for all the possible reduction ratio. An interesting aspect that result from this graph is the tendency of the absorbed current to remain more constant while decreasing the reduction ratio: this is clearly visible from the slope of the line, which is very high with a high reduction ratio (light blue line) and lower with a low reduction ratio (green line)

The selected configuration for this specific application will be the last one, showing a sustainable dynamic load of 10000 N, a gear ratio of 100 and a speed of 5 mm/s. The stroke will be chosen after the following parametric analysis, since it depends on the configuration of the hinge points.

The only problem which results from the adoption of this linear actuator is the sustainable static load, which is limited to 18100 N for each actuator: considering the presence of two actuators, the sustainable static load will be of 36200 N, which is way lower than the required one. For this reason, there will be the need of projecting a specific static brake which can sustain the remaining load. This component will be discussed later on, as function of the load that it has to sustain.

In order to continue with the parametric analysis, the next step is the definition of the dimensions of the selected CON60 configuration, in particular the distance between the two hinge points of the actuator. To do that, the following CAD and table will be used, taken from the Concens catalogue.

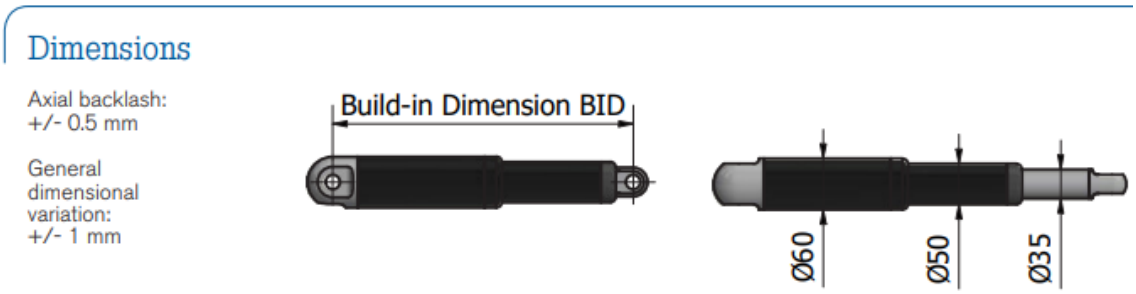

Build-in Dimension 'BID'				
Gear Ratio	Standard	Hall	Harsh Enviroment	Emergency lowering/spline
All ratios	358 + stroke	+ 15	+ 25	+ 31/+ 10
Stroke length > 400 mm + 25 mm not HE-version Stroke lengths > 750 mm + 100 mm (On request)				

Figure 3.7 General dimensions of the CON60 linear actuator [15]

Considering the need of both the Hall sensor and the Harsh Environment protection, the total length will be equal to 398 mm.

3.1.1 Parametric analysis

This analysis is performed in order to define the hinge point configuration of this specific component and in particular the arm distance between the force coming from the static load and that one from the actuator. To do that, first of all it is necessary to draw a scheme of the mechanism configuration, specifying the hinge point, the distance between them and the angles that their connection creates.

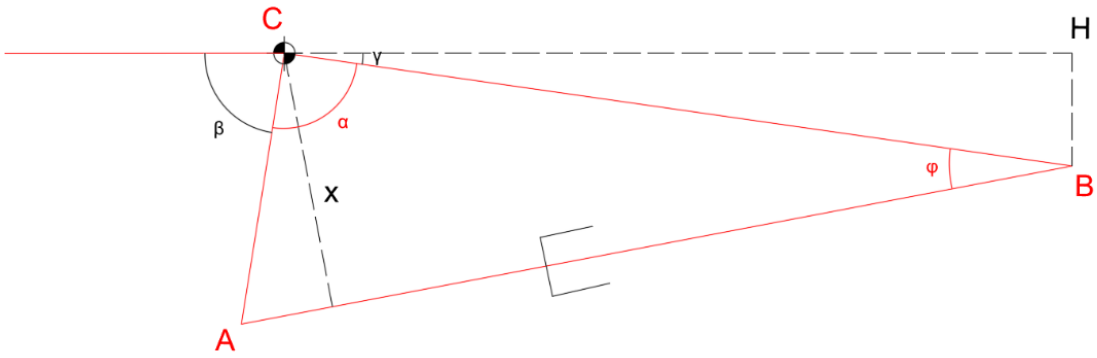

Figure 3.8 Schematic sketch of the position of the hinge points of the linear actuator solution

The next step is the definition of all the distance and angles which are present in the drawing, in particular the arm distance x. The following table summarizes these calculations.

CH	**440,00**	**mm**
BH	**15,00**	**mm**
BC	**440,26**	**mm**
γ	**0,03**	**rad**
AC	**105,00**	**mm**
β	**90,00**	**°**

	α [rad]	α [°]	AB [mm]	φ [rad]	x [mm]	AB INCLINATION [rad]
UP	1,89	108,05	483,21	0,21	90,96	0,17
MID	1,54	88,05	449,11	0,24	102,87	0,20
DOWN	1,19	68,05	412,66	0,24	103,90	0,20

Table 3.2 General dimensions of the positioning of the hinge points for the linear actuator solution

From these calculations, the lowest resulting arm distance is 90 mm, which means that the actuators should sustain a static load equal to 47415 N. Of course, this value is way greater than that one sustainable by the actuators, which means that a static brake capable of sustaining a load equal to 11215 N has to projected.

However, another problem came out from this analysis, and it is the impossibility to place the actuators inside the already existing cart where the old piston was placed, due to the great actuators' length, even if they are the most compact solution available on the market. For this reason, another parametric analysis was performed, this time placing the actuators in "reverse" position, which means under the passerella and no more inside the cart. In this way, there is no more the length problem since the passerella has a lot of available space in the horizontal direction. However, there is not so much space in the width and height direction, but this can be dealt using the appropriate connection that can avoid any interference during the movement. The following is the parametric analysis performed with the Inventor software.

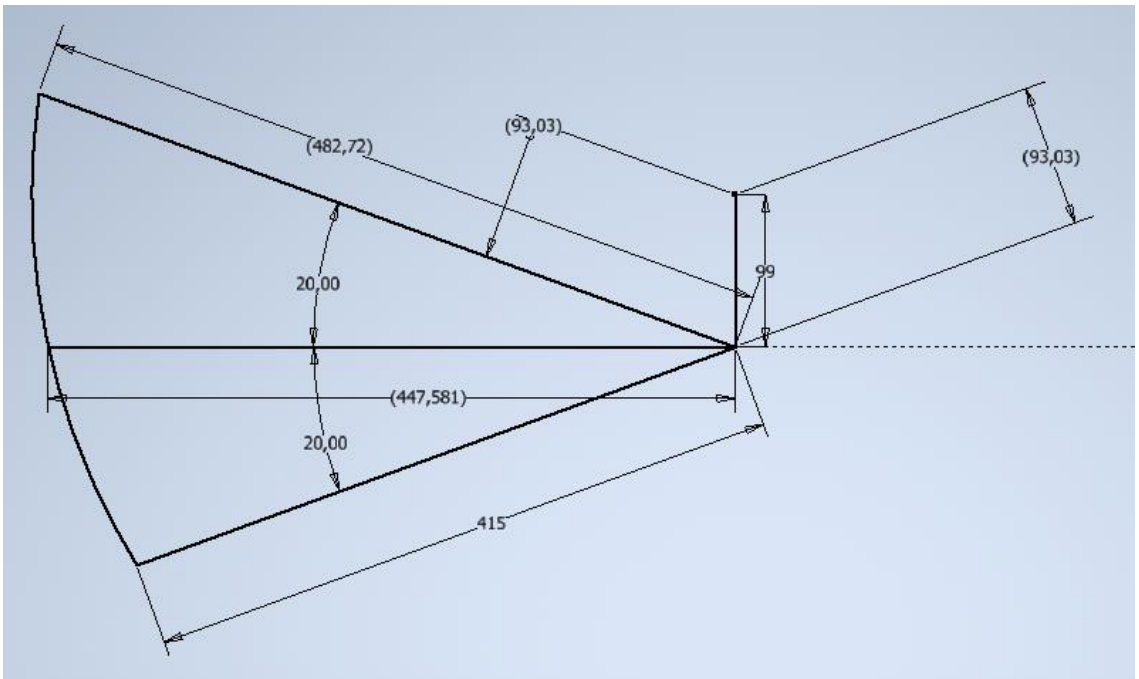

Figure 3.9 Schematic sketch of the "reversed" linear actuator solution (dimensions in mm)

From this analysis, can be seen that the lowest arm increase to 93 mm, which means that the static force sustainable by the actuators should be 45885,5 N, lower than before but still greater than the maximum load sustainable by the CON60.

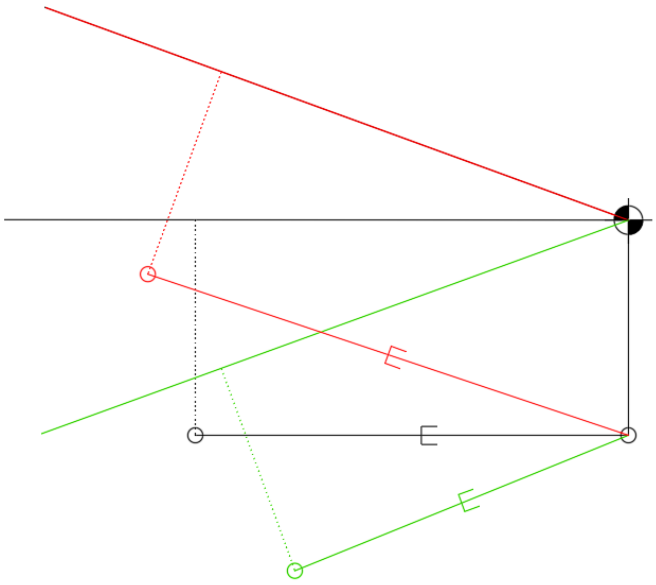

Figure 3.10 Schematic sketch of the "reversed" linear actuator solution

3.1.2 Components design

This part of the dissertation will be dedicated to showing the design of the components created ad hoc for this project, in particular the hinge point of the actuators on the passerella and on the movable cart placed inside the box, but also the movable cart will be designed as well.

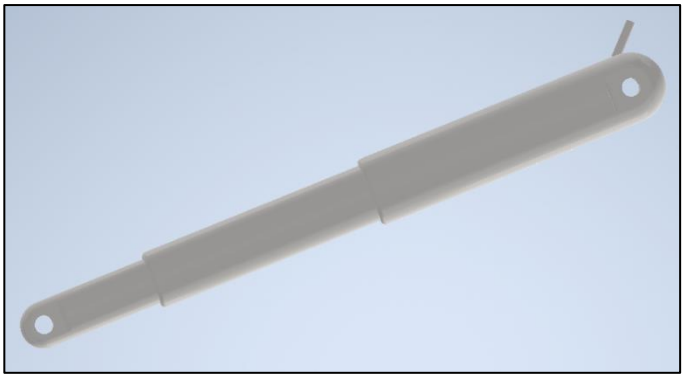

Figure 3.11 Design of the CON60 linear actuator

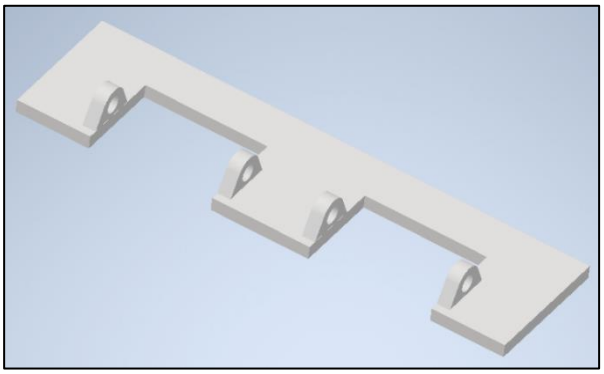

Figure 3.12 Design of the support for the CON60 actuator placed under the walkable part of the gangway

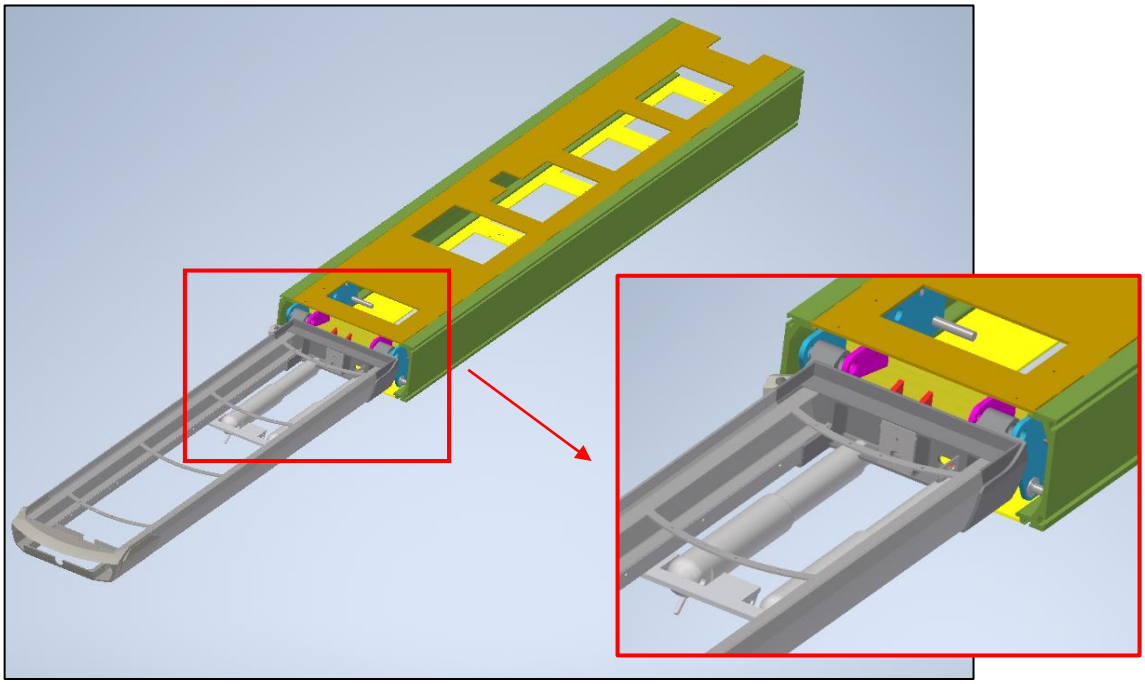

Figure 3.13 Positioning of the actuators with detailed view in red

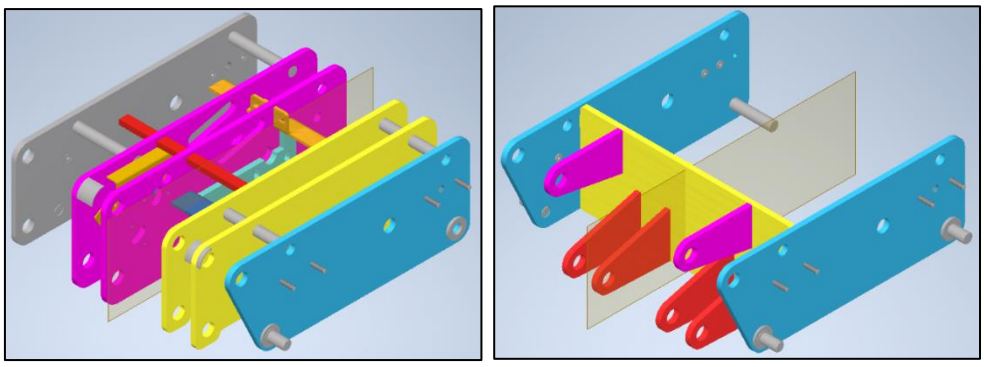

Figure 3.14 Design of the CON60 mounting inside the box

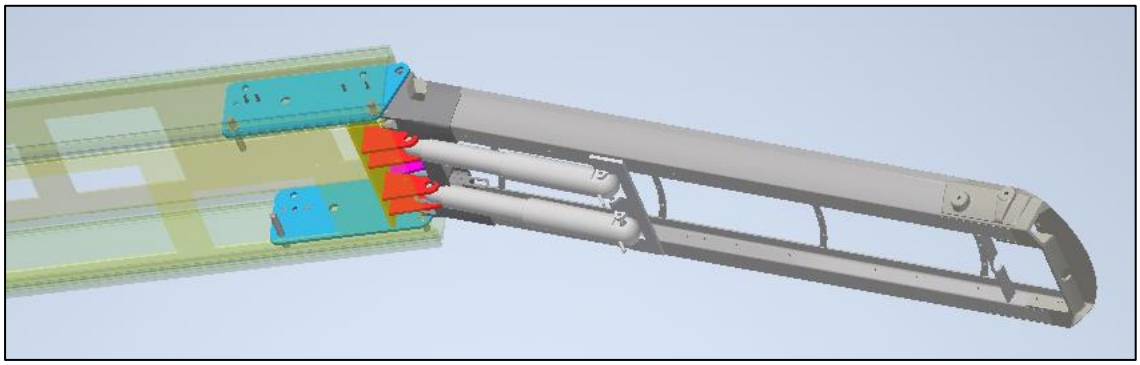

Figure 3.15 Bottom-side view of the gangway inclined towards the sea

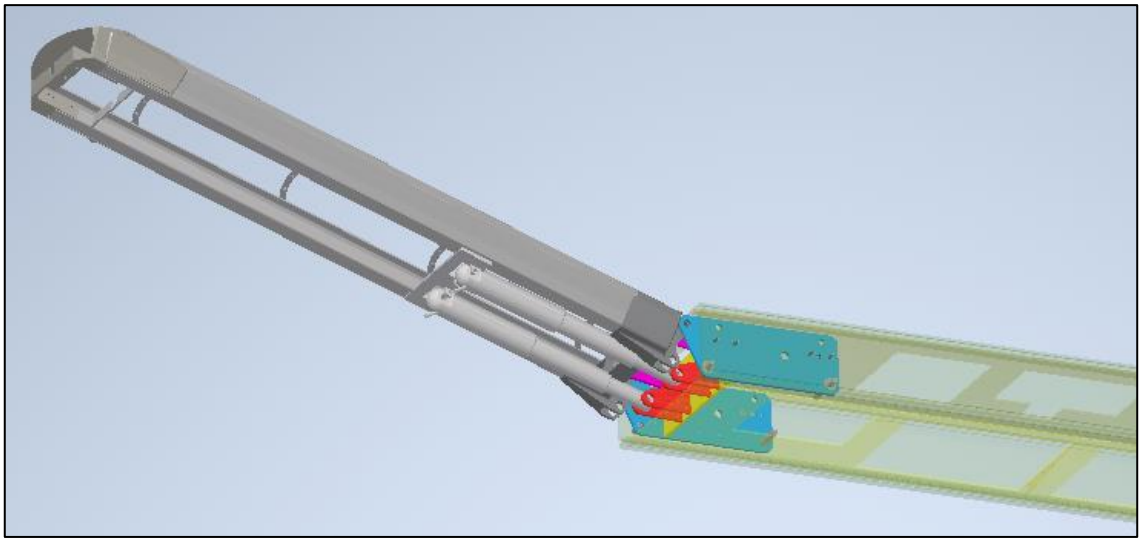

Figure 3.16 Bottom-side view of the passerella inclined towards the sky

3.1.3 Preliminary static brake design

Once the design of the actuators and their hinge points have been defined ensuring an arm distance equal to 93mm at least, now it is necessary to design the static brake that should sustain the remaining static load. However, this brake will not be designed in a very detailed way, but it will be just a qualitative design in order to understand if it is possible, which mechanism could perform it and the amount of force that is necessary to hold in position the gangway using this mechanism. The proposed solutions will be two: the first one is a simple cam which rotates together with the passerella, while the second one is a static disk brake, like that one of cars.

– **Cam solution**

This solution is made using a simple cam which in in direct contact with the vertical face of the passerella placed in the end nearest to the movable cart. In this way, when the gangway is static, the load is transferred to the cam through the contact point, and then it is transferred to the hinge point of the cam itself. When the passerella goes up or down, instead, the cam rotates itself to maintain the contact point with the vertical shape; of course, since the passerella rotates around its hinge point, its vertical face tends to go away from the cam when going up, while does the opposite behavior when going down: for this reason, the shape of the cam has to be carefully designed. To do that, it possible to take the CAD of the gangway in different gangway position, from fully up to fully down, and some position in the middle. The contact point evolution during the whole movement will be the cam shape. The software Autocad will be used for this purpose.

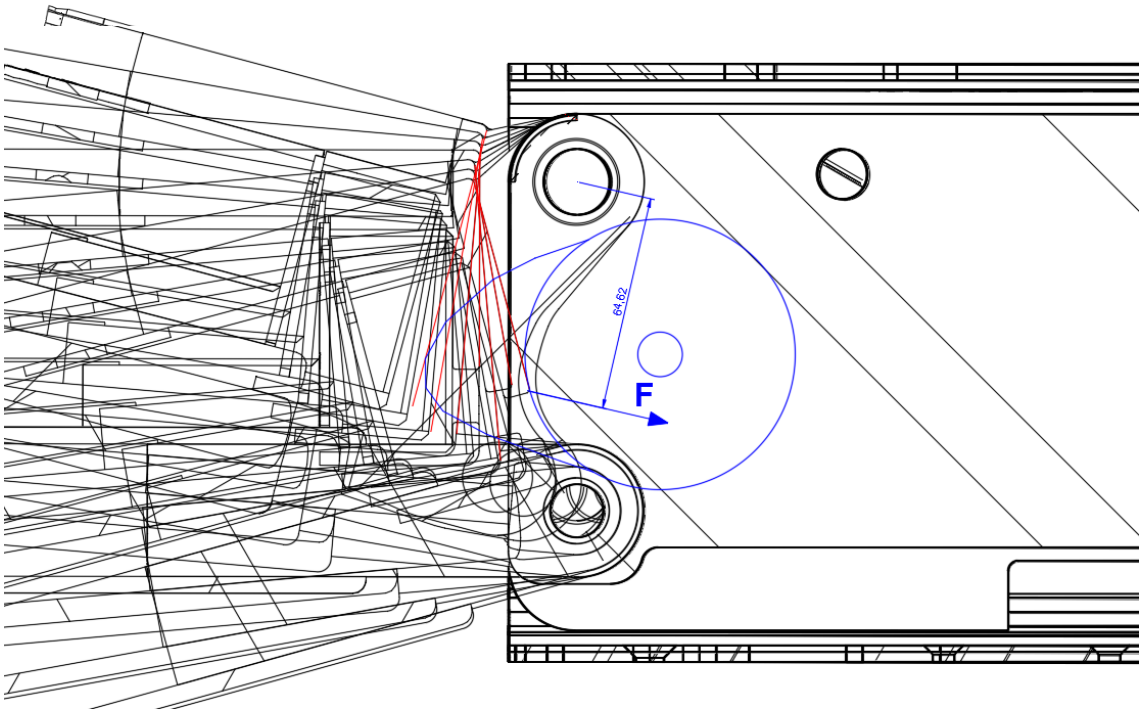

Figure 3.17 Preliminary sketch of the required shape for the cam solution

The following are the calculations done in order to define a qualitative amount of force that the cam should sustain in the contact point.

$F_{static} = 150\ kg$

$l = 2900\ mm$

$F_{con60} = 18100\ N$

$b_{con60} = 93\ mm$

$b_{cam} = 64{,}62\ mm$

$$F_{static} \cdot l = 2\,F_{con60} \cdot b_{con60} + x \cdot b_{cam} \tag{3.6}$$

$$x = \frac{F_{static} \cdot l - 2\,F_{con60} \cdot b_{con60}}{b_{cam}} \tag{3.7}$$

$$x = \frac{150 \cdot 9{,}81 \cdot 2900 - 2 \cdot 18100 \cdot 93}{64{,}62} = 13939{,}18\ N \tag{3.8}$$

– **Static disk brake**

The second solution is based on a mechanism quite similar to that one used to slow down the wheels of a car during the braking phase. However, there is fundamental difference, which is the stativity of the mechanism: in fact, it works only as a static brake, which means that it works just when the passerella is already stopped and it has the function to hold it in position. This aspect could be an advantage since there is no wear of the brake pads and also a greater friction coefficient, since the static one is always greater than the dynamic one. To obtain a qualitative design of the position and dimensions of both the disk and the brake calipers the software Autocad was used.

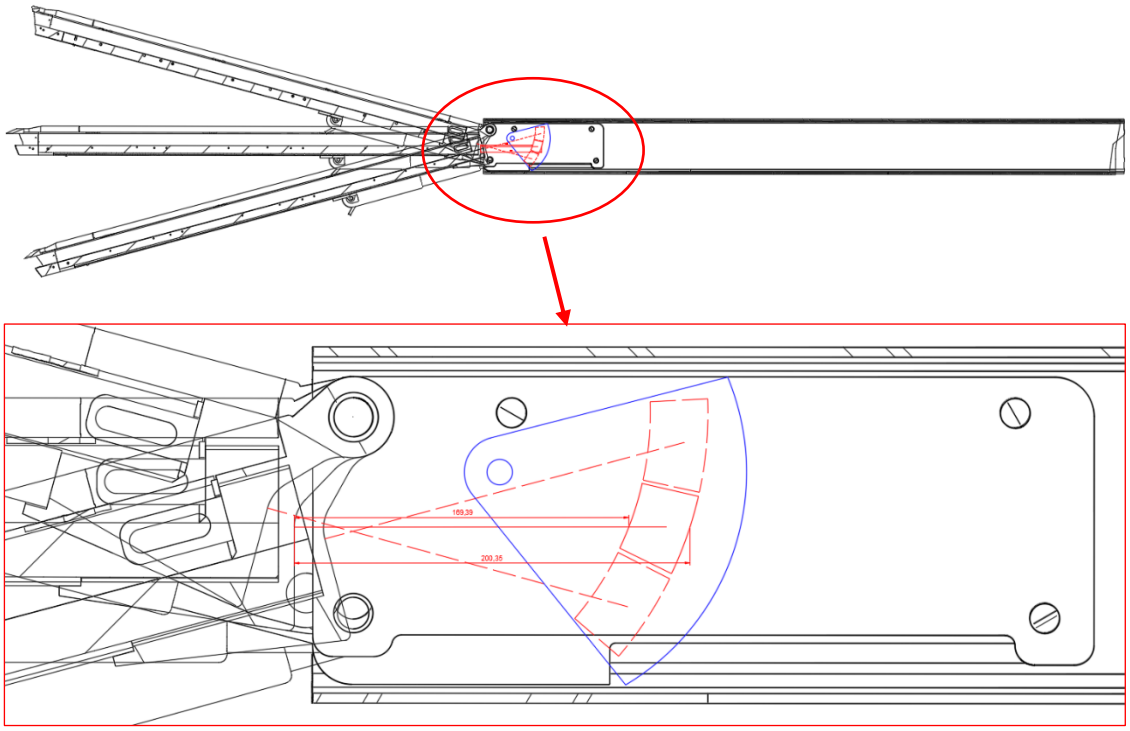

Figure 3.18 First configuration for the design of the static disk brake (config A)

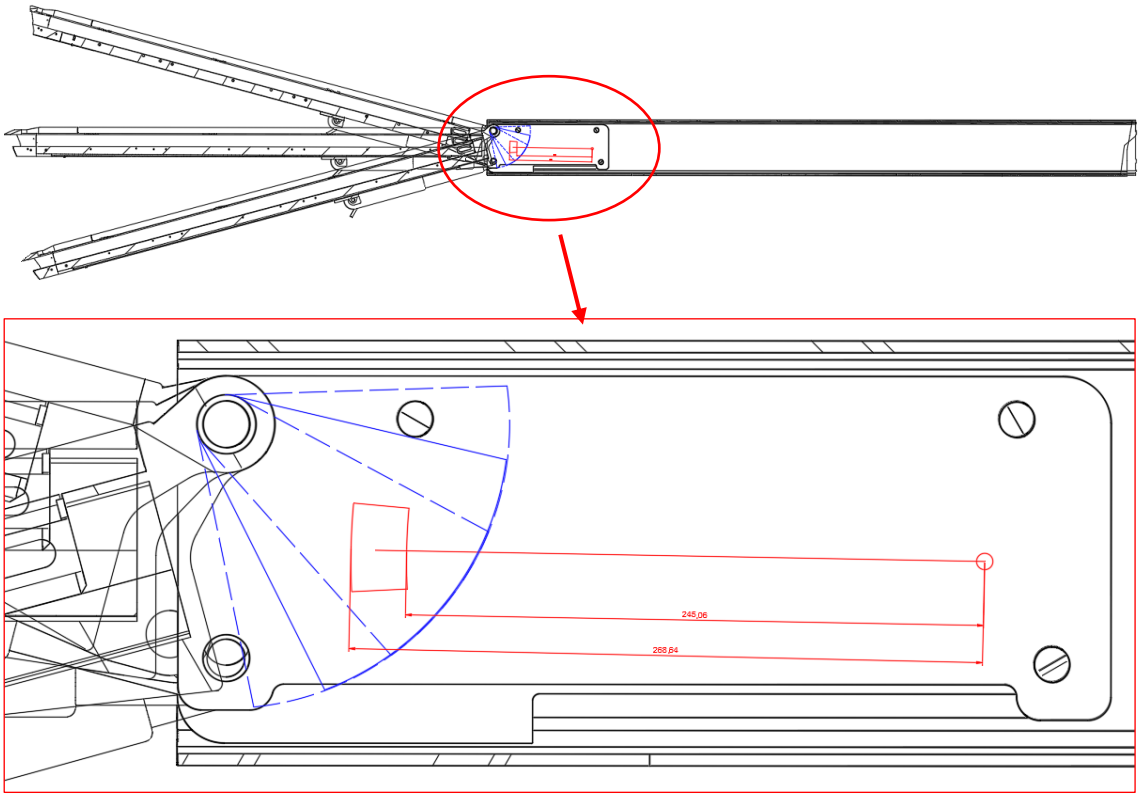

Figure 3.19 Second configuration for the design of the static disk brake (config B)

As it can be seen form these pictures, there are a lot of possible configurations: in particular, the configuration A shows the brake calipers connected with the passerella, representing the moving element, while the disk is static and connected to the cart placed inside the box. The configuration B, instead, is the opposite situation, where the disk is movable and connected with the gangway, while the brake calipers are static and hinged to the cart. The advantage of the configuration B is the possibility of having a greater calipers radius, which will reduce the force required to the calipers to hold the gangway in position.

The following are the calculations done in order to obtain a qualitative amount of force that has to applied by the brake calipers on the disk, both in configuration A and B. The material for the brake pads and disk is supposed to be AISI 316, which means with a static friction coefficient equal to 0,8 [16].

$F_{static} = 150\ kg$

$l = 2900\ mm$

$F_{con60} = 18100\ N$

$b_{con60} = 93\ mm$

$f = 0{,}8$

$$F_{static} * l = M_b + 2 \cdot F_{con60} \cdot b_{con60} \tag{3.9}$$

$$M_b = f\ F_b \frac{r_e + r_i}{2} \tag{3.10}$$

$$F_b = \frac{F_{static} \cdot l - 2 \cdot F_{con60} \cdot b_{con60}}{f\ \frac{r_e + r_i}{2}} \tag{3.11}$$

REQUIRED FORCE FOR CONFIGURATION A

$r_e = 200\ mm$

$r_i = 169\ mm$

$$F_b = \frac{150 \cdot 9{,}81 \cdot 2900 - 2 \cdot 18100 \cdot 93}{0{,}8 \cdot \frac{200 + 169}{2}} = 6102{,}64\ N \tag{3.12}$$

REQUIRED FORCE FOR CONFIGURATION B

$r_e = 268\ mm$

$r_i = 245\ mm$

$$F_b = \frac{150 \cdot 9{,}81 \cdot 2900 - 2 \cdot 18100 \cdot 93}{0{,}8 \cdot \frac{268 + 245}{2}} = 4381{,}08\ N \tag{3.13}$$

3.2 Nut and screw solution

This second solution came out after the necessity to obtain a system capable of satisfying both the dynamic and the static requirement, without adding external components like in the previous case with the static brake. This solution is very similar to the one proposed for the previous telescopic movement, where the rotation of the screw is transformed in linear motion of the nut, directly connected with the passerella. In this way, when the nut moves towards the end of the screw, the passerella goes towards the sky, while when the nut moves towards the top of the screw, the gangway goes down.

In order to understand the feasibility of this mechanism, it is necessary to define the dimensions of the coupling between the nut and the screw capable of satisfying the dynamic requirement. The selected screw material is the AISI 316 as before, while the selected nut material is an alloy of bronze and aluminum, which guarantees a good resistance against the marine corrosion but also a good sliding capability against the AISI 316 screw. However, this selection strongly influences the dimensions of the mechanism, since the smallest nut shows an inner diameter of 30 mm. The dimensions of all the available bronze-aluminum nut are reported here from the CONTI's catalogue [10].

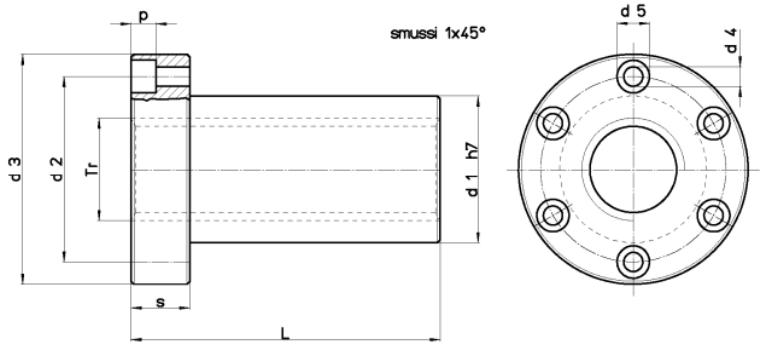

Codice per chiocciola **DESTRA**	Codice per chiocciola **SINISTRA**	**Diametro per passo**	n° principi	**d1** mm	**d2** mm	**d3** mm	**d4** mm	**d5** mm	**p** mm	**L** mm	**s** mm	**n°** fori per viti	Viti di fissaggio (classe 8.8)	Peso kg/cad.	**At** mm^2 (1)
HAL 30 A R	HAL 30 A L	**Tr 30x6**	1	40	53	68	6,5	11	6,5	90	18	6	M6	0,712	3816
HAL 35 A R	--	**Tr 35x6**	1	50	63	78	8,5	14	8,5	105	20	6	M8	1,222	5277
HAL 40 A R	HAL 40 A L	**Tr 40x7**	1	55	68	84	8,5	14	8,5	120	25	6	M8	1,622	6880
HAL 40 I R	--	**Tr 40x10**	1	55	68	84	8,5	14	8,5	120	25	6	M8	1,684	6597
HAL 50 A R	HAL 50 A L	**Tr 50x8**	1	65	80	100	10,5	17	10,5	150	30	6	M10	2,590	10840
HAL 50 I R	--	**Tr 50x10**	1	65	80	100	10,5	17	10,5	150	30	6	M10	2,670	10600
HAL 60 A R	--	**Tr 60x9**	1	75	95	118	12,5	19	12,5	180	35	6	M12	3,982	15700

Figure 3.20 CAD drawing and general dimensions of the bronze-aluminum available nuts

The calculations done in this way are very similar to those ones previously done for the telescopic movement, and they are reported in the following table. The equation adopted for the radial velocity is the (2.3), for the angular velocity of the screw is the (2.4), for the sliding velocity of the nut against the screw the (2.10), for the admissible $p \cdot v_{st}$ the (2.12) and for the calculated $p \cdot v_{st}$ the (2.13).

SCREW	PITCH	MEAN DIAMETER [mm]	THREAD ANGLE [°]	THREAD ANGLE [rad]	RADIAL VELOCITY [mm/s]	ω [rpm]
KAM 30	6	26,71	4,03	0,07	42,58	**30,44**
KAM 35	6	32,23	3,25	0,06	52,83	**31,31**
KAM 40	7	36,74	3,30	0,06	52,03	**27,05**
KAM 50	8	46,27	3,10	0,05	55,39	**22,87**
KAM 60	9	55,78	2,57	0,04	66,84	**22,88**

NUT	CONTACT AREA At [mm^2]	SUPERFICIAL CONTACT PRESSURE p [N/mm^2]	V_{st} [m/min]
HAL 30 A R	3816	4,45	2,60
HAL 35 A R	5277	3,22	3,31
HAL 40 A R	6880	2,47	3,29
HAL 50 A R	10840	1,57	3,38
HAL 60 A R	15700	1,08	4,59

NUT	$V_{st\ graph}$ [m/min]	$P*V_{st\ max}$	INERTIA FORCE FACTOR	$P*V_{st\ adm}$	$P*V_{st\ calc}$
HAL 30 A R	**4,50**	20,05	0,80	16,04	11,58
HAL 35 A R	7,00	22,55	0,80	18,04	10,68
HAL 40 A R	8,00	19,77	0,80	15,81	8,13
HAL 50 A R	15,00	23,52	0,80	18,82	5,31
HAL 60 A R	20,00	21,66	0,80	17,32	4,97

Table 3.3 Summary table of the calculations performed on the available nuts and screws

For these calculations, the first assumption that was made is a linear velocity of the nut equal to 3 mm/s: this because the complete vertical movement of the passerella (± 20°) has to be performed in less than 30 seconds, which means that the nut should compete its stroke during this time. Considering a general stroke of 70 mm and a mean time of 23 s, the resulting linear velocity is 3 mm/s. Moreover, it was considered only the dynamic

force requirement, since all the movements are performed without people on the passerella, as already stated. The distance between the application point of the dynamic force, which is the hinge point of the gangway with the box, and the application point of the force produced by the moving nut is considered equal to 79 mm, as it was before with the hydraulic solution. Once the parametric analysis will be performed, the specific arm distance for this solution will be defined and these calculations will be updated so that the previous considered parameters are still verified. For what concern the static force, it is necessary to keep in mind that it is a load applied to the mechanism only when it is not moving, which means that the sliding velocity of the nut against the screw is equal to zero. Looking at the graph 3.1, the sustainable superficial contact pressure for a bronze nut when its sliding velocity is equal to zero is equal to 30 N/mm^2, greater than the superficial contact pressure characterizing this specific situation, which is equal to 14 N/mm^2 for the lowest as possible superficial contact pressure and with the previous assumption. The following are the calculations done in this way.

$$p = \frac{F_{static}}{A_t} = \frac{54017}{3816} = 14{,}16\ \frac{N}{mm^2}$$

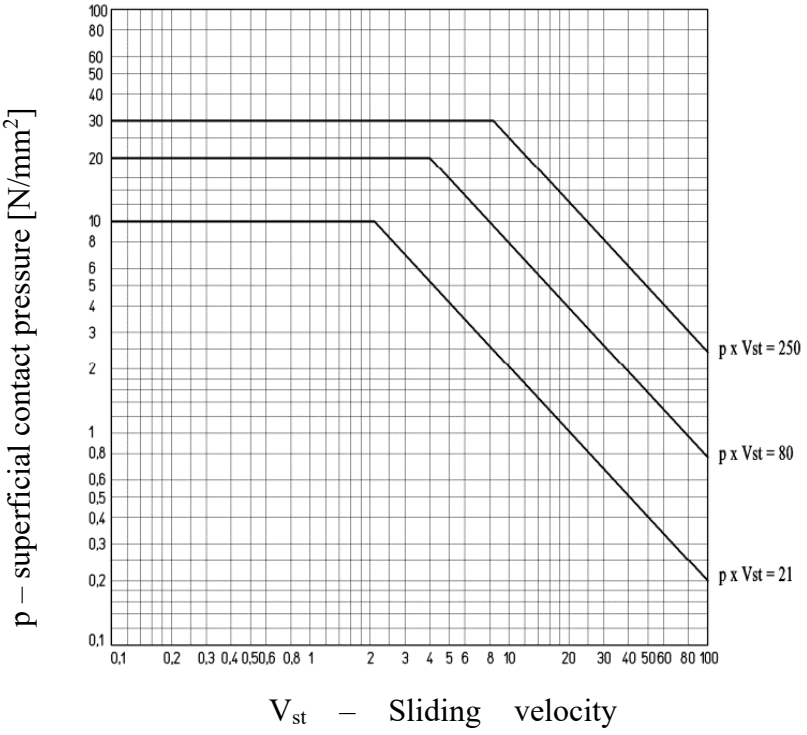

Plot 3.3 Reference plot for the definition of the admissible sliding velocity for the bronze-aluminum nut [10]

Finally, it is possible to denote that alle the possible nut diameter satisfies both requirements, which means that they are all suitable for the solution, still remembering that the smallest as possible solution will be better due to the lack of space.

3.2.1 Gear motor selection

Once the calculations on the nut and screw dimensions have been done, it is possible to obtain also a qualitative value for the required motor torque, the required angular velocity to move the nut at the required linear velocity. From this data, it is possible to select a suitable coupling between a motor and a gear train, keeping in mind also the available space inside the movable cart.

– **Motor selection**

After a very detailed market analysis, the chosen motor will be the brushless DC motor "62 dMove" sold by the Dunkermotoren company, in particular the "62x45" configuration. The following are the characteristics of this specific motor [17].

Data/ Technische Daten		BG 62x45 *dCore*
Nominal voltage/ Nennspannung	VDC	24
Nominal current/ Nennstrom	A[1]	5.1
Nominal torque/ Nennmoment	Nm[1]	0.27
Nominal speed/ Nenndrehzahl	rpm[1]	3210
Stall torque/ Anhaltemoment	Nm[**1]	2.11
Maximum torque/ Maximales Moment	Nm[**1]	2.11
No load speed/ Leerlaufdrehzahl	rpm[1]	3855
Nominal output power/ Dauerabgabeleistung	W[1]	91
Maximum output power/ Maximale Abgabeleistung	W	182
Torque constant/ Drehmomentkonstante	Nm A^{-1}[**1]	0.067
Terminal Resistance/ Anschlusswiderstand	Ω[**1]	0.52
Terminal inductance/ Anschlussinduktivität	mH[**1]	0.95
Starting current/ Anlaufstrom	A[**1]	38.7
No load current/ Leerlaufstrom	A[**1]	0.7
Demagnetisation current/ Entmagnetisierungsstrom	A[**1]	≥ 70
Rotor inertia/ Rotor Trägheitsmoment	gcm^2	262
Weight of motor/ Motorgewicht	kg	1.4

Figure 3.21 Design of the BG 62x45 motor

Table 3.4 General characteristics of the BG 62x45 motor

This motor is a 3-phase Brushless DC motor with high quality 4-pole rare neodymium magnets, a very innovative solution with low noise level and low cogging forces. Since it is a BLDC motor, there will be the need of encoder to control the position of the rotor, which is also directly available from the same company. There is moreover a solution for sensorless control which is available on request, but the presence of some kind of sensors will be more reliable since there are human beings involved in this project.

This motor has been selected primarily as function of the required motor torque. In order to obtain this parameter, it is necessary first of all to obtain the efficiency of the coupling between the selected nut and screw, using this equation:

$$\eta = \frac{1 - f \bullet \mathrm{tg}\alpha}{1 + \frac{f}{\mathrm{tg}\alpha}}$$

η = efficiency
f = dynamic friction coefficient between screw and nut
α = thread angle

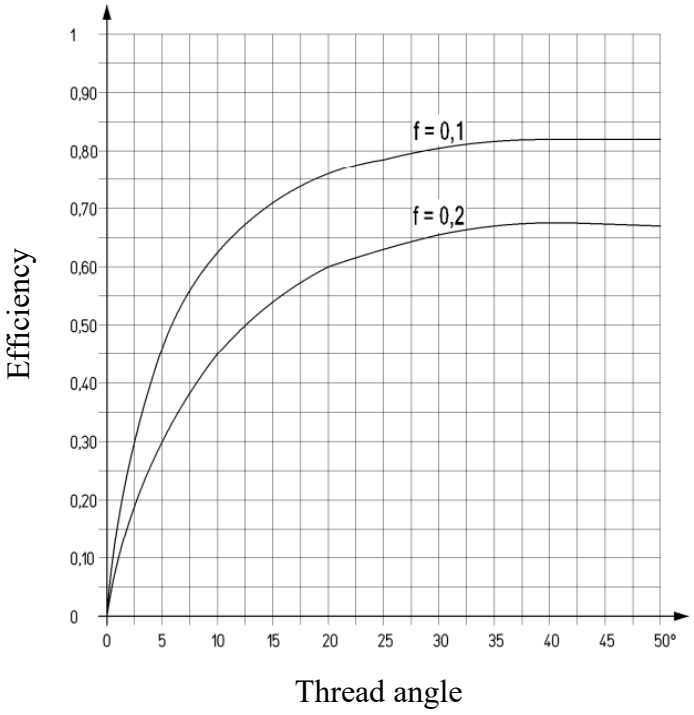

Plot 3.4 Reference plot for the calculation of the efficiency of the transmission between nut and screw [10]

$$\eta = \frac{1 - 0{,}2 \cdot \tan\,(3{,}25°)}{1 + \frac{0{,}2}{\tan\,(3{,}25°)}} = 0{,}2186 \qquad (3.14)$$

$$\eta = \frac{1 - 0{,}1 \cdot \tan\,(3{,}25°)}{1 + \frac{0{,}1}{\tan\,(3{,}25°)}} = 0{,}3601 \tag{3.15}$$

The first one is the efficiency of the mechanism during the starting phase, where the friction between the nut and the screw is higher and equal to 0,2, while the second one is the dynamic efficiency of the transmission with a friction coefficient equal to 0,1, as it is also visible from the graph 3.2.

Once that the two efficiencies have been obtained, it is possible to calculate the required torque both during the starting phase and during the dynamic operation. To do that, it is possible to use this equation:

$$C = \frac{F \bullet P}{2\,\pi\,\eta\,1000}$$

C = torque [Nm]
F = axial force on the nut [N]
P = screw pitch [mm]
η = efficiency

$$C = \frac{17425 \cdot 6}{2 \cdot \pi \cdot 0{,}2186 \cdot 1000} = 76{,}2\ Nm \tag{3.15}$$

$$C = \frac{17425 \cdot 6}{2 \cdot \pi \cdot 0{,}3601 \cdot 1000} = 46{,}2\ Nm \tag{3.16}$$

Looking at the torque Vs speed curve which characterize this specific motor configuration, it is possible to see that the highest as possible torque that can be deliver is 1,5 Nm at very low angular velocity. Considering a reduction ratio of 100, which is usually the highest as possible for 2 stage epicyclical gear train, the maximum available torque is around 150 Nm, verifying both requirements. The specific working point of the motor will be analyzed more in detail once the gear train has been selected.

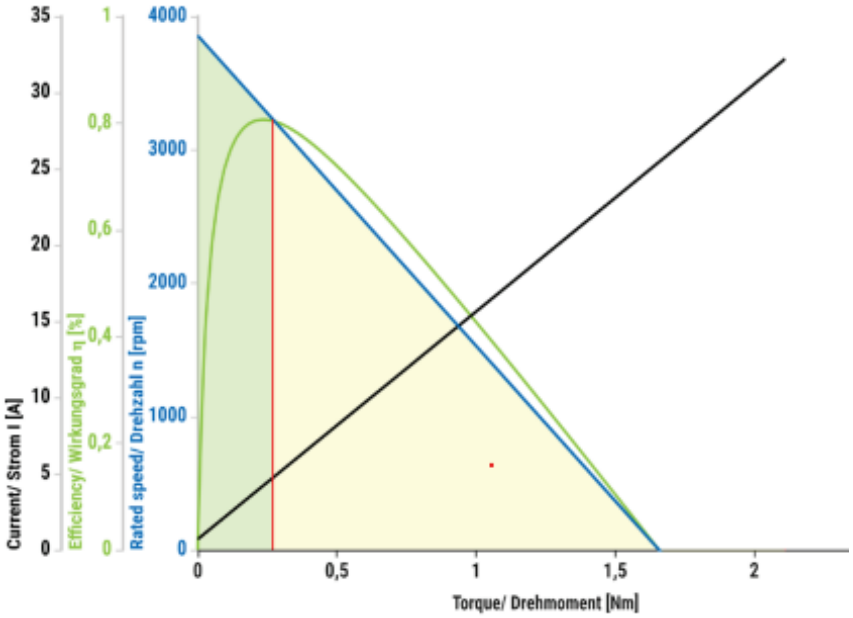

Plot 3.5 Characteristic plot of the BG 62 x 45 motor, showing current, efficiency and speed of rotation as function of the produced torque [17]

– **Gear train selection**

The selection of a suitable gear train was made considering that its reduction ratio should be around 100 in order to reach both the torque and angular velocity requirements. Moreover, another very important characteristic is its overall dimensions, which should be as low as possible while ensuring the torque transmissibility. After a very detailed market analysis, it was clear that the smallest gear trains available were the ones of the Wittestein company. Between them, the smallest model which is able to transmit the required starting torque is the CP 025 MF. The reduction ratio will be exactly 100, which is also the highest as possible. All the others feature, along with the CAD drawings, are shown below [8].

Figure 3.22 Design of the CP 025 MF gear train

				2-stadi			
Rapporto di riduzione		**i**		**100**	Forza assiale max. [c]	F_{2AMax}	N	1600
Coppia max. [a] [b] [e]		T_{2a}	Nm	144	Forza radiale max. [c]	F_{2QMax}	N	1200
Coppia di accelerazione max. [e] (max. 1000 cicli per ora)		T_{2B}	Nm	90	Coppia di ribaltamento max.	M_{2KMax}	Nm	54
Coppia di emergenza [a] [b] [e] (fino a 1000 volte durante la vita del riduttore)		T_{2Not}	Nm	187	Rendimento a pieno carico	η	%	95
Velocità nominale media in ingresso [d] (a T_{2N} e temperatura ambiente di 20°C)		n_{1N}	rpm	3600	Peso (inclusa flangia di adattamento standard)	m	kg	3,7
Velocità max. in ingresso		n_{1Max}	rpm	7000	Rumorosità (per i e n_1 di riferimento consultare cymex®)	L_{PA}	dB(A)	≤ 62
Coppia senza carico media [b] (a n_1=3000 rpm e e temp. misurata sul riduttore di 20°C)		T_{01Z}	Nm	0,21	Temperatura max. ammissibile sulla carcassa		°C	+90
Momento d'inerzia (riferito all'ingresso)	E 19	J_1	10^{-4}·kgm²	0,54	Temperatura ambiente		°C	da –15 a +40
Diametro morsetto calettatore [mm]	G 24	J_1	10^{-4}·kgm²	1,4	Lubrificazione			a vita
					Senso di rotazione			concorde tra ingresso e uscita
					Grado di protezione			IP 64

Table 3.5 General characteristics of the CP 025 MF gear train [8]

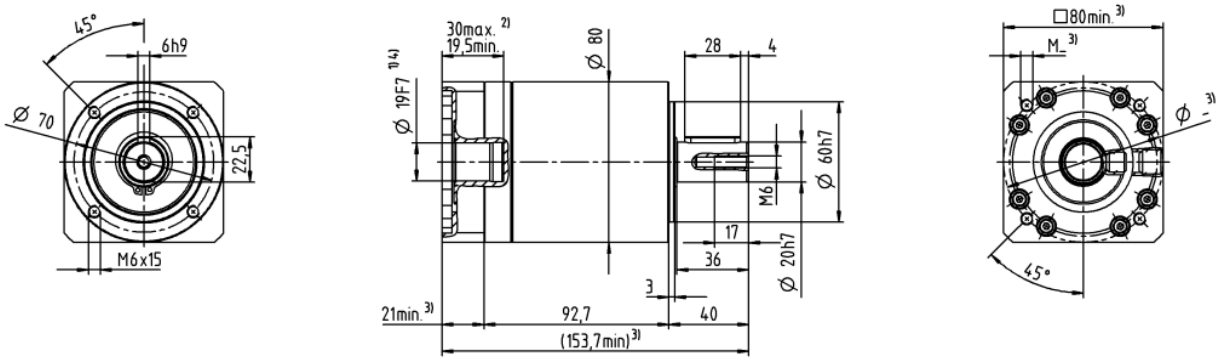

Figure 3.23 CAD drawings of the CP 025 MF gear train [8]

The problems related with this model are two: the first one is the class protection, which is lower than the required one for a mechanism under constant water exposure, but it can be dealt with the company using specific painting on the gearbox without reducing its internal efficiency. The second one, instead, is the considerable overall dimensions: even if it is one of the most compact solutions available on the market, it is still quite big, which means that there will be the need of a very detailed parametric analysis and probably also some modification of the external shape of the gear train, without changing the internal functioning.

Once that all the components have been defined it is possible to summarize the results, also the check the feasibility of the project and to avoid errors during the development phase, where they are still correctable without relevant consequences.

The following is the table which summarize the features of the selected coupling between nut and screw.

SCREW	PITCH	MEAN DIAMETER [mm]	THREAD ANGLE [°]	THREAD ANGLE [rad]	RADIAL VELOCITY [mm/s]	ω [rpm]
KAM 35	6	32,23	3,25	0,06	52,83	31,31

NUT	CONTACT AREA At [mm^2]	SUPERFICIAL CONTACT PRESSURE p [N/mm^2]	V_{st} [m/min]	$V_{st\ graph}$ [m/min]	$P*V_{st\ max}$	INERTIA FORCE FACTOR	$P*V_{st\ adm}$	$P*V_{st\ calc}$
HAL 35 A R	5277	3,22	3,31	7,00	22,55	0,80	18,04	10,68

Table 3.6 Summary of the calculations performed on the selected coupling between nut and screw

Then, taking the selected motor and gear train, it is possible to summarize the input and output features of the complete mechanism, checking if the match the nut and screw requirements.

SCREW	MOTOR TORQUE [Nm]	MOTOR SPEED [rpm]	REDUCTION RATIO	OUTPUT TORQUE [Nm]	OUTPUT SPEED [rpm]
35 x 6	0,8	2200	100	80	22

Table 3.7 General characteristics of the designed mechanism

As it is visible from the graph 3.4, during the starting phase the motor can transmit up to 1,5 Nm, with a very low angular velocity, which is very useful to overcome the high static friction between the nut and the screw. Once that a stationary condition has been reached, characterized by a complete dynamic condition, the required torque diminishes while the angular velocity increase, until the working point has been reached. Looking at the graph 3.4 once again, it is clear that the selected working point is not the optimal one, since the required output torque during the dynamic condition is higher than the nominal value. However, it is necessary to keep in mind that this mechanism will be actuated one or two times per day, which allows to work in more severe condition with respect to a continuous operation. Finally, considering an average rotational speed of the screw equal to 22 rpm, a complete moving from fully up to fully down will be performed in about 33 seconds, which meet the requirements.

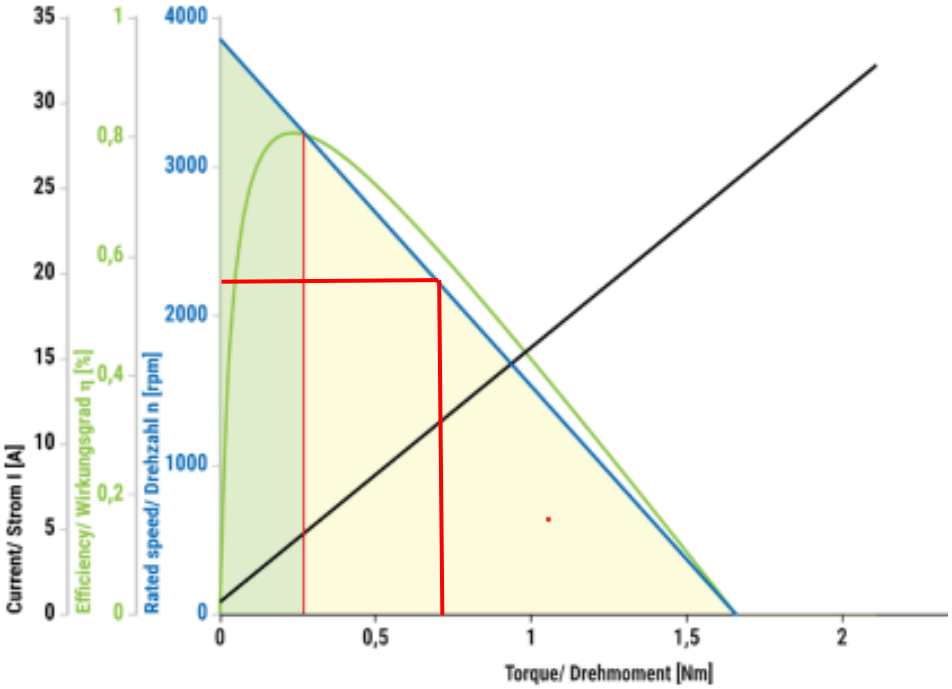

Plot 3.6 Working point of the BG 62 x 45 motor [17]

3.2.2 Parametric analysis

Once that all the components have been selected and the preliminary requirements have been verified, it is necessary to perform the parametric analysis, which allows to define the hinge points location of the whole mechanism. From this analysis the final result will be the effective arm distance between the application point of both the static and dynamic moment and the application point of the force coming out from the actuation mechanism. Once that this effective arm distance will be defined, the previous calculations will be updated and the requirements will be verified once again, since a little change in the arm distance can result in a huge change in the applied force and consequently the mechanism could no longer sustain the new resulting load. This analysis will be performed first of all using Excel, were all the distances and the angles will be calculated using trigonometric equations. Then the results will be used to draw a preliminary sketch of the mechanism on the Autocad software in order to understand the effective dimensions of the mechanism, verifying if it fits inside the movable cart.

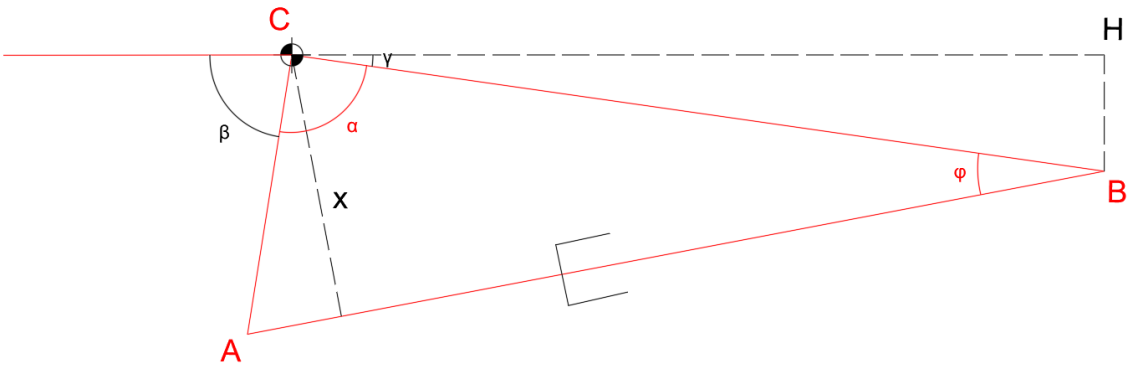

Figure 3.24 Schematic sketch of the position of the hinge points of the nut and screw solution

CH	383,55	mm
BH	34,60	mm
BC	385,11	mm
γ	0,09	rad
AC	103,30	mm
β	73,40	°

	α [rad]	α [°]	AB [mm]	φ [rad]	x [mm]	AB INCLINATION [rad]
UP	2,12	121,41	447,71	0,20	75,84	0,11
MID	1,77	101,41	417,99	0,24	93,29	0,15
DOWN	1,42	81,41	383,52	0,27	102,56	0,18

Table 3.8 General dimensions of the positioning of the hinge points for the nut and screw solution

Looking at the results of this analysis, the smallest as possible arm distance is 75 mm, which is lower than arm distance used to calculate the required dynamic force from the nut and screw mechanism, which means that all the calculations have to been updated.

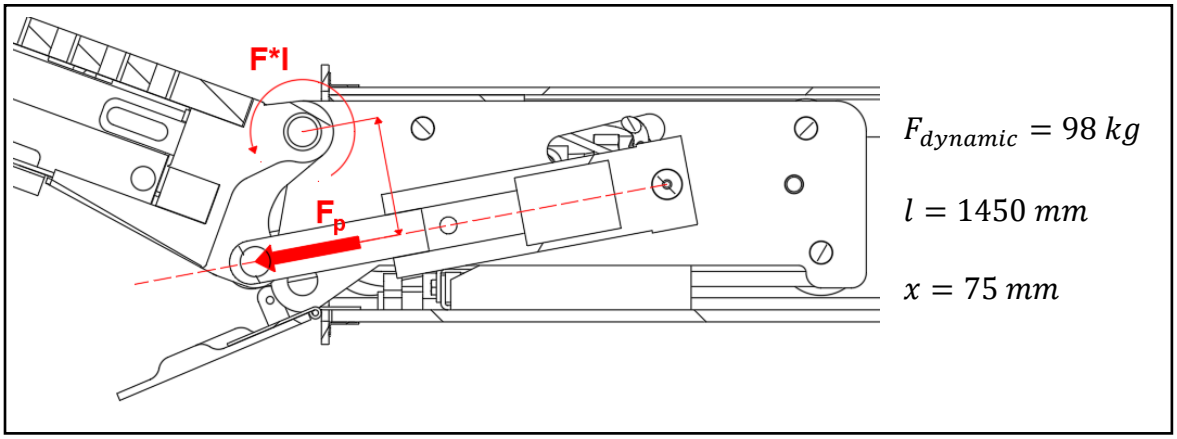

$$F_{p\ dynamic} = \frac{F_{dynamic} \cdot l}{x} \tag{3.17}$$

$$F_{p\ dynamic} = \frac{98 \cdot 9{,}81 \cdot 1450}{75} = 18586{,}68\ N$$

Once that the new dynamic force requirement has been defined, it is possible to update all the nut calculations, in order to verify both the sliding and the static requirements.

NUT	CONTACT AREA At [mm^2]	SUPERFICIAL CONTACT PRESSURE p [N/mm^2]	V_{st} [m/min]
HAL 30 A R	3816	4,87	2,60
HAL 35 A R	5277	3,52	3,31
HAL 40 A R	6880	2,70	3,29
HAL 50 A R	10840	1,71	3,38
HAL 60 A R	15700	1,18	4,59

NUT	$V_{st\ graph}$ [m/min]	$P*V_{st\ max}$	INERTIA FORCE FACTOR	$P*V_{st\ adm}$	$P*V_{st\ calc}$
HAL 30 A R	4,31	21,00	0,80	16,80	12,66
HAL 35 A R	5,96	21,00	0,80	16,80	11,67
HAL 40 A R	7,77	21,00	0,80	16,80	8,89
HAL 50 A R	12,25	21,00	0,80	16,80	5,80
HAL 60 A R	17,74	21,00	0,80	16,80	5,44

Table 3.9 Update of the calculations performed on the nut

From this table, it is clear that the sliding velocity requirements are still verified after the increase of the dynamic force: the calculated $p \cdot v_{st}$ is lower than admissible one for all the possible nut diameters, which means that they are all suitable for the current application.

The following step is the updating of the static requirement: to do that, it is necessary to calculate the new superficial contact pressure in static condition and verify if it is still lower than the 30 N/mm^2, which can be considered as the maximum sustainable superficial contact pressure for a bronze – aluminum nut.

To obtain the superficial contact pressure, first of all it is necessary to obtain the new static force and this equation can be used:

$$F_{p\ static} = \frac{F_{static} \cdot l}{x} \tag{3.18}$$

$$F_{p\ static} = \frac{150 \cdot 9{,}81 \cdot 2900}{75} = 56898\ N$$

Once that the new static force requirement has been defined, it is possible to update also the superficial contact pressure in the static situation, using this equation:

$$p = \frac{F_{\ static}}{A_t} = \frac{56898}{3816} = 14{,}91\ \frac{N}{mm^2} \tag{3.19}$$

Since this value is still way lower than the maximum 30 N/mm^2, also the new static requirement can be considered satisfied, which means that all the requirements are satisfied with the projected arm distance of 75 mm.

3.2.3 Components design

This part of this dissertation will be dedicated in showing the evolution of the design of the various components which are present inside the mechanism, starting from the CAD drawing, followed by the preliminary design, the final design and the final assembly.

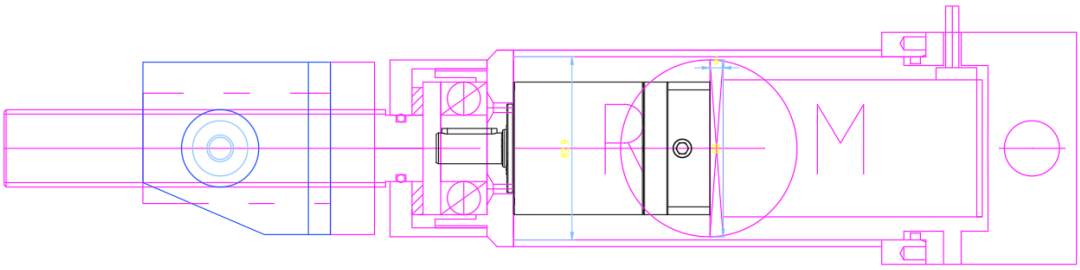

Figure 3.25 Autocad drawing of the whole mechanism designed

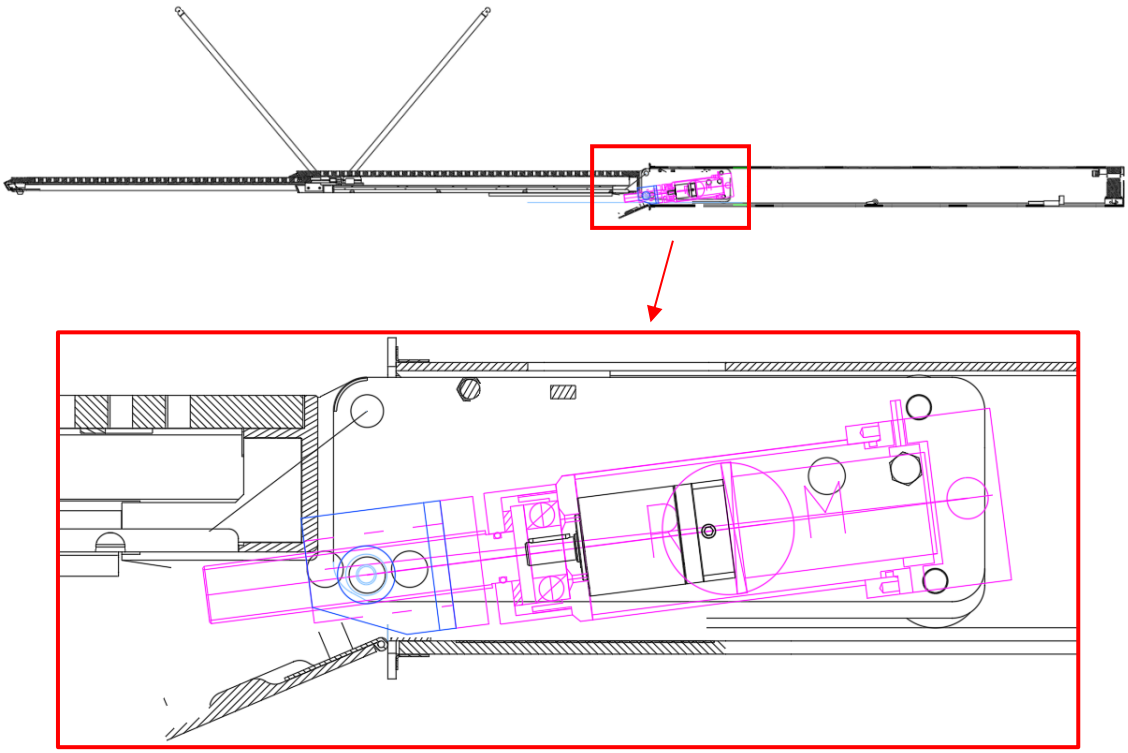

Figure 3.26 Autocad drawing of the positioning of the mechanism inside the passerella, in red a more zoomed view

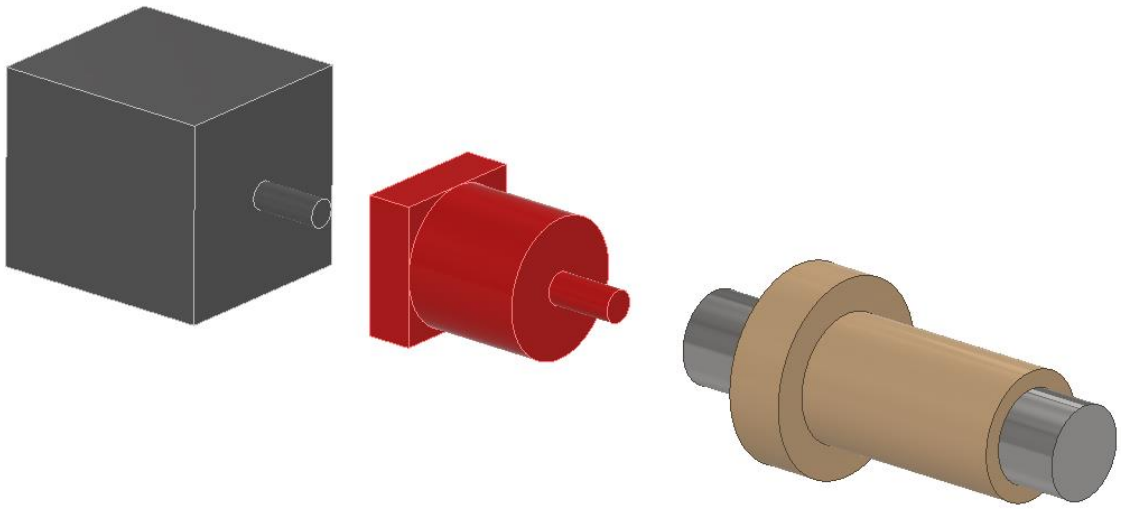

Figure 3.27 Preliminary design of the main components of the mechanism

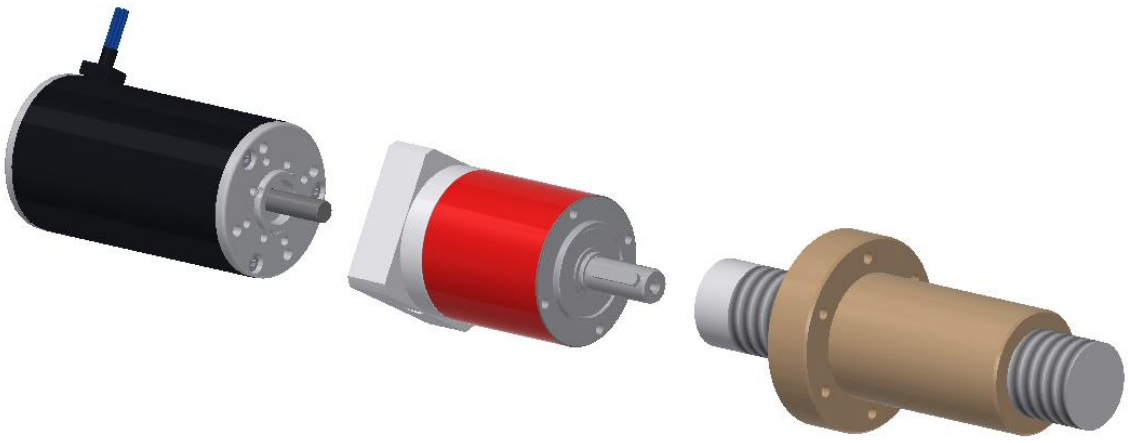

Figure 3.28 Final design of the main components of the mechanism

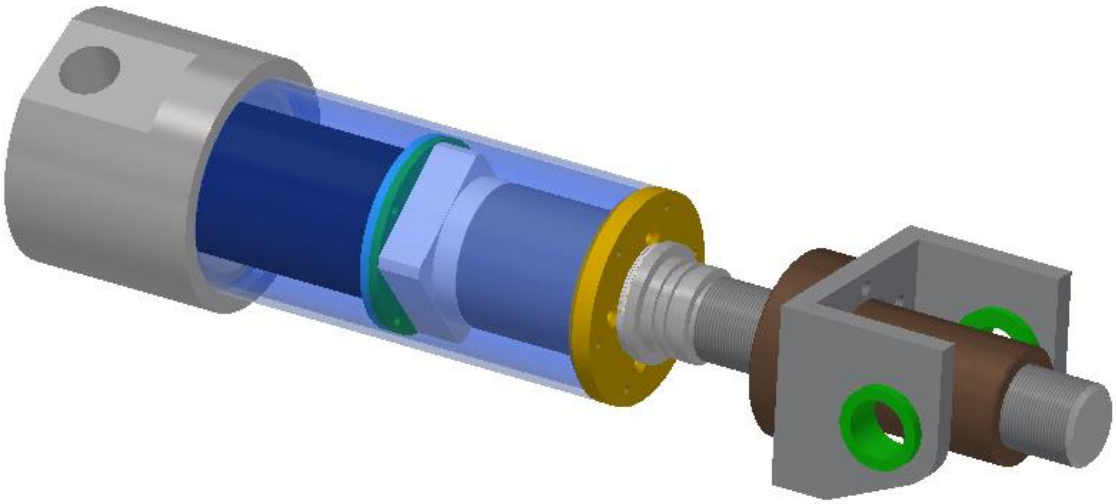

Figure 3.29 Final design of the whole mechanism, already with the joints and supports of the main components and intrusion protection where necessary

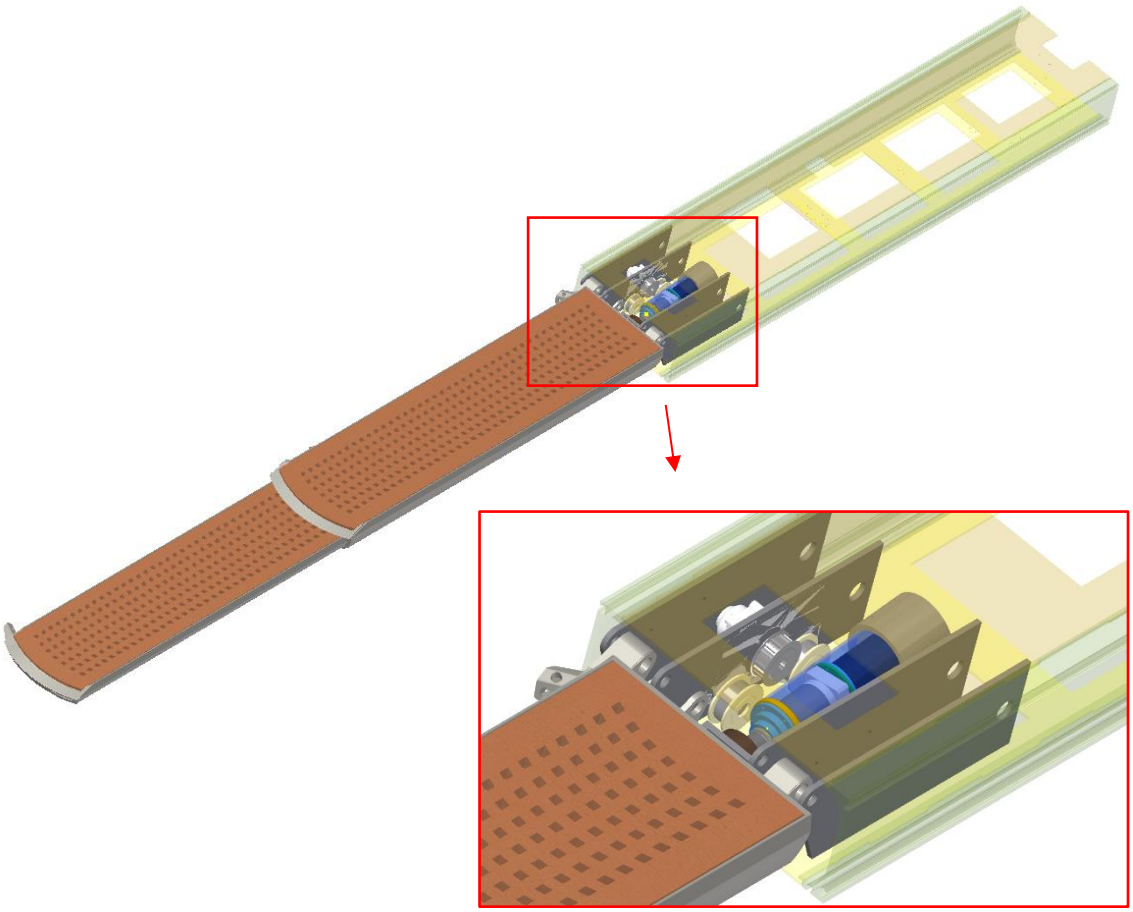

Figure 3.30 Isometric view of the positioning of the final mechanism

4. Energetic Analysis

The last chapter of this dissertation will be dedicated in analyzing the energy consumption of both the hydraulic and the electric solution, in order to have a more detailed view of the advantages and improvements of the electric solution with respect to the hydraulic one but also the weak points, where future efforts could be concentrated.

4.1 Hydraulic solution

For what concerns the hydraulic solutions, the first calculations are aimed at defining the required pressure drop and oil capacity for each actuator. These results will be interesting for the definition of the efficiencies of the systems but also for understanding the amount of waste in terms of energy, pressure drop and capacity for each actuator. As a matter of fact, they are all connected to the same pressure pump, which is designed to satisfy the most demanding requirement from the actuators. As a consequence, all the exceeding pressure drop is relieved using non-return valves placed at the intake manifold of the actuators, while the exceeding oil returns to the reservoir, representing a strong waste in terms of energy consumption.

The second part is dedicated to the definition of a typical cycle performed by the gangway, obtaining in this way the running time of the pressure pump: as a matter of fact, the pressure pump runs continuously during the whole cycle time, which means that the energy drawn by the pump is function of this cycle time.

4.1.1 First movement: exiting from the box

For this first movement, the adopted hydraulic motor has the following characteristics.

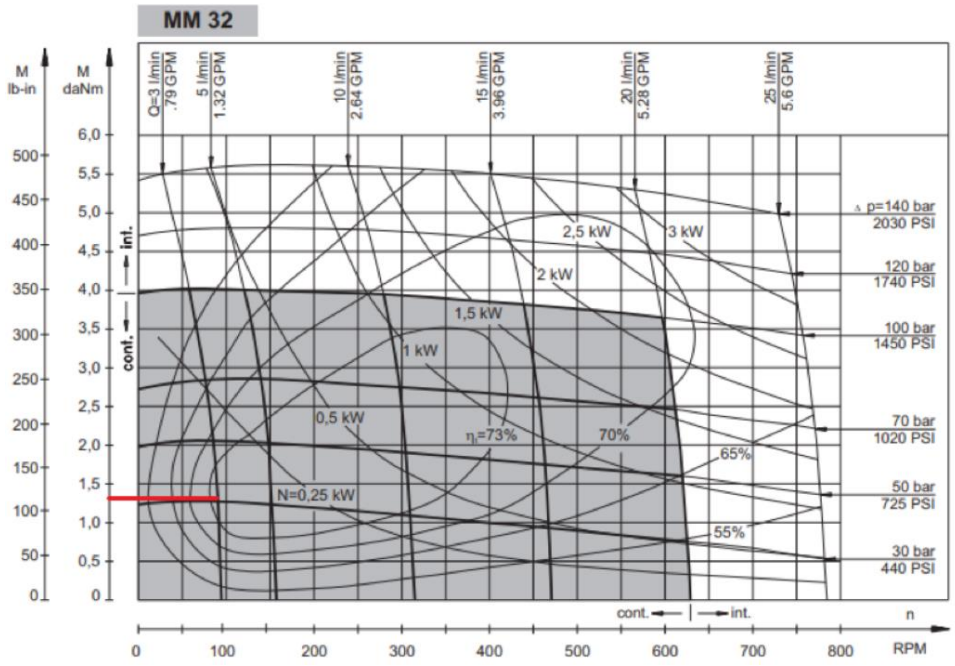

Plot 4.1 Characteristic plot of the hydraulic motor used for exiting from the box

$$Engine\ capacity\ (c.c.) = 32\ \frac{cm^3}{rev}$$

$$\Delta p = 97 - 70 = 27\ bar$$

$$\eta_t = 0{,}76$$

$$M = 13\ Nm$$

$$M = \frac{c.c.\ \cdot\ \Delta p\ \cdot\ \eta_{m,h}}{20\ \cdot\ \pi} \tag{4.1}$$

$$\eta_{m,h} = \frac{M\ \cdot\ 20\ \cdot\ \pi}{c.c.\ \cdot\ \Delta p} = \frac{13\ \cdot\ 20\ \cdot\ \pi}{32\ \cdot\ 27} = 0.94 \tag{4.2}$$

$$\eta_v = \frac{\eta_t}{\eta_m} = \frac{0{,}76}{0{,}94} = 0{,}81 \tag{4.3}$$

$$Q = \frac{c.c.\ \cdot\ \omega}{1000\ \cdot\ \eta_v} = \frac{32\ \cdot\ 100}{1000\ \cdot\ 0{,}81} = 3{,}95\ {}^{l}/_{min} \tag{4.4}$$

4.1.2 Second movement: telescopic elongation / compression

For the second movement, the adopted hydraulic piston has the following characteristics.

$\Delta p_{push} = 40 - 19 = 21\ bar$

$\Delta p_{pull} = 77 - 33 = 44\ bar$

$stroke\ (s) = 1200\ mm$

$t_{push} = 17\ s$

$t_{pull} = 12\ s$

$v_{push} = \frac{s}{t} = \frac{1200}{17} = 70{,}6\ {}^{mm}/_{s}$

$v_{pull} = \frac{s}{t} = \frac{1200}{12} = 100\ {}^{mm}/_{s}$

$d_p = 32\ mm$

$d_s = 18\ mm$

$A = \pi \cdot \left(\frac{d_p}{2}\right)^2 = \pi \cdot \left(\frac{32}{2}\right)^2 = 8{,}04\ cm^2$

$a = \pi \cdot \left(\frac{d_s}{2}\right)^2 = \pi \cdot \left(\frac{18}{2}\right)^2 = 2{,}55\ cm^2$

$$Q_{push} = \frac{v \cdot A}{166{,}67} = \frac{70{,}6 \cdot 8{,}04}{166{,}67} = 3{,}41\ {}^{l}/_{min} \quad (4.5)$$

$$Q_{pull} = \frac{v \cdot (A - a)}{166{,}67} = \frac{70{,}6 \cdot (8{,}04 - 2{,}55)}{166{,}67} = 3{,}30\ {}^{l}/_{min} \quad (4.6)$$

4.1.3 Third movement: inclination of the gangway

The following are the characteristics of the hydraulic piston adopted for the third movement.

$F_p = 98\ kg$

$l = 2877\ mm$

$b_{piston}\ (0°) = 89\ mm$

$b_{piston}\ (+20°) = 79{,}2\ mm$

$C.S. = 1{,}1$

$t_{push} = 20\ s$

$t_{pull} = 15\ s$

$stroke\ (s) = 55\ mm$

$v_{push} = \frac{s}{t} = \frac{55}{20} = 2{,}75\ {}^{mm}/_{s}$

$v_{pull} = \frac{s}{t} = \frac{55}{15} = 3{,}6\ {}^{mm}/_{s}$

$d_p = 50\ mm$

$d_s = 35\ mm$

$A = \pi \cdot \left(\frac{d_p}{2}\right)^2 = \pi \cdot \left(\frac{50}{2}\right)^2 = 19{,}63\ cm^2$

$a = \pi \cdot \left(\frac{d_s}{2}\right)^2 = \pi \cdot \left(\frac{35}{2}\right)^2 = 9{,}62\ cm^2$

$$F\ (0°) = \frac{F_p\ \cdot\ g\ \cdot\ \frac{l}{2}}{b_{piston}} = \frac{98\ \cdot\ 9{,}81\ \cdot\ \frac{2877}{2}}{89} = 15538{,}8\ N \qquad (4.7)$$

$$F\ (+20°) = \frac{F_p\ \cdot\ \cos\ (20°)\ \cdot\ g\ \cdot\ \frac{l}{2}\ \cdot\ \cos\ (20°)}{b_{piston}} =$$

$$= \frac{98\ \cdot \cos\ (20°) \cdot 9{,}81\ \cdot\ \frac{2877}{2}\ \cdot \cos\ (20°)}{79{,}2} = 15418{,}9\ \ N \qquad (4.8)$$

$$F_{C.S.}\ (each\ piston) = \frac{F\ (0°)\ \cdot\ C.S.}{2} = \frac{15538{,}8\ \cdot\ 1{,}1}{2} = 8546{,}1\ N \qquad (4.9)$$

$$\Delta p = \frac{F}{A} = \frac{8546{,}1}{\pi\ \cdot\ 25^2} = 4{,}35\ MPa = 43{,}5\ bar \qquad (4.10)$$

$$Q_{push} = \frac{v\ \cdot\ A}{166{,}67} = \frac{2{,}75\ \cdot\ 19{,}63}{166{,}67} = 0{,}324\ {}^{l}/_{min} \qquad (4.11)$$

$$Q_{pull} = \frac{v\ \cdot\ (A - a)}{166{,}67} = \frac{3{,}6\ \cdot\ (19{,}63 - 9{,}62)}{166{,}67} = 0{,}216\ {}^{l}/_{min} \qquad (4.12)$$

4.1.4 Pressure pump

The adopted pump which has to satisfy all the previous requirements about the hydraulic motor and the two hydraulic piston is a Gear Pump connected to a Permanent Magnet Direct Current electric motor with a nominal power of 800 W and a DC voltage of 24 V. This gear pump works with a constant volumetric flow and a constant pressure drop, but the three different actuators work with a different pressure drop and a different volumetric flow. For this reason, the working point of the gear pump it is selected in such a way that it can satisfy the most demanding requirement, while all the exceeding flow or pressure drop in the other actuators are wasted using specific valves at the input port of the actuators. The following are the characteristics and the selected working point of this gear pump.

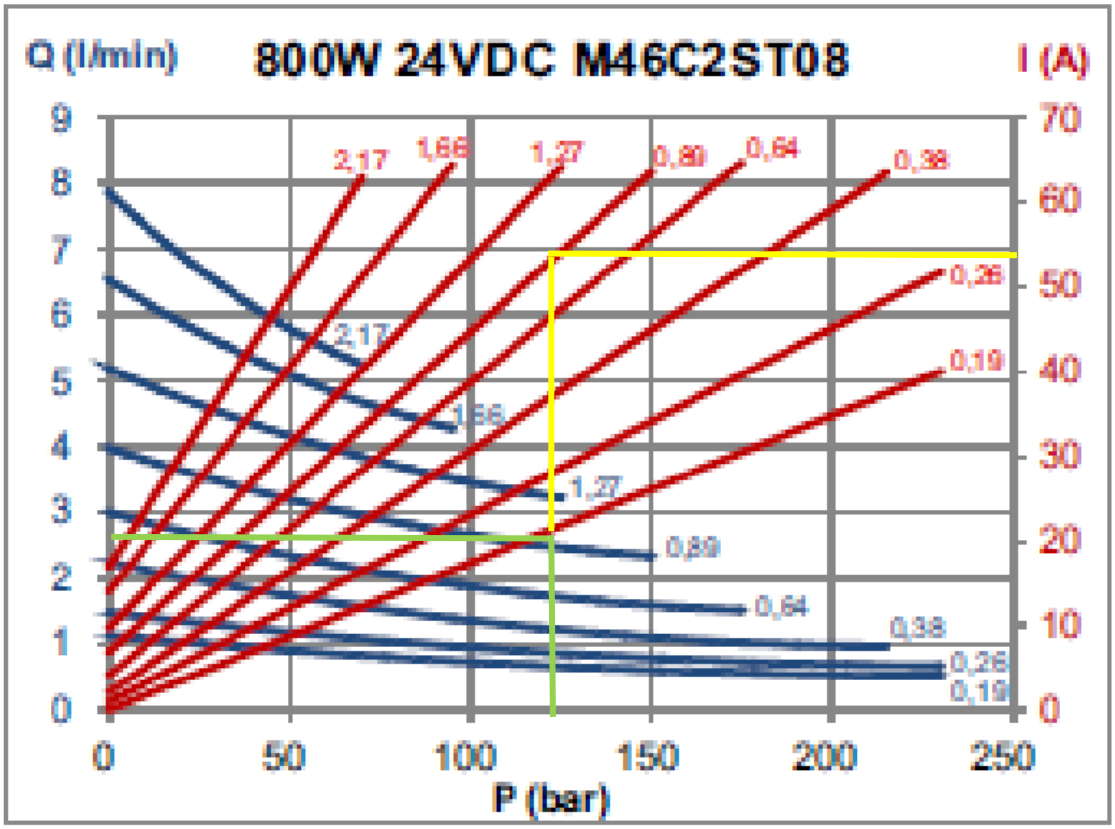

Plot 4.2 Characteristic plot of the pressure pump showing both the capacity and the drawn current as function of the build-up pressure

$volumetric\ capacity\ (c.c.) = \ 0{,}89\ {}^{cm^2}/_{rev}$

$\Delta p \ = \ 120\ bar$

$Q_p \ = \ 2{,}8\ {}^{l}/_{min}$

$V_{DC} \ = \ 24\ V$

$I_{120\ bar} \ = \ 55\ A$

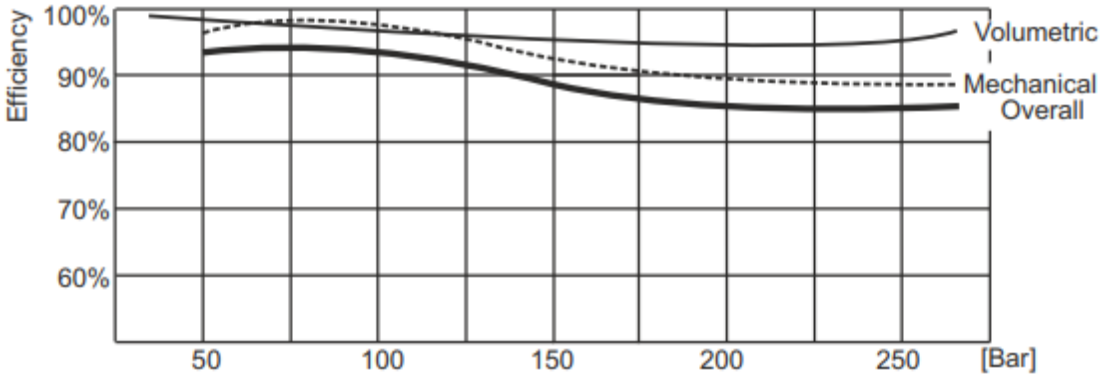

Plot 4.3 Efficiencies plot directly taken from the pump catalogue

$$\eta_p \ = \ \eta_{vol} \ \cdot \ \eta_{mech} \ \cdot \ \eta_{overall} \ = \ 0{,}96 \ \cdot \ 0{,}96 \ \cdot \ 0{,}92 \ = \ 0{,}85 \qquad (4.13)$$

$$P_{th} \ = \ Q_p \ \cdot \ \Delta p \ = \ \frac{2{,}8 \ \cdot \ 120}{0{,}6} \ = \ 560\ W \qquad (4.14)$$

$$P_{abs} \ = \ V \ \cdot \ I = \ 24 \ \cdot \ 55 \ = 1320\ W \qquad (4.15)$$

$$\eta_t \ = \ \frac{P_{th}}{P_{abs}} \ = \ \frac{560}{1320} = 0{,}42 \qquad (4.16)$$

In order to define the total energy absorbed by the pump during the actuation of the gangway, it is necessary to define a cycle which will be also used for determining the energy absorbed by the electric solution during the same cycle. The two values will be finally compared.

4.1.5 Cycle time definition

- Exiting from the box: 7 s
- Telescopic elongation: 17 s
- Inclination of the gangway towards the sky: 10 s
- Return of the gangway on horizontal position: 7 s
- Telescopic compression: 12 s
- Entering inside the box: 7 s

$$\text{TOTAL CYCLE TIME} = 60 \text{ s}$$

$$E_{abs\,hyd} = P_{abs} \cdot t_{cycle} = 1320 \cdot 60 = 79{,}2\ kJ \qquad (4.17)$$

Once the cycle time has been defined, it is possible to consider both the maximum working time and the required idle cool-down time. Once they have been obtained, they will be compared with the cycle in order to define if they meet the requirements or not.

To obtain these values, it is necessary to use the "Motor Ratings" diagram in this way:

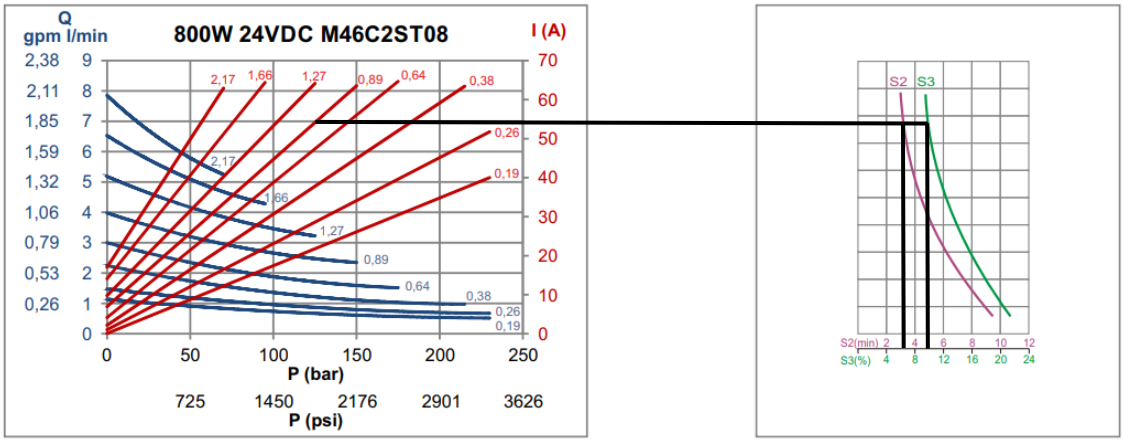

Plot 4.4 Matching of the two plots of the pressure pump; the plot on the right is used for the calculation of the idle cooling time

From the graph above it is possible to see that the maximum working time for this motor-pump is 3 minutes (S2 curve) while the S3 curve is about 10 %, which means that after 3 minutes of working, the pump should be idle for cooling for at least 30 minutes. Considering our working cycle of 60 s, the first requirements about the maximum working is met, while the second requirements is strongly dependent on the behavior of the customer: as a matter of fact, not all the customers respect the cooling idle time, and they actuate the gangway even if its motor is not completely cooled. This wrong behavior is not so influent on the performances of the passerella, which means that it still works even if it is not completely cooled; however, it is clear that this behavior can reduce the life of this component, increasing its wear. Moreover, since the considered cycle time is 60 s, the cooling time should be around 10 minutes, which is not a huge amount of time.

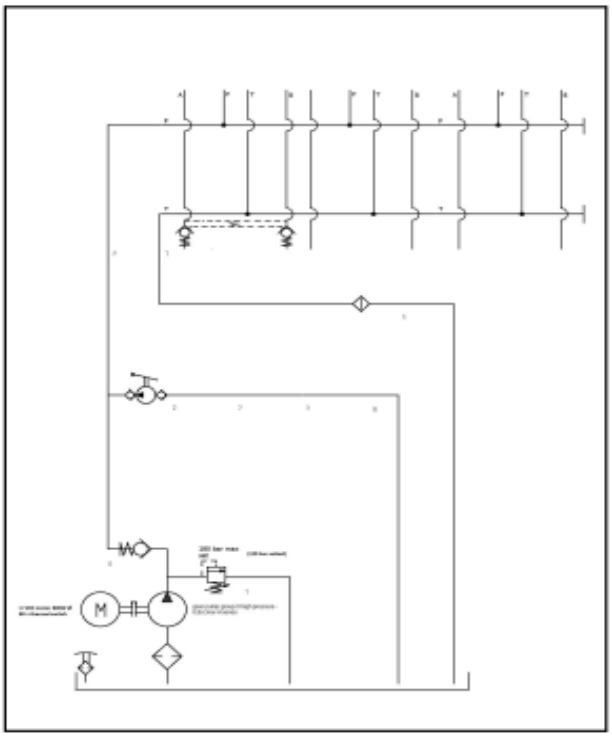

Figure 4.1 Hydraulic scheme of the pressure pump

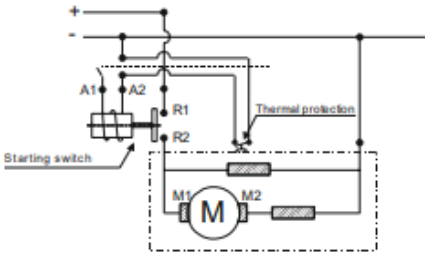

Figure 4.2 Electric connection scheme of the motor

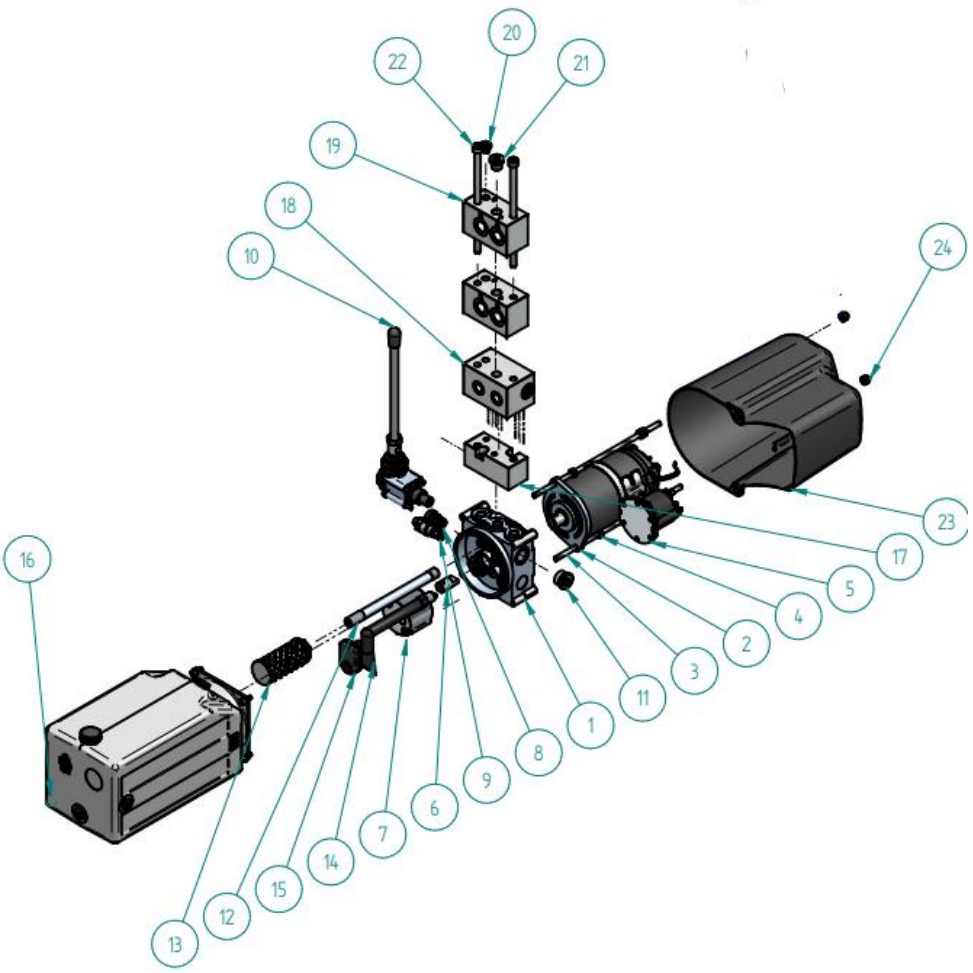

Figure 4.3 Exploded view of the pressure pump assembly

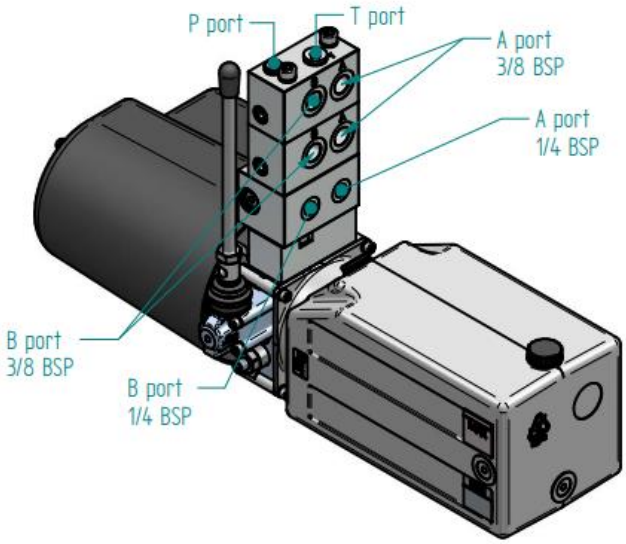

Figure 4.4 External design of the pressure pump assembly

4.2 Electric solution

For what concerns the electric solution, first of all it is necessary to define the working points of all the motors that can satisfy the requirements. Once that the working points have been defined, it is possible to take the current drawn by the motors at that specific speeds and torque. In this way, the effective power absorbed by the motors can be obtained and multiplying this value for the working time of each motor, the effective energy consumed by each motor can be obtained as well. As it is clear, the electric situation is slightly different from the hydraulic one for what concerns the cycle time: the pressure pump works continuously during the whole cycle time, while the same cannot be said for the electric motors. As a matter of fact, they work one at a time, just for their own running time, which is the one necessary to complete the assigned movement. For these reasons, in order to calculate the total energy absorbed, it necessary to multiply the instantaneous power absorbed by each motors with their own working time, and finally sum up these three values.

4.2.1 1° Movement: exiting from the box

– **Motor reductor**: "RAO – 4" (Sir)

$C = 13\ Nm$

$\omega = 60\ rpm$

$t = 10\ s$

$V_{DC} = 24\ V$

$I = 9\ A$

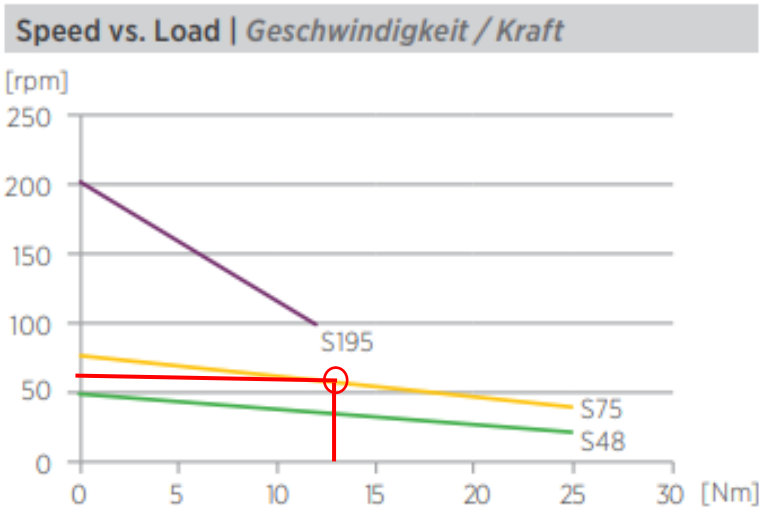

Plot 4.5 Torque Vs speed plot of the RAO - 4 motor

$$P_{th} = C \cdot \omega = 13 \cdot 60 \cdot \frac{\pi}{30} = 81{,}7\ W \tag{4.18}$$

$$P_{abs} = V_{DC} \cdot I = 24 \cdot 9 = 216\ W \tag{4.19}$$

$$\eta = \frac{P_{th}}{P_{abs}} = \frac{81{,}7}{216} = 0{,}38 \tag{4.20}$$

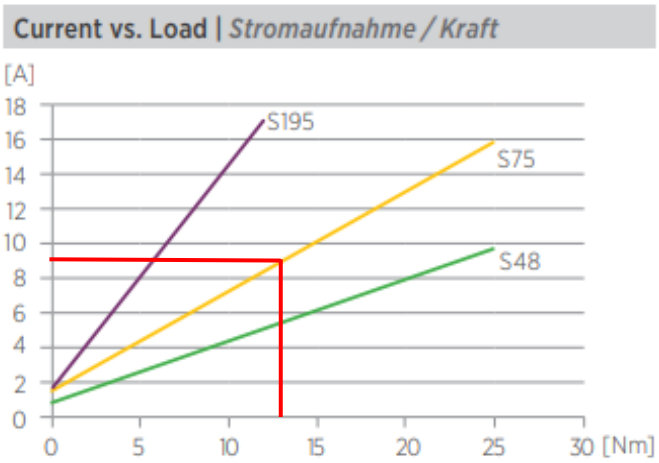

Plot 4.6 Drawn Current Vs Torque of the RAO - 4 motor

4.2.2 2° Movement: telescopic elongation / compression

- **Motor:** BG 42 x 30 (Dunkermotoren)
- **Gear train:** CPK 015 MF (i = 100)

In this energetic analysis, the adopted electric solution for the telescopic movement is a little bit different form the solutions proposed in this dissertation. The following are the data fundamental for the calculation of the energy spent during the movement.

$C = 0{,}6\ Nm$

$\omega = 2300\ rpm$

$t = 26\ s$

$V_{DC} = 24\ V$

$I = 10\ A$

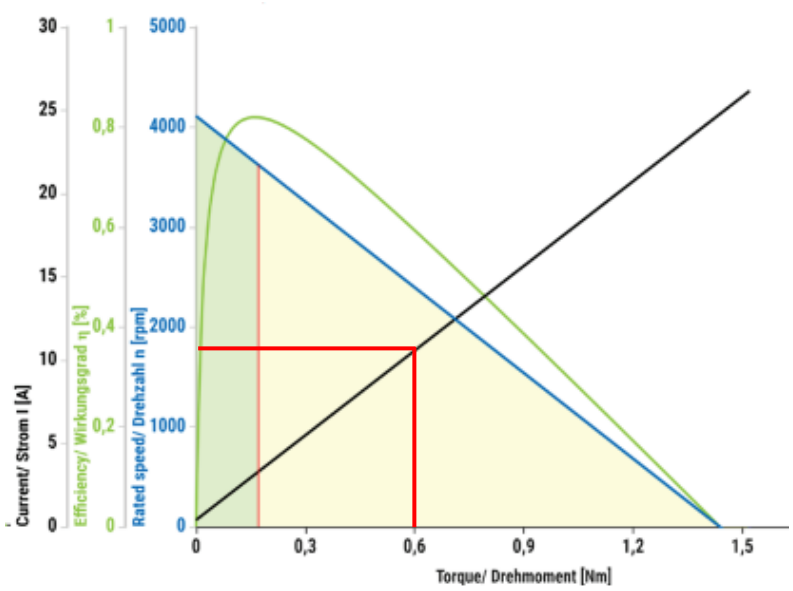

Plot 4.7 Characteristic plot of the BG 42 x 30 motor

$$P_{th} = C \cdot \omega = 0.6 \cdot 2300 \cdot \frac{\pi}{30} = 144{,}5\ W \qquad (4.21)$$

$$P_{abs} = V_{DC} \cdot I = 24 \cdot 11 = 264\ W \qquad (4.22)$$

$$\eta = \frac{P_{th}}{P_{abs}} = \frac{144{,}5}{264} = 0{,}55 \qquad (4.23)$$

4.2.3 3° Movement: inclination of the gangway

- **Motor:** BG 62 x 45 (Dunkermotoren)
- **Gear train:** CP 025 MF (Wittestein)

$stroke\ (s) = 65\ mm$

$v\ =\ 2{,}27\ \ {}^{mm}/_{s}\ \ (linear\ velocity\ of\ the\ nut)$

$t = \dfrac{{}^{s}/_{2}}{v}\ =\ \dfrac{{}^{65}/_{2}}{2{,}27}\ \cong 15\ s$

$F\ =\ 12000\ N$

$screw/nut\ pitch\ (p)\ =\ 6\ mm$

$\eta_{t\ static}\ =\ 0{,}2186$

$\eta_{t\ dynamic}\ =\ 0{,}3601$

$$C_{static}\ =\ \frac{F\ \cdot\ p}{2\ \cdot\ \pi\ \cdot\ \eta_{t\ static}\cdot 1000}\ =\ \frac{12000\ \cdot\ 6}{2\ \cdot\ \pi\ \cdot\ 0{,}2186\ \cdot 1000}\ =\ 52{,}4\ Nm \quad (4.24)$$

$$C_{dynamic}\ =\ \frac{F\ \cdot\ p}{2\cdot\pi\cdot\eta_{t\ dynamic}\cdot 1000}\ =\ \frac{12000\ \cdot\ 6}{2\cdot\pi\cdot 0{,}3601\ \cdot 1000}\ =\ 31{,}82\ Nm \quad (4.25)$$

$\eta_{CP\ 025}\ =\ 0{,}95$

$$C_{tot\ static}\ =\ \frac{C_{static}}{\eta_{CP\ 025}}\ =\ \frac{52{,}4}{0{,}95}\ =\ 55{,}2\ Nm \quad (4.26)$$

$$C_{tot\ dynamic} = \frac{C_{dynamic}}{\eta_{CP\ 025}} = \frac{31{,}82}{0{,}95} = 33{,}5\ Nm \qquad (4.27)$$

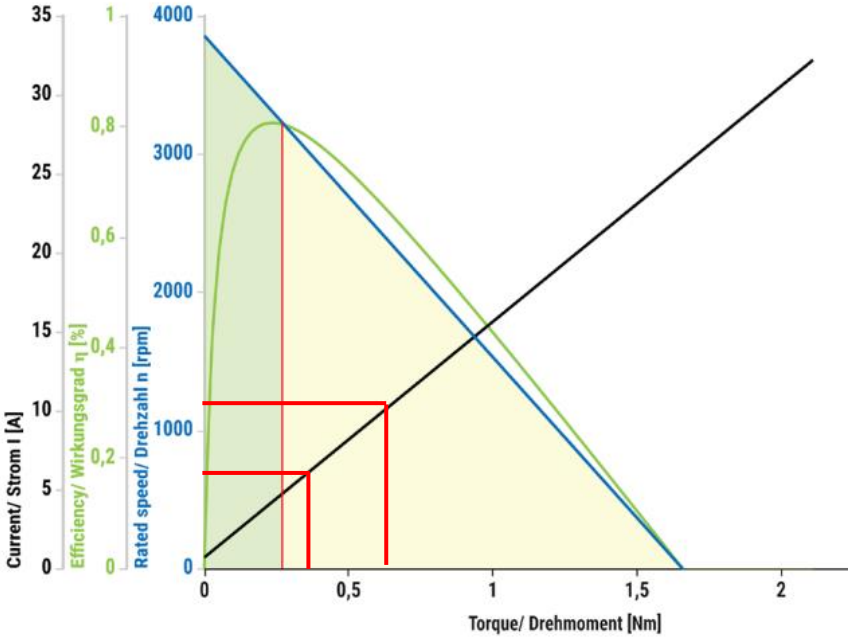

Plot 4.8 Characteristic plot of the BG 62 x 45 motor

$$P_{abs\ static} = V_{DC} \cdot I = 24 \cdot 11 = 264\ W \quad x\ 1\,\text{sec} \qquad (4.28)$$

$$P_{abs\ dynamic} = V_{DC} \cdot I = 24 \cdot 6 = 144\ W \quad x\ 14\,\text{sec} \qquad (4.29)$$

Cycle time definition

- Exiting from the box: 10 s ***(t_1)***
- Telescopic elongation: 26 s ***(t_2)***
- Inclination of the gangway towards the sky: 15 s ***(t_3)***
- Return of the gangway on horizontal position: 15 s ***(t_3)***
- Telescopic compression: 26 s ***(t_2)***
- Entering inside the box: 10 s ***(t_1)***

TOTAL CYCLE TIME = 102 s

$$E_{abs\,1} = P_{1\,abs} \cdot t_1 = 216 \cdot 10 = 2160\,J \tag{4.30}$$

$$E_{abs\,2} = P_{2\,abs} \cdot t_1 = 264 \cdot 26 = 6864\,J \tag{4.31}$$

$$E_{abs\,3} = P_{3\,abs\,static} \cdot t_{3\,static} + P_{3\,abs\,dynamic} \cdot t_{3\,dynamic} = \\ = 264 \cdot 1 + 144 \cdot 14 = 2280\ J \tag{4.32}$$

$$E_{abs\,el} = E_{abs\,1} + E_{abs\,2} + E_{abs\,3} = 2160 + 6864 + 2280 = 11{,}3\ kJ \tag{4.33}$$

5. Conclusions

Finally, after all the analyses that has been performed, it is possible to draw some conclusions on the performances of the electric solution with respect to the hydraulic one. This work was aimed at the definition of a new solution to overcome a series of drawbacks showed by the hydraulics, such as the risk of oil spillage inside the marine environment, leading to a strong pollution problem, which is completely avoided by the electric solution. Moreover, the energy consumed by the electric motors can be produced in a green way, such us using for example solar panel to recharge the batteries connected to the gangway's motors. In this way, the impact on the environment will be strongly reduced, taking a further step towards the total sustainable energy consumption.

This aspect leads to the second most important improvement which characterize the electric solution, which is the reduced energy consumption of whole system, strongly highlighted by the previous energetic analysis. As a matter of fact, while the hydraulic solution presents an energy consumption of about 80 kJ during a whole cycle, the electric solution consumes only 11,3 kJ during the same cycle, even if the overall running time is almost doubled. This result is very important, because one again it reduces the impact on the environment of this kind of solution.

The fact that the running time of the motors is increased can be seen as a drawback, but this aspect is strongly related to the dimensions of the electric motors: as a matter of fact, in order to reduce the space occupied by the mechanisms, it is necessary to use motors as small as possible, which means with lower available power. Having the possibility to adopt motors showing the same overall dimensions but a greater available power will surely overcome this problem. Another important improvement of the electric solution is the overall weight reduction: as a matter of fact, there is no more the need of a pressure pump and its motors, while the electric mechanism weight much less than the hydraulic counterparts. Moreover, all the components aimed at the transport of the pressured oil from the pump to the actuators will disappear, leaving the place to the lighter electric

cables. All of these factors will lead to a weight reduction not only of the gangway, but also of the complete boat.

On the other hand, the electric solution shows also some drawbacks, first of all the increase in the overall dimensions of the passerella. This is mainly related to technology behind the electric project, which is not advanced as it is the hydraulic one; however, the electric world is still in development, which means that more compact and powerful solution will arrive on the market. Last but not least, it is necessary to take into account also the price of the two solutions: unfortunately, the electric solution presents a cost of production greater than the hydraulic one, which results in a higher price on the market of the final product: this is mainly due to the fact that the electric market is not fully developed like the hydraulic one, with less competitors and consequently higher prices. On the other hand, the electric solution could be seen as a long-term investment, since its consumption is way lower than the hydraulic one, leading to important savings over the years.

In conclusions, the electric gangway can be seen as a very interesting solution, with several improvements both in term of performances and design, and nowadays is already achievable with the components available on the market. However, it is still in development and it cannot achieve the same performances of the hydraulic one, mainly to the fact that the electric motors and consequent mechanisms are not as avant-garde as the hydraulic ones, but this does not mean that they will never be, as we all hope.

6. References

[1] Agency for Toxic Substances and Disease Registry (ATSDR), *Toxicological profile for hydraulic fluid,* Atlanta, GA: Department of Health and Human Services, Public Health Service, 1997.

[2] Rainford solutions , «IP Ratings & Standards Explained,» 2020. [Online]. Available: https://rainfordsolutions.com/products/ingress-protection-ip-rated-enclosures/ip-enclosure-ratings-standards-explained/.

[3] Renesas Electronics Corporation, «What are Brushless DC Motors,» 2018. [Online]. Available: https://www.renesas.com/us/en/support/engineer-school/brushless-dc-motor-01-overview.

[4] Kollmorgen Experts, « Kollmorgen Experts,» 2 Marzo 2021. [Online]. Available: https://www.kollmorgen.com/en-us/blogs/_blog-in-motion/articles/how-does-stepper-motor-work/.

[5] NDR srl, «RIDUTTORE EPICICLOIDALE: VANTAGGI APPLICATIVI,» 2020. [Online]. Available: https://www.ndr.it/riduttore-epicicloidale-vantaggi/.

[6] Thomas Publishing Company, «All About Bevel Gears - What They Are and How They Work,» 9 Giugno 2022. [Online]. Available: https://www.thomasnet.com/articles/machinery-tools-supplies/bevel-gears/#:~:text=Share%3A,whose%20axes%20do%20not%20intersect..

[7] Dunkermotoren , *Catalogo BG 65 x 75,* 2022.

[8] WITTESTEIN , *Catalogo prodotti alpha Basic Line & alpha Value Line,* 2022.

[9] SIDERMARIOTTI s.r.l., «SCHEDA TECNICA ACCIAIO AISI 316,» [Online]. Available: https://www.sidermariotti.it/acciaio-inox/austenitici/316.html.

[10] CONTI, *Catalogo Viti Trapezoidali,* 2022.

[11] T. R. Carlo Ferraresi, Meccanica Applicata, Torino: C.L.U.T., 2007.

[12] Musola Metalli S.p.a., «Bronzo all'Alluminio (Leghe Rame – Alluminio),» 2019. [Online]. Available: https://www.venditabronzo.it/dati-tecnici-bronzo/bronzo-alluminio.html.

[13] Musola Metalli S.p.a., «PA6-G + MOS2,» 2020. [Online]. Available: https://www.materieplastiche.eu/poliammidi/pa-6-g-mos-2.html.

[14] Elip Tagliente s.r.l., *Catalogo Motori ElipTagliente,* 2020.

[15] Concens, *Catalogo CON60,* 2022.

[16] H. a. F. F. a. O. A. Doğan, «Comparative study of wear mechanism of surface treated AISI 316L stainless steel,» *Industrial Lubrication and Tribology,* pp. 76-83, marzo 2003.

[17] Dunkermotoren , *Catalogo BG 62 x 45,* 2022.

Acknowledgements

Vorrei dedicare le ultime righe di questa tesi ad alcune persone importanti e molto speciali per me, che con loro contributo mi hanno permesso di realizzare tutto ciò.

Innanzitutto, vorrei ringraziare l'Ingegner Bernardo Perez della Opacmare, supporto fondamentale nella realizzazione di questa tesi ma soprattutto persona splendida, sempre disponibile e gentile, senza di te questo elaborato non esisterebbe.

In secondo luogo, vorrei ringraziare il mio relatore, il Professor Mirko Baratta, e il mio co-relatore, il Professor Andrea Cavagnino, i quali mi hanno guidato e aiutato in questo ultimo percorso verso la fine dei miei studi.

Vorrei ringraziare inoltre tutta la mia famiglia e i miei amici, che hanno allietato le mie giornate con divertimenti, risate e stimoli di ogni genere, grazie di cuore a tutti.

In particolare, vorrei ringraziare mia sorella Giulia, la mia spalla e la mia ancora dal mio primo giorno di vita, i miei genitori Bruno e Paola, per avermi permesso di raggiungere questo traguardo di cui vado profondamente fiero, e la mia fidanzata Micol, per la sua dolcezza e il suo amore.

Infine, vorrei fare un ringraziamento speciale al team FKSKK, per avermi aiutato sotto il profilo accademico nel corso di tutti questi anni, ma soprattutto per avermi insegnato che l'università non ti lascia solo un diploma, ma anche degli amici fantastici che spero di avere al mio fianco per tutta la vita.